COASTAL INUNDATION MODELING FOR COASTAL GEORGIA THROUGH AUTOMATED UNSTRUCTURED FINITE MESH GENERATION

by

GRANT BILDERBACK

(Under the Direction of Matthew V. Bilskie)

ABSTRACT

Storm surge is the deadliest and costliest aspect of tropical storms and hurricanes. To accurately simulate hurricane storm surge, numerical models should include an up-to-date and accurate representation of the coastal landscape. Contemporary storm surge models leverage unstructured, finite element meshes to resolve complex coastal geometries while balancing computational efficiently. A substantially new development in mesh generation across the coastal floodplain includes the representation of significant vertical features such as dunes and highways. In addition, newly introduced mesh technology has evolved to allow for automated meshing. An unstructured mesh with integrated vertical features was generated using automatic mesh generation software for coastal flood research and real-time hurricane landfalling prediction purposes. The thesis presents the development of an unstructured storm surge model mesh for coastal Georgia using the latest mesh generation tools and the most recently available topographic and bathymetric data.

INDEX WORDS: Storm Surge, ADCIRC, Hydrodynamic Modeling, Numerical Modeling, Mesh Generation

COASTAL INUNDATION MODELING FOR COASTAL GEORGIA THROUGH AUTOMATED UNSTRUCTURED FINITE MESH GENERATION

by

GRANT BILDERBACK

B.S., The University of Georgia, 2022

A Thesis Submitted to the Graduate Faculty of The University of Georgia in Partial Fulfillment of the Requirements of the Degree

MASTER OF SCIENCE

ATHENS, GEORGIA

2023

COASTAL INUNDATION MODELING FOR COASTAL GEORGIA THROUGH AUTOMATED UNSTRUCTURED FINITE MESH GENERATION

by

GRANT BILDERBACK

Major Professor:	Matthew V. Bilskie
Committee:	Felix Santiago-Collazo
	Catherine Edwards

Electronic Version Approved:

Ron Walcott

Dean of the Graduate School

The University of Georgia

August 2023

DEDICATION

For those who lost their lives to Hurricane Ian

ACKNOWLEDGEMENTS

Without those around me, none of my achievements, past, present, or future, would be possible. The consistent love, encouragement, and support from family, friends, colleagues, and professors is what made this attainable, and I cannot summarize into enough words how grateful I am to each and every one of them. First, I would like to give a special thank you to Dr. Matthew Bilskie. Prior to joining the COAST lab as one of Dr. Bilskie's graduate students, I was without a project or funding, with my undergraduate graduation soon around the corner, and he took a chance on me. I cannot convey gratitude enough, so to you Dr. B -- thank you. To my committee members, Dr. Felix Santiago-Collazo and Dr. Catherine Edwards, I am extremely grateful for all the time and support you have given me and am ecstatic to have done this by your sides.

I joined the COAST lab as an undergraduate student in the summer of 2021. At the time, it was just myself, Dr. Bilskie, Dr. Viyaktha Hithaishi Hewageegana, and M.S. student Sheppard Medlin. Dr. Bilskie and the COAST lab afforded me the opportunity to discover a discipline within engineering I came to love -- coastal engineering. Rejoining the lab the following summer as a graduate student, I received nothing but support and friendship from those within COAST and the surrounding IRIS labs. I would like to give a special thanks to my lab mates: Rebecca Stanley, Caraline Miller, Ada Chimzulukeme Agbogu, Aditya Gupta, Bobby Fiegelist, Frank McQuarrie, Matheus Fagundes, Nashid Mumtaz, Oscar Gutierrez Villegas, Lauryn Falkenstein, Lina Cardenas, Sarah Moore, and Hannah Lim. Thank you all for supporting my project, as well as the

often-times confused student behind it. Your friendships are extremely valuable to me and I cannot wait to see where each of your individual research takes you.

I would like to give an important shout-out to my University of Georgia College of Engineering family. To our faculty and staff: Lauren Anglin, Sean McGarity, Josh Cooke, and others -- thank you for making the University of Georgia College of Engineering my home for the last 5 years. A special thanks to Amber Juncker and Dr. Stephan Durham, whose consistent advice, support, and friendship are a large reason that I am here today. To my fellow engineering friends and the College of Engineering Student Ambassadors, thank you for making engineering at UGA my home. You made this whole engineering thing well worth it. I couldn't possibly have made it this far without each of you.

Lastly, I would like to thank my family and friends. To my closest friends I met along the way, thank you for building me up when I was down and supporting my dream of becoming an engineer. To my girl, Caitlyn Brown: your smile, laughter, love, and encouragement pushed me to become the man I am today. And to my family: thank you for your love and support of me and this whole engineering thing. Each of you contributed to my completion of this project and thesis through both your interest and your love. And to you, Mom and Dad. My gratitude for you and the consistent sacrifices you made to get me to where I stand today cannot be put into words. From the financial support to the facetime calls where I walk you through running a code and everything in between, I am so grateful and blessed to call you Mom and Dad. I love you both and could not be here without you.

Glory, glory to the University of Georgia. Go Dawgs.

TABLE OF CONTENTS

LIST OF TABLES

LIST OF FIGURES

1.0 | INTRODUCTION

As time has progressed, the frequency of tropical cyclone development in the North Atlantic has increased, and the strength of storms has become more severe (Intergovernmental Panel on Climate Change (IPCC), 2022; Mudd et al., 2014). The meteorological community widely agrees that this is a result of climate change and the subsequent increase of both sea levels and ocean temperature (Intergovernmental Panel on Climate Change (IPCC), 2022; Lin et al., 2012). This increase in frequency and severity, paired with sea level rise has put coastal communities at a heightened level of vulnerability, both in respect to infrastructure as well as human life (Yasuda et al., 2014).

There are a multitude of detrimental impacts that can come from tropical activity. The most damaging is the flooding caused by storm surge (*Storm Surge Overview*, n.d.). Storm surge is the temporary rise in sea level as a result of decreasing atmospheric pressure and the angular winds that come with a tropical cyclone. The stronger the winds and the lower the pressure, typically the higher the storm surge (*Storm Surge Overview*, n.d.). Geographic factors also play a role in the impact of storm surge (M. V. Bilskie, Hagen, et al., 2012; M. V. Bilskie et al., 2015; Gao, 2021; *Storm Surge Overview*, n.d.). With regards to climate change, both the rising sea levels and increased ocean temperatures are estimated to result in an increase in both frequency and intensity of the storms and thereby the storm surge (Intergovernmental Panel on Climate Change (IPCC), 2022; Mcinnes et al., 2003; Yasuda et al., 2014)

During the landfall of a tropical system, storm surge values are highest where winds come ashore (Sebastian et al., 2019; *Storm Surge Overview*, n.d.). This phenomenon can be seen in the recent instances of Hurricane Ian (2022) and Hurricane Irma (2017) in Florida, where both made

landfalls on the west coast of Florida, and regions north of the eye saw a decrease in sea level due to the offshore winds, while the south end saw an increase.

Additionally, the impact from storm surge can be affected by certain bathymetric and topographic features (Bilskie, Hagen, et al., 2012; Tognin et al., 2021). Features such as barrier islands and marsh vegetation can serve as obstacles to the progression of storm surge, whereas concave shoreline features such as bays and river mouths can actually intensify storm surge's effects (Sebastian et al., 2019; Tognin et al., 2021). Bathymetric elements such as depth and bathymetric slope also have effects upon storm surge's intensity (Hagen et al., 2006; Resio & Westerink, 2008).

The North Atlantic Hurricane basin is one of the most active regions for tropical activity in the world (Villarini et al., 2012). The destructive capabilities of these storms have been felt throughout the Americas and elsewhere. In recent years, hurricanes such as Ian (2022), Katrina (2005), and Sandy (2012) have highlighted the destructive capability of storm across the East and Gulf Coast (Bunya, 2010; Georgas et al., 2014). One of the vulnerable regions along the U.S. coastline is known as the South Atlantic Bight (SAB), the concave shoreline region extending from the Florida Keys to Cape Hatteras, North Carolina (Figure 1.1) (Park et al., 2022; Thomas et al., 2019). Georgia coastline, near the midpoint of the SAB, is characterized by a complex marshland and barrier island ecosystem, defined by extensive tidal channels and creeks, swamps, and low-lying flat plains (Park et al., 2022).

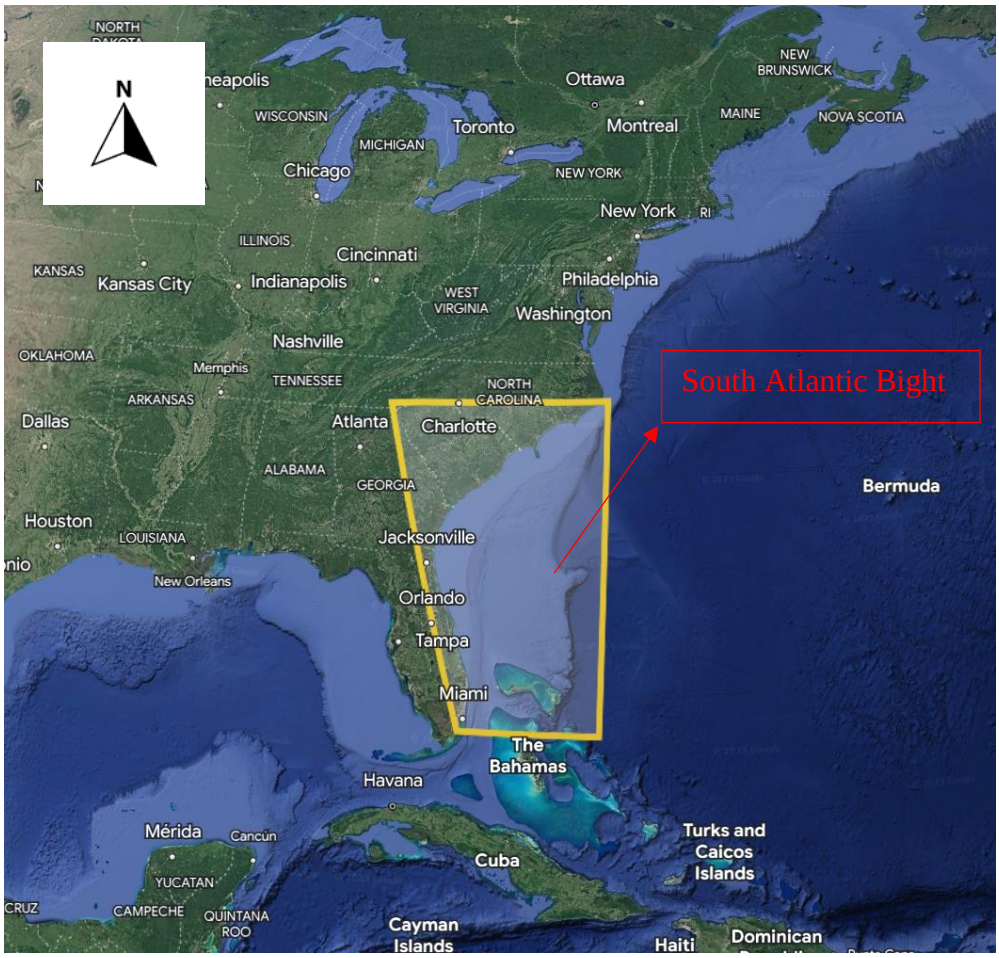

Figure 1.1 Location of South Atlantic Bight within the North Atlantic

Georgia has 14 major barrier islands, many of which are uninhabited or have low population density. There are, however, several developed islands with a higher population density, such as that of Saint Simons, Tybee, and Jekyll Islands, as well as metropolitan areas such as Savannah that are not far from the shoreline and are at risk of storm surge events (Park et al., 2022). Georgia has experienced tropical systems in the past that brought significant surge to its coast, such as Hurricane David (1979) that brought surge depth of upwards of a meter high in the streets of Brunswick and estimated higher values in other areas of the state (Hebert, 1980). In more recent years, storm surge from Hurricanes Ian (2022) and Irma (2017) brought destructive surges

to the state, and have reaffirmed the need for updated coastal infrastructure and other defensive measures to protect against future storms (Park et al., 2022).

One of the most important aspects in preventing loss of life from hurricanes and their storm surge is meteorological forecasting, particularly storm surge forecasting (Kohno et al., 2018). Storm surge prediction and modeling a field that is consistently developing and changing, with various of different models used to predict storm surge (Kohno et al., 2018). Storm surge is typically predicted using computer models that simulate the behavior between the ocean and the land in respect to meteorological and tidal forcing during a hurricane event (Luettich et al., 1992). These models use data collected from a variety of sources, including weather satellites, buoys, and aircraft to simulate water levels and wave conditions (Kohno et al., 2018; Luettich et al., 1992).

ADCIRC (Advanced Circulation Model) is a widely used numerical model designed for simulating the hydrodynamics of coastal and oceanic systems. It is specifically developed to study storm surge and flooding caused by severe weather events such as hurricanes. ADCIRC utilizes the finite element method to solve the shallow water equations, accurately representing the interactions between wind, waves, tides, and complex coastal features like islands, estuaries, and river inflows. By simulating the dynamic behavior of water levels, currents, and associated processes, ADCIRC helps predict coastal flooding and aids in the development of effective mitigation strategies and response plans. For this thesis, ADCIRC will be used as the modeling software for simulating storm surge and tides for the coast of Georgia.

Prior to running ADCIRC, one must obtain a mesh of the region they would like to model storm surge (Luettich et al., 1992). A mesh for ADCIRC refers to the discretization of the model domain into a set of finite elements. In other words, a mesh is a collection of non-overlapping elements, or triangles, connected by nodes, or points, that span the domain of the geographical

area the user would want to model, such as that of the mesh in Figure 1.2 (Luettich et al., 1992; Roberts et al., 2019). The mesh serves as the basis for numerical calculations in ADCIRC and provides the framework for solving the governing equations of the model (Dietrich et al., 2012; Luettich et al., 1992). For this thesis, ADCIRC will be fed in an unstructured, finite element mesh with integrated geographic elements.

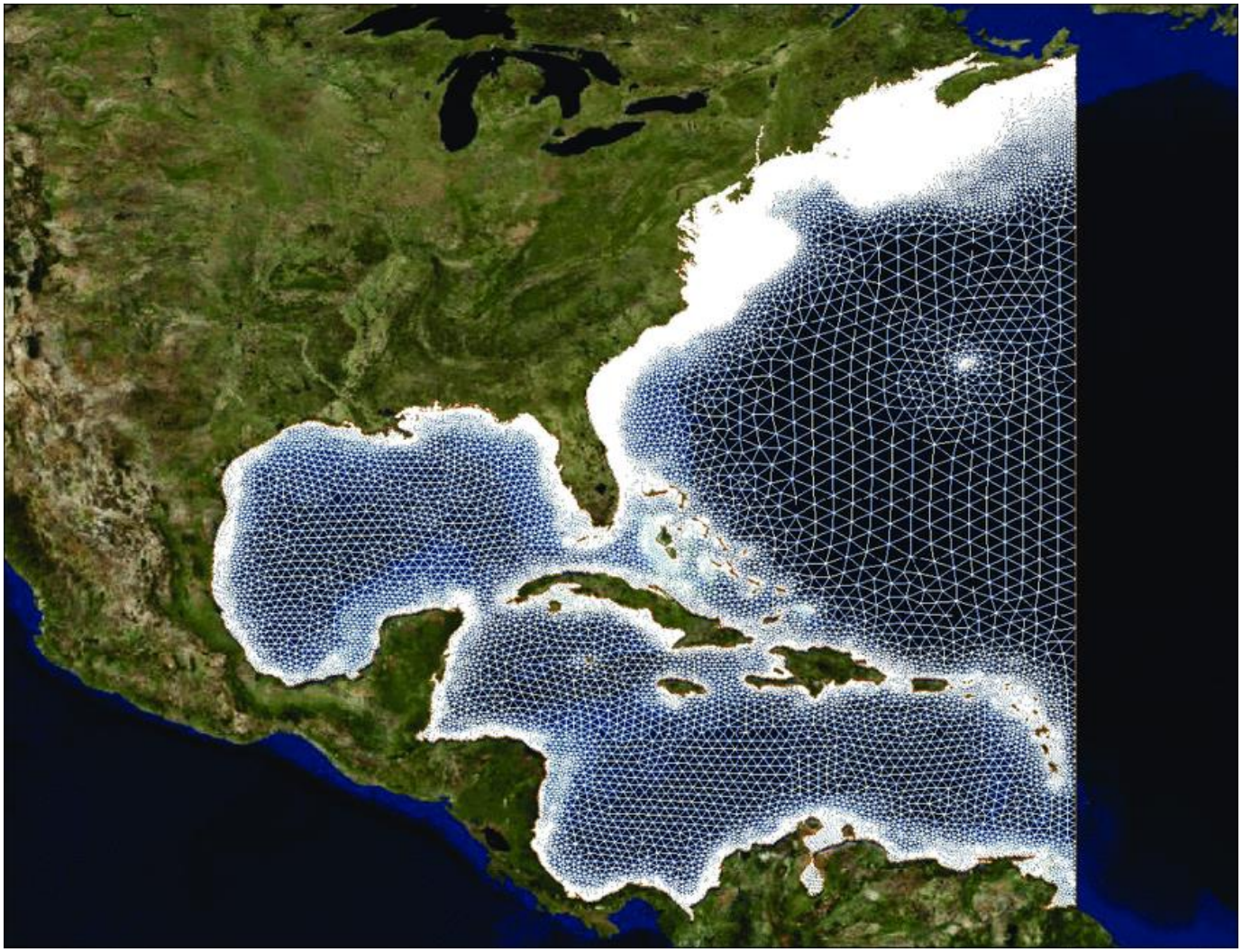

Figure 1.2 Large domain unstructured mesh

The particular mesh development software used in this study is OceanMesh2D (OM2D) (Roberts et al., 2019). Compared to other meshing software, OM2D is semi-automated and generates quality unstructured finite meshes quickly (Roberts et al., 2019).

One of the main developments in meshing integration of impactful geographic features, such as vertical features (VFs) and thalwegs (M. V. Bilskie, Hagen, et al., 2012; Gao, 2021). Thalwegs indicate the region within a stream or channel of lowest elevation, and play a role in the way floodwaters propagate up said channels (M. V. Bilskie, Hagen, et al., 2012; Velasquez-Montoya et al., 2023). VFs are geographic points of significance along the terrain that extrude out above the surrounding areas (M. V. Bilskie et al., 2015; Gao, 2021). For example, certain features with small surface areas such as dunes, levees, roads, and railways that extrude above the surrounding terrain will not always be resolved when developing a bathymetric and topographic map, but still have a significant effect upon coastal inundation (M. V. Bilskie et al., 2015; Hu et al., 2022). In coastal flood modeling, these features can significantly impact the propagation and behavior of storm surge and other coastal hazards. VFs can greatly influence the dynamics of coastal ocean circulation, and their accurate representation is essential for reliable simulations of coastal flooding (Luettich et al., 1992).

Due to Georgia's complex coastline and comprehensive geography and bathymetry, a mesh including geographical features such as channels and VFs is required to sufficiently model coastal inundation scenarios with a high level of accuracy (Park et al., 2022). With the development of advanced, rapid meshing technologies such as OM2D and numerical modeling software, ADCIRC, real-time storm surge modeling during cyclonic events can be performed with a higher level of accuracy at quicker runtimes (Dietrich et al., 2012; Roberts et al., 2019).

This thesis aims to answer the following two research questions:

1. *Can vertical features be automatically extracted from a large domain DEM?*
2. *Can vertical features and thalwegs be integrated into unstructured meshes developed by automated mesh generation software?*

2.0 | LITERATURE REVIEW

2.1 | Overview

The process of modeling storm surge and coastal inundation consists of multiple steps, all of which play a role in the efficiency and accuracy of a model. Automated mesh generation software can be an alternative to manual mesh generation, and can prove more effective for storm surge modeling with the incorporation of certain geographical features into the meshing constraints. This literature review examines four main topics: 1) the rising vulnerability of coastal regions to storm surge; 2) storm surge modeling; 3) VF and thalweg extraction, and 4) semi-automated mesh development.

2.2 | The Rising Vulnerability of Coastal Regions to Storm Surge

Coastal regions are home to a significant proportion of the global population and are of great ecological, economic and cultural importance (Intergovernmental Panel on Climate Change (IPCC), 2022). However, they are increasingly vulnerable to natural hazards such as hurricanes, sea-level rise, and flooding, exacerbated by human activities such as coastal development and climate change (Bathi & Das, 2016; Intergovernmental Panel on Climate Change (IPCC), 2022).

Sea-level rise and coastal flooding are two of the most significant threats facing coastal regions (Bathi & Das, 2016). According to IPCC, sea-level rise is projected to continue throughout the 21st century, with significant impacts on coastal areas (Intergovernmental Panel on Climate Change (IPCC), 2022). The report also highlights the need for adaptation measures, including the relocation of communities, infrastructure, and ecosystems (Intergovernmental Panel on Climate Change (IPCC), 2022). Furthermore, it has been indicated by 2050 coastal flooding could affect up to 300 million people globally, causing significant economic losses and social disruption

(Hinkel et al., 2014). As sea-levels rise, the buffer between coastal communities diminishes (Hinkel et al., 2014). The increased water levels further increases those communities' vulnerability to storm surge, as inundation can occur from weaker storms comparatively from when sea levels were lower (Mcinnes et al., 2003).

The increased in storm frequency and intensity in tandem with sea level rise as a result of climate change has resulted in coastal regions becoming increasingly more vulnerable to flooding (Intergovernmental Panel on Climate Change (IPCC), 2022; Mudd et al., 2014). Hurricanes have become more intense in recent years due to climate change, leading to more significant damage to coastal communities (Lin et al., 2012). Storm surge, which is the rise in sea level caused by a hurricane, is widely considered to be the most damaging factor of a hurricane. One study found that storm surge was responsible for 49% of the economic losses caused by Hurricane Sandy in 2012. The study also found that the height of storm surge was the single most important factor in determining the amount of damage caused by the hurricane (Georgas et al., 2014).

Storm surge is caused by the intense winds and low pressure at the center of a tropical storm. The winds push the ocean water towards the shore, causing it to rise above its normal level. This rise in sea level can be catastrophic, as it can cause flooding and damage to coastal infrastructure. In fact, storm surge is responsible for most of the deaths and damage caused by tropical storms (*Storm Surge Overview*, n.d.). Storm surge's costliness is a result of its expanse over a large area, affecting hundreds of miles of coastline while penetrating up to several miles inland (Bathi & Das, 2016). In addition, storm surge can occur quickly and shift throughout a storm's progression, making it difficult for people to evacuate in time in the area the storm will ultimately make landfall (Ghorbanzadeh et al., 2021).

The damage caused by storm surge can be long-lasting. Flood waters can damage buildings, infrastructure, and other structures, leading to costly repairs and reconstruction. In addition, storm surge can cause saltwater intrusion into freshwater resources, leading to long-term environmental damage (Hu et al., 2022). The surge not only can affect the immediate area, but also the wider region, as it can disrupt fisheries and other industries that rely on the coastal environment (Panthi et al., 2022). Other factors such as those related to local politics and economics also affect how damaging storm surge can be, as some communities that have not valued updating coastal infrastructure to both the increase in storm severity as well as sea level rise are more vulnerable than those who have adjusted to the climactic and geomorphic changes (Helderop & Grubesic, 2019).

Another reason why storm surge is so damaging is that it can be difficult to predict. This is due to the prediction of storm surge in real-time storm scenarios being highly dependent on meteorological forecasting of the incoming tropical cyclone (Dietrich et al., 2012; Thomas et al., 2019). Factors such as the size and intensity of the hurricane, the shape of the coastline, and the depth of the water can all affect the height and extent of storm surge (Irish et al., 2008; Sebastian et al., 2019; *Storm Surge Overview*, n.d.). While scientists have made significant progress in understanding the factors that contribute to storm surge, there are still many challenges in predicting its height, extent, and timing (Bode & Hardy, 1997; Kohno et al., 2018).

One of the primary reasons why storm surge is difficult to predict is its dependence on a wide range of factors. These include the size and intensity of the hurricane, the shape of the coastline, the depth of the water, and the topography of the land, amongst others According to one study, storm surge is highly dependent on the size and intensity of the hurricane (Irish et al., 2008). A larger and more intense hurricane is likely to produce a higher storm surge, all other things being

equal. In addition, the shape of the coastline can have a significant impact on the height and extent of storm surge (Irish et al., 2008). For example, a coastline with a wide and shallow shelf will experience a more extensive storm surge than a coastline with a steep drop-off. These complex interactions between different factors make it challenging to predict the height and extent of storm surge accurately.

A further challenge in predicting storm surge is the difficulty in modeling the complex interactions between different factors. Storm surge is influenced by a range of factors, including wind speed and direction, ocean currents, tidal patterns, and geographic obstacles (M. V. Bilskie et al., 2015; *Storm Surge Overview*, n.d.). Modeling these complex interactions is challenging and requires advanced computational techniques. In addition, different models may produce different results, leading to further uncertainty in the prediction of storm surge (Lin et al., 2010). For example, the impact of storm surge can be influenced by human activities, such as the construction of coastal infrastructure, such as levees, dams, roads, and other features (Hu et al., 2022). These unexpected events can make it challenging to accurately predict the height and extent of storm surge, as they may not be typically accounted for in predictive models (Zhang et al., 2000).

In conclusion, storm surge is a complex and challenging phenomenon to predict. The dependence on a wide range of factors, the limited availability of data, the difficulty in modeling complex interactions, and the impact of unexpected events all contribute to the challenge of predicting storm surge accurately. These difficulties in predicting storm surge increases the overall vulnerability of coastal regions. Even with recent progress in storm surge modeling, there are still dependencies on meteorological forecasting. As a hurricane's path shifts, estimated storm surge amounts will change. With further developments in the modeling of a hurricane's path, the ability to estimate storm surge will become more effective (Kohno et al., 2018).

2.3 | Storm Surge Modeling

Storm surge and coastal inundation has been modeled previously using an array of techniques (Kohno et al., 2018). Technologies used to predict storm surge include satellite data, radar, buoys and tide gauges, machine learning, and numerical models (Bode & Hardy, 1997). These are all used, often times in collaboration, within the process of storm surge prediction. Information gathered from satellites is used to track storms and monitor ocean and atmospheric conditions, which can help improve the accuracy of storm surge predictions (Bunya, 2010; Feng et al., 2012). Radar technology is used to track the movement of storms and measure precipitation and wind patterns, which can help determine the potential for storm surges. Buoys and tide gauges measure water levels in real-time and provide crucial information about storm surges. Machine learning algorithms are used to analyze large amounts of data from various sources and make more accurate predictions of storm surges (Sun et al., 2021). Numerical models, such as the SLOSH and ADCIRC models, are used to simulate storm surges and provide predictions for specific locations (Dietrich et al., 2012; Luettich et al., 1992; *Sea, Lake, and Overland Surges from Hurricanes (SLOSH)*, n.d.).

The main type of numerical models used to predict storm surge are hydrodynamic models (Kohno et al., 2018; Luettich et al., 1992). Hydrodynamic models simulate the flow of water and predict how storm surges will impact coastlines. Hydrodynamic models consider the shape of the coastline, bathymetry and other factors that can affect the flow of water during a storm surge (Luettich et al., 1992).

The use of hydrodynamic numerical models for real time storm surge prediction is highly dependent upon tropical storm modeling (Kohno et al., 2018; Li & Nie, 2017). There are a range of different tropical storm models used worldwide, each of which will individually predict the path

a storm will take, the speed at which the storm will progress along the line, and the strength of the storms along that line, in terms of both atmospheric pressure and wind speeds. Understanding each of these factors is necessary in developing an accurate storm surge model (M. V. Bilskie et al., 2022). These models are ran consistently throughout a storm's progression, and thus storm surge models must be ran concurrently, as the projected path will become more accurate with time (Li & Nie, 2017). It has also been shown that from 1970 until 2005, tropical storm track errors have decreased across all sides of a storm's prediction history and thus the models have consistently become more accurate (Cangialosi & Landsea, 2016). As tropical storm track and intensity models improve, storm surge models will improve at a commensurate rate (Li & Nie, 2017).

In the United States, several different models are used to predict storm surge during hurricanes, including the Sea, Lake, and Overland Surges from Hurricanes (SLOSH) model, which was developed by the National Oceanic and Atmospheric Administration (NOAA) specifically for the prediction of storm surge during hurricanes. The SLOSH model takes into account a wide range of factors, including the size, strength, and speed of the hurricane, as well as the shape of the coastline and the local topography (*Sea, Lake, and Overland Surges from Hurricanes (SLOSH)*, n.d.).

Other models used in the United States include the Advanced Circulation (ADCIRC) model, developed by Westerink and Luettich for the U.S. Army Corps of Engineers, and the Simulating Waves Nearshore (SWAN) model, which was developed at Delft University of Technology (Booij et al., 2015; Luettich et al., 1992). Both models are often used in tandem to simulate the propagation of waves and water levels along the coast during hurricane events, and to predict the potential impacts of storm surge on coastal communities (Dietrich et al., 2012). ADCIRC is specifically designed to simulate the behavior of water levels and currents during

storm surge events, as well as predict tidal fluctuations (Dietrich et al., 2012; Luettich et al., 1992). ADCIRC uses a finite element method to solve the shallow water equations and considers a variety of factors, including wind forcing, tides, and pressure gradients (Luettich et al., 1992). On the other hand, SWAN is designed to simulate the behavior of waves in coastal and offshore regions (Booij et al., 2015). SWAN is spectral wave model to simulate the propagation and transformation of waves due to wind forcing, currents, and bottom friction (Booij et al., 2015; *Coastal Model Applications and Field Measurements- Tools and Standards for Ocean Modeling | U.S. Geological Survey*, n.d.).

ADCIRC is a numerical model used to predict the flow of water and the impact of storm surges. ADCIRC considers wind patterns, pressure changes, and other factors associated with storms to simulate the flow of water and predict the height and extent of storm surges (Luettich et al., 1992). Compared to other models, the ADCIRC model is more flexible and can be adapted to different coastal environments, which makes it useful for predicting storm surges in a variety of locations (Turan et al., 2018).

The ADCIRC model can be coupled with other models, such as the SWAN model, to provide a more complete prediction of the impact of storm surges (Bunya et al., 2010; Dietrich et al., 2012). The ADCIRC model provides predictions of the overall flow of water and height of storm surges, while the SWAN model focuses on the wave component and predicts the impact of waves on coastlines (Dietrich, Zijlema, et al., 2011).

ADCIRC was developed using the shallow water equations (SWE), which are partial differential equations used to determine the behavior of water in shallow regions (Luettich et al., 1992). These equations are originally derived from the Navier-Stokes equations, and will allow ADCIRC to determine the overall water surface elevation and currents during a storm, through

geographic input data (Luettich et al., 1992). SWAN is based on the wave action balance equation and uses the Gauss-Seidel sweeping method to be able to provide wave height and direction fields, which is then fed back to ADCIRC (Dietrich et al., 2012; Zijlema, 2010). The coupled model can then simulate the combined effects of storm surge and waves on the coastal region selected by the user (Dietrich et al., 2012).

The governing equations that drive ADCIRC and SWAN require numerous inputs regarding the storm that causes the surge, as well as the environment the surge occurs in (Dietrich et al., 2012). These begin with determining the domain size of the region the user wishes to model. It has been shown that larger domains result in more accurate inundation estimates, due to their inclusion of certain oceanographic features such as continental shelves and their physical interactions with both the coast and the basin (Blain et al., 1994). The domain that storm surge will be predicted is mapped by the mesh. The mesh is the spatial discretization of ADCIRC, and dictates where water levels are simulated (Luettich et al., 1992).

ADCIRC will then read in a variety of other datasets, including specified nodal attributes or properties associated with each computational node in the finite element mesh. The user may also include datasets which specify model parameters such bottom and surface roughness, Manning's N and time step, and several others, all of which allow the model to further specific parameters that affect the modeled storm surge's magnitude (Luettich et al., 1992).

Manning's n, also known as Manning's roughness coefficient, is a parameter used to characterize the roughness or friction between a fluid flow and the boundary it interacts with, such as a channel bed, river banks, or ocean floor. Manning's n represents the resistance to flow caused by the roughness elements in the channel or water body. It is used in various hydrodynamic models

and equations, including the computation of water flow velocities, determination of hydraulic roughness, and calculation of flow rates in open channels (Passeri et al., 2012).

The value of Manning's n depends on the characteristics of the boundary, including the surface roughness, vegetation, obstructions, and other factors. It is typically determined through empirical observations, field measurements, or by using established reference tables that provide estimates for different types of surfaces. The Manning's n value is dimensionless and can vary within a range depending on the type of flow and the specific hydraulic conditions. Smoother surfaces, such as concrete channels, tend to have lower Manning's n values, indicating less friction, while rougher surfaces, like natural streams or vegetated areas, have higher values, indicating higher friction (Passeri et al., 2012).

By assigning appropriate Manning's n values to different parts of a computational model, such as in ADCIRC, the model can account for the effects of bottom roughness and simulate the influence of friction on water flow velocities and patterns accurately. It is important to note that Manning's n is specific to each modeling application, and accurate calibration or estimation of Manning's n values for the specific hydraulic conditions and boundary characteristics is crucial for obtaining reliable simulation results (Passeri et al., 2012).

Manning’s n values can be gathered through multiple sources, but in the mesh developed as a part of this study, CCAP was utilized. The Coastal Change Analysis Program (CCAP) is a long-term initiative led by the United States Geological Survey (USGS) to study and analyze coastal change and land cover dynamics along the shoreline of the United States. Its primary goal is to provide reliable and consistent information about coastal land cover changes, erosion, and habitat loss over time (*C-CAP Regional Land Cover and Change*, n.d.).

The CCAP utilizes remote sensing data, particularly high-resolution aerial imagery and satellite imagery, to capture and analyze changes in coastal land cover. By comparing images from different time periods, the program can identify and quantify changes in land cover types such as beaches, dunes, wetlands, urban areas, and other coastal habitats.

One of the main objectives of the Coastal Change Analysis Program is to monitor and document coastal land cover changes. By assessing changes in land cover, the CCAP seeks to understand the impacts of erosion, sedimentation, sea-level rise, storms, and other coastal processes. The program provides valuable information on the rates and patterns of change for different coastal regions (*C-CAP Regional Land Cover and Change*, n.d.).

A key aspect of the CCAP is its commitment to providing consistent and accessible data. The program aims to ensure that its land cover data and analysis are consistent across different coastal regions, allowing for comparisons and understanding of broader coastal change trends. The CCAP makes its data publicly available, facilitating access for researchers, managers, and the general public. The Coastal Change Analysis Program has produced land cover and change data for multiple time periods and regions within the United States. The data is typically organized into various land cover categories and can be accessed through the USGS National Land Cover Database (NLCD) or specific CCAP data products (*C-CAP Regional Land Cover and Change*, n.d.).

2.4 | Mesh Generation

The mesh for ADCIRC can be either structured or unstructured (Figure 1.3). A structured mesh has a regular geometric structure, such as a grid of squares or rectangles, while an unstructured mesh does not have a regular structure, and the nodes and elements are distributed arbitrarily throughout the domain (Roberts et al., 2019). How elements and nodes are distributed

are based on certain criteria set by the user (Hagen et al., 2006; Roberts et al., 2019). For more specific and accurate modeling, an unstructured mesh is required to achieve the desired resolution due to the complexity of the coast geography (Westerink et al., 2008). The process of generating a mesh involves several steps, including selecting appropriate element types, determining the number of elements needed, and assigning nodal coordinates to create the mesh (Westerink et al., 2008). The mesh quality, such as the element size and shape, is important as it affects the accuracy and stability of the model (M. V. Bilskie, Hagen, et al., 2012; Hagen et al., 2006; Westerink et al., 2008). Therefore, mesh optimization techniques may be applied to refine the mesh and improve its quality. Overall, the mesh plays a crucial role in the accuracy and reliability of the ADCIRC model and is a critical component in simulating coastal inundation and flooding events (Luettich et al., 1992).

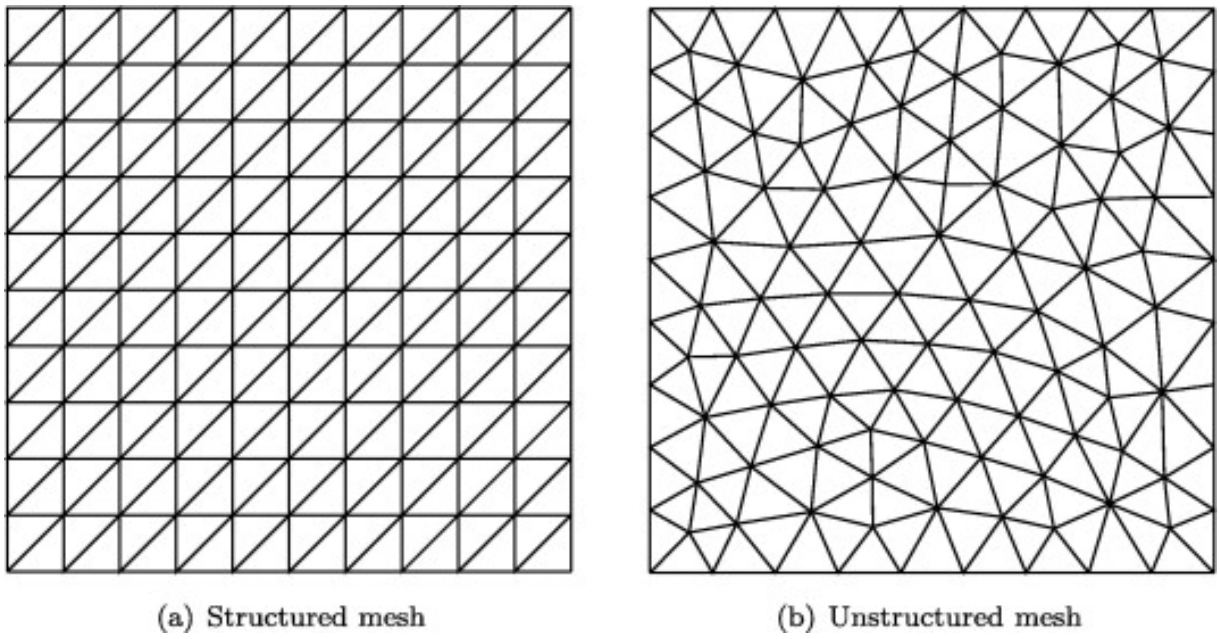

Figure 1.3 Structured versus unstructured mesh (Hiester et al., 2014)

The development of an unstructured mesh for ADCIRC involves several steps, including preprocessing, mesh generation, mesh optimization, and mesh quality assessment (Roberts et al.,

2019; Westerink et al., 2008). Preprocessing involves preparing the input data for the mesh generation software, such as topography and bathymetry data, boundary conditions, and other model inputs (Luettich et al., 1992; Westerink et al., 2008). Once the input data is ready, the mesh generation software is used to create the unstructured mesh.

Throughout the history of storm surge modeling, the process of mesh generation has undergone significant transformations to meet the evolving demands of computational modeling techniques and computational fluid dynamics. The objective of mesh generation is to discretize the computational domain into smaller elements or cells, enabling the accurate simulation of storm surge (Hagen et al., 2006; Roberts et al., 2019).

In the early stages of storm surge modeling, structured grids were commonly employed. These grids featured regular shapes and uniform cell sizes, which facilitated straightforward implementation. However, they struggled to represent complex coastal geometries and irregular coastlines effectively (Kojima, 2005). As computational capabilities advanced, unstructured grids emerged as a popular alternative for storm surge modeling. Unstructured grids offered increased flexibility in capturing intricate coastal features, such as irregular shorelines, islands, and estuaries (M. V. Bilskie, Hagen, et al., 2012; Gao, 2021; Roberts et al., 2019). They facilitated higher mesh resolution near the coastline and critical features like estuarine channels and VF (M. V. Bilskie, Hagen, et al., 2012; M. V. Bilskie et al., 2015; Gao, 2021).

With the advent of high-performance computing, automated mesh generation techniques gained prominence (Bunya et al., 2010; Roberts et al., 2019). These techniques, including the utilization of software tools like OM2D, enabled dynamic grid adaptation. Automated mesh generation employs adaptive strategies that refine the mesh resolution based on predefined criteria in regions of interest. This approach optimizes computational resources allocation, leading to

enhanced accuracy while reducing computational costs (M. V. Bilskie et al., 2020; Bunya et al., 2010; Roberts et al., 2019).

Mesh generation involves dividing the computational domain into a set of triangular or quadrilateral elements. The mesh generation process can be done in various ways, such as by using a Delaunay triangulation or advancing front method (P. Frey & George, 2008; Hagen et al., 2002). In the Delaunay method, a set of nodes is created, and the triangles are formed by connecting the nodes in such a way that no nodes lie inside the circumcircle of any triangle (P. J. Frey et al., 1998; Weatherill & Hassan, 1994). In the advancing front method, the mesh is generated by sweeping a front across the computational domain, connecting nodes as it moves along (P. J. Frey et al., 1998; Löhner & Parikh, 1988). The Delaunay triangulation method does not take much time to run, and is used more frequently in automated mesh generation (Hagen et al., 2002, 2006; Roberts et al., 2019).

Recent developments in mesh generation techniques have also embraced the integration of topographic data and remote sensing technologies. High-resolution elevation data from LiDAR, satellite imagery, and aerial photographs contribute to accurate representation of coastal features, enabling refinement of meshes along shorelines and thalwegs (M. V. Bilskie, Hagen, et al., 2012; Coggin, 2008; Gao, 2021).

One of the frequently used mesh generation software is SMS (Sahoo & Bhaskaran, 2018). SMS (Surface-water Modeling System) is a software package developed by Aquaveo that specializes in modeling and simulation of surface water systems. SMS provides a comprehensive set of tools and capabilities for working with geospatial data, creating and manipulating mesh structures, and visualizing and analyzing simulation results (AQUAVEO, n.d.).

One of the key aspects that sets SMS apart from older mesh generation technologies is its emphasis on integrating GIS (Geographic Information System) functionality with meshing capabilities. SMS allows users to seamlessly import and work with GIS data, including DEMs, aerial imagery, and vector datasets such as rivers, lakes, and land boundaries. This integration enables users to leverage the power of geospatial data in generating high-quality meshes for surface-water modeling (M. V. Bilskie et al., 2015).

SMS offers an intuitive and user-friendly graphical interface that makes it easier for users to interact with the software. It provides a range of visualization tools, allowing users to dynamically view and manipulate meshes, assign boundary conditions, and visualize simulation results (M. V. Bilskie, Akhavian, et al., 2012). The graphical interface also facilitates the creation and editing of meshes, with tools for generating meshes from scratch, refining and optimizing existing meshes, and incorporating geometric and bathymetric data (Macchione et al., 2019).

SMS also provides advanced mesh editing and manipulation tools, such as mesh smoothing, refinement, and adaptation, which help improve the quality and resolution of meshes (M. V. Bilskie, Akhavian, et al., 2012; M. V. Bilskie et al., 2015). Additionally, it offers tools for incorporating boundary conditions, defining material properties, and assigning attributes to different parts of the mesh, enabling users to accurately represent the physical properties and behavior of the modeled system (Blanton & Luettich, 2023).

Furthermore, SMS supports a wide range of simulation models, including hydraulic, hydrologic, and water quality models, facilitating comprehensive analysis and simulation of surface-water systems. It provides seamless integration with popular simulation engines, enabling users to easily set up simulations, run them, and visualize the results within the SMS environment (AQUAVEO, n.d.).

Historically, the generation of unstructured meshes has progressively developed and become more comprehensive over time (M. V. Bilskie et al., 2015; Hagen et al., 2006; Westerink et al., 2008). One of the important developments in mesh generation is the inclusion of geographic data to dictate the mesh generation. Geographic data, such as channel thalweg lines, VFs, and LiDAR assessed DEMs, can have a significant impact on automated mesh development for numerical modeling applications (Bates et al., 2003; M. V. Bilskie et al., 2015). These data provide critical information on the topography and bathymetry of the system being modeled, which can be used to guide the mesh generation process. For example, channel thalwegs can be used to define the location and orientation of channels and other topographic features, while VF lines can be used to guide the placement of nodes within an overland mesh (Gao, 2021; Roberts et al., 2019). LiDAR assessed DEMs can provide highly accurate elevation data that can be used to create high-resolution meshes that capture the fine-scale sloping of the domain being modeled (Maune, 2007; Roberts et al., 2019). By incorporating these types of geographic data into the mesh generation process, automated mesh development tools can create more accurate and efficient meshes that better represent the topography and bathymetry of the system being modeled.

After the mesh is generated, it may require optimization to ensure that it is well suited for the ADCIRC model. Mesh optimization involves adjusting the nodes and element shapes to improve the mesh quality, which is a measure of how well the mesh represents the geometry of the computational domain. Various mesh optimization techniques are available, including the Laplacian smoothing method and the Delaunay-based optimization method (Boender, 1994). Once the mesh is optimized, it is assessed for quality to ensure that it meets the desired specifications for the ADCIRC model. Mesh quality can be assessed using various measures, such as element shape, aspect ratio, and mesh size distribution (Boender, 1994). The quality assessment is done to

ensure that the mesh is well suited for the ADCIRC model and that the simulation results are accurate and reliable (Roberts et al., 2019).

The evolution of mesh generation in storm surge modeling has transitioned from structured grids to unstructured grids and, more recently, embraced automated techniques like OM2D (Roberts et al., 2019). These advancements have enhanced the ability of models to capture complex coastal geometries, providing accurate simulations of storm surge events. The integration of high-resolution data further contributes to improved mesh quality, enabling more precise coastal planning, risk assessment, and disaster management (M. V. Bilskie, Hagen, et al., 2012; M. V. Bilskie et al., 2015; Bunya et al., 2010; Gao, 2021).

OM2D is an open-source software tool specifically designed for generating two-dimensional unstructured meshes for coastal and oceanographic modeling. It provides a user-friendly interface and a range of features to facilitate the creation of high-quality computational meshes for numerical simulations (Roberts et al., 2019).

OM2D focuses on generating meshes that accurately represent coastal and oceanic features, such as shorelines, islands, estuaries, and complex bathymetry. It considers the varying resolution requirements of different regions within the domain to ensure efficient and accurate modeling of hydrodynamic processes. The software incorporates advanced mesh generation algorithms, including Delaunay triangulation and advancing front methods, to create high-quality unstructured meshes. It also offers options for refining the mesh resolution in specific areas of interest, such as nearshore regions or around coastal structures, allowing for greater detail and accuracy in those areas (Roberts et al., 2019) (Figure 2.1).

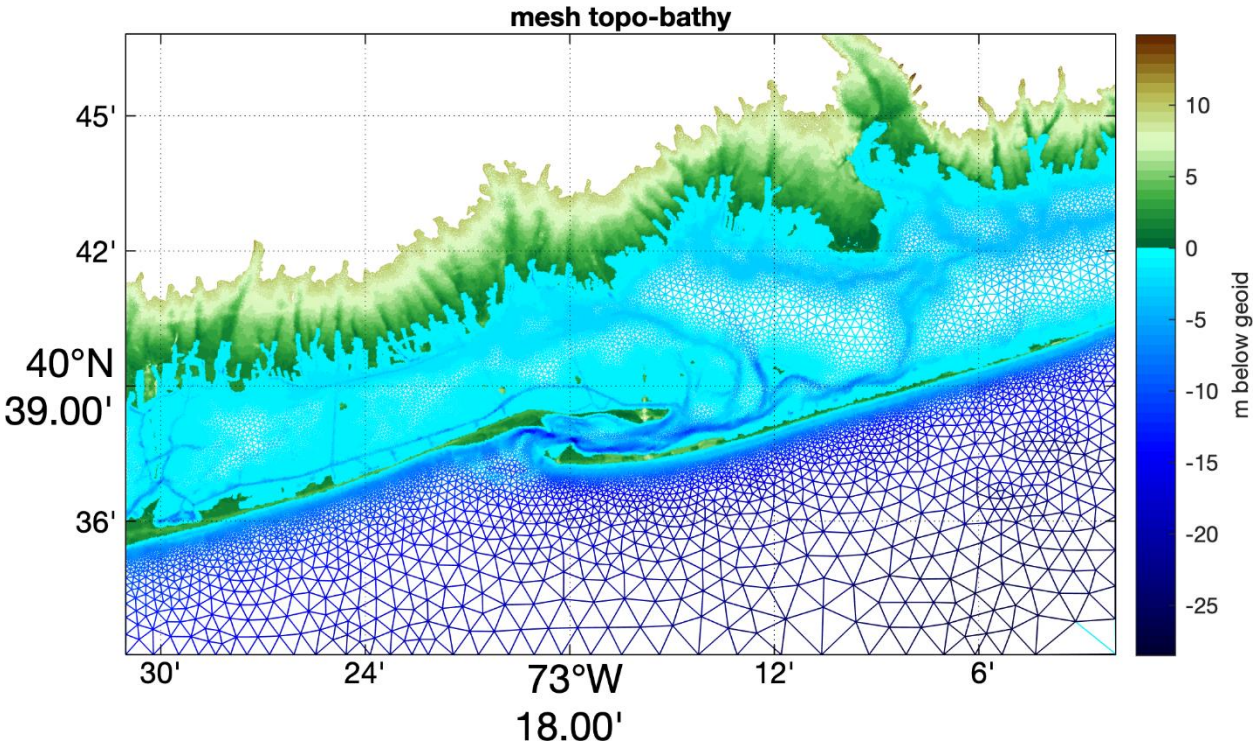

Figure 2.1 Example of OM2D developed mesh with resolution of coastal channels

OM2D supports various input data formats, including topographic data, elevation models, and coastline data, which can be used to guide the mesh generation process. It provides tools for preprocessing the input data, visualizing the mesh, and exporting the generated mesh in formats compatible with popular numerical modeling software. One notable feature of OM2D is its ability to handle large-scale coastal domains efficiently, making it suitable for modeling applications at regional or global scales. The software is continually being developed and enhanced by a community of researchers and practitioners in the field of coastal and oceanographic modeling (Roberts et al., 2019).

2.5 | Geographic Data Collection

Accurate physical depiction of geographical features including bathymetry, topography, and certain geographical inundation barriers that affect how coastal floods can be modeled (M. Bilskie, 2012; Gallien et al., 2014; Gao, 2021). High quality unstructured meshes that are used in storm surge modeling have certain mesh specifications as it relates to geographic features, and thus it is critical to a high functioning storm surge model that the mesh includes these features (M. Bilskie, 2012; Gallien et al., 2014). The geographic data required to develop these meshes come from Digital Elevation Models (*DEM*), and computerized files that contain wet/dry boundaries, VFs, and thalwegs.

2.5.1 | Digital Elevation Models

Improvement in the estimation of storm surges has come with the development of newer modeling technology (Kohno et al., 2018). Some of the improvements in the technology however are a result of progress in geographic data collection technology, such as lidar (M. V. Bilskie et al., 2020). Developments in LiDAR allows for higher resolution in a *Digital Elevation Model* (DEM) (Figure 2.2). A DEM is a digital representation of the surface of the Earth, or other planetary body, that provides information on the elevation, or height, of the terrain at each point on a regular grid (Wolock & Price, 1994). DEMs are typically generated using remote sensing data, such as satellite imagery or LiDAR (Light Detection and Ranging) data, and are widely used in a variety of applications, including geographic information systems, hydrological modeling, and land use planning. DEMs can be used to create topographic maps, calculate slope and aspect, and derive other terrain-related information (Bunya et al., 2010; Wolock & Price, 1994). However, pertinently to storm surge modeling, LiDAR developed DEMs can also be used for the development of a *fort.14* mesh (Liu, 2008; Roberts et al., 2019).

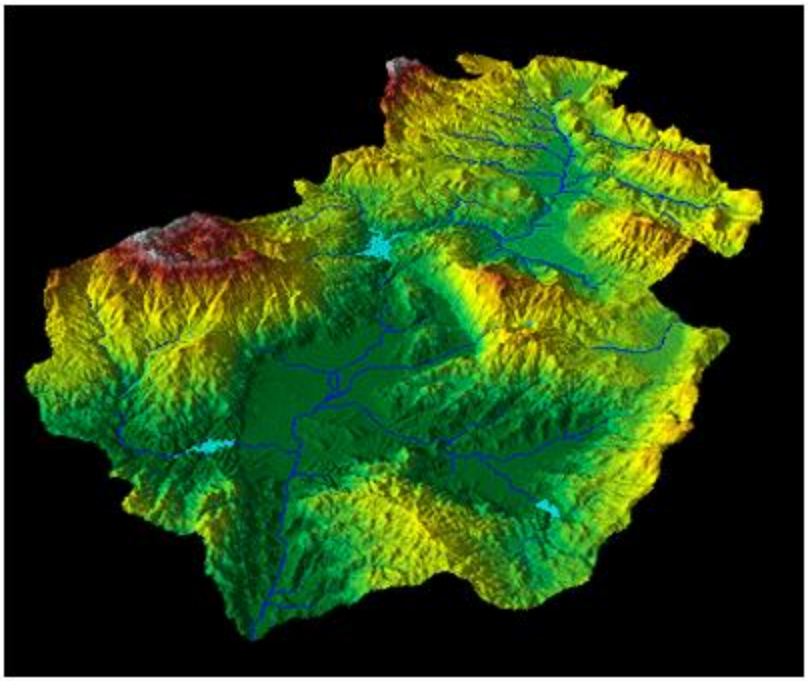

Figure 2.2 Example Digital Elevation Model (DEM) Raster Layer (*Exploring Digital Elevation Models—ArcMap | Documentation*, n.d.)

Although not foolproof, LiDAR developed DEMs will assess elevation of the bare-earth terrain while disregarding man-made structures and vegetation (Maune, 2007). The DEM is made up of square cells, spaced in a uniform pattern across the graphed domain (Maune, 2007). DEMs will differ based upon their 'resolution', which is the sizing of the two-dimensional cells which houses elevation data for that specific section. Each square cell of the DEM represents an interpolated elevation value of the bare-earth terrain gathered in the LiDAR assessment (M. Bilskie, 2012; Maune, 2007). High-resolution DEMs will have cell sizes as low as 1 square meter, with higher-resolution DEMs ranging as high as 25 square meters, although DEM resolution is constrained by the LiDAR data that is provided (Florinsky, 1998). The resolution size of a DEM has a major bearing on data size, and thus upon run-times in computer modeling scenarios. There can be errors however, with estimated RMS error in certain commonly used SRTM DEM being

calculated at 17.76 meters (Mukherjee et al., 2013). New LiDAR technology has improved upon this however, and newer localized DEMs have been found to have higher accuracy in their topographic assessments, especially with introduced filtering techniques to fix cells where structures or vegetation may be interfering with the LiDAR (M. Bilskie, 2012; Liu, 2008).

2.5.2 | VF and Thalweg Identification

VFs refer to physical geographic structures that have statistically significant heights and elevations above a surrounding reference area (M. V. Bilskie et al., 2015; Gao, 2021). In the context of coastal inundation, VFs play a crucial role in influencing the extent and impact of flooding during storm events. These features can include natural elements such as dunes, cliffs, and bluffs, as well as built structures like seawalls, levees, and highways (M. V. Bilskie et al., 2015; Gao, 2021) (Figure _).

VFs have a significant impact on coastal inundation due to their ability to alter the flow of water and act as barriers or conduits for storm surge. Their presence can influence the propagation of water inland and affect the magnitude and spatial distribution of flooding (Gallien et al., 2014; Gao, 2021). For instance, elevated natural features like dunes can act as buffers, absorbing and dissipating wave energy, thereby reducing the extent and intensity of flooding in areas behind them (M. V. Bilskie et al., 2015; Gallien et al., 2014; Gao, 2021). On the other hand, VFs can also channelize and concentrate water, potentially leading to localized flooding in certain areas (Hu et al., 2022).

The precise impact of VFs on coastal inundation depends on various factors, including their height, shape, orientation, and the characteristics of the storm event. Tall VFs can create shadowing effects, causing areas behind them to be relatively protected from storm surge, while low-lying features may offer minimal protection (Tognin et al., 2021) . Additionally, the interaction between VFs and coastal topography plays a role in amplifying or attenuating floodwaters, resulting in complex patterns of inundation (Gao, 2021; Hu et al., 2022; Tognin et al., 2021).

High-resolution elevation data, such as DEMs from LIDAR, can help capture the detailed topographic features that affect flood patterns (M. V. Bilskie et al., 2015; Gao, 2021). There have been numerous studies that have developed ways of extracting VFs out of topographic maps such as DEMs, where VFs were computerized into lines made up of coordinates (Coggin, 2008; Gao, 2021). Further studies then found methods to use the extracted VFs and then turn them into fixed polylines, where a mesh could have node points along the VFs (M. V. Bilskie et al., 2015). Holding the fort.14 nodes along VFs allows for models such as ADCIRC to not linearly interpolate over the VFs, and rather ensure that the highest elevation points are depicted, and then model inundation around those points (M. V. Bilskie et al., 2015; Gao, 2021).

The study by Gao (2021) utilized methods previously developed by Coggin (2008) and Bilskie (2015) to automate the process through python functions in her code, *PyVF* (Gao, 2021) (Figure 2.3). Gao's code implemented *ArcMap* functions using the toolbox, *TauDEM* to delineate a watershed using an input DEM, as first used by Coggin (Coggin, 2008; Gao, 2021). Then, once the watershed had been constructed, Gao's code then extracted VFs from the surrounding topographic environment through a series of ArcMap functions that turned the features into polylines, as first done by Bilskie (M. V. Bilskie et al., 2015; Gao, 2021). The code was then able transform the polyline into a shapefile that could be utilized in mesh development. Incorporating these features into numerical models allows for more realistic simulations and better predictions of flood risk, helping communities and decision-makers to plan and implement effective coastal management strategies (M. V. Bilskie et al., 2015; Gallien et al., 2014; Gao, 2021).

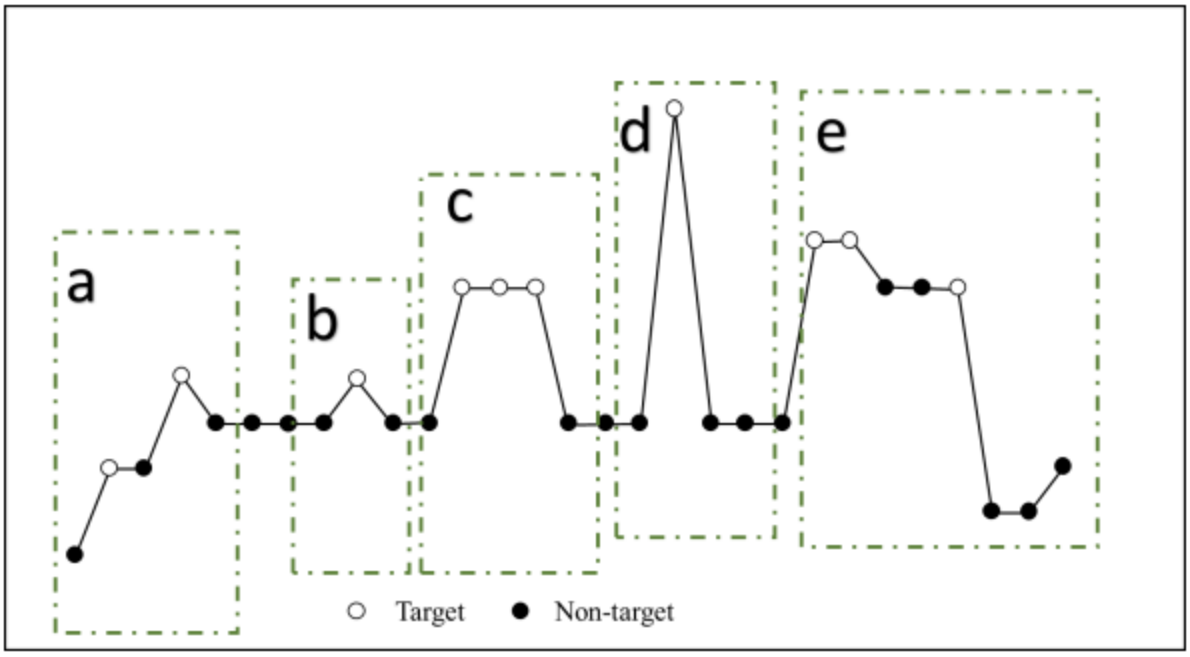

Figure 2.3 Example of VFs on a horizontal terrain profile chosen using PyVF (Gao, 2021)

Similarly to that of VFs, how channels are mapped can affect precision of storm surge modeling (M. V. Bilskie, Hagen, et al., 2012). Thalwegs are critical features in hydrology and coastal engineering, representing the deepest path of a river or channel. They follow sinuous courses along the channel bottom, reflecting the line of maximum flow velocity (Westerink et al., 2008). In the context of storm surge modeling, the resolution of the computational mesh along the thalweg plays a crucial role in accurately simulating and predicting flood events.

Higher mesh resolution specifically along the thalweg can greatly improve storm surge modeling (M. V. Bilskie, Hagen, et al., 2012). By using smaller mesh elements, a more detailed representation of flow characteristics within the channel can be achieved once ran in ADCIRC.

This enhanced resolution allows for a more accurate depiction of flow dynamics, capturing the intricate patterns and interactions that occur during coastal inundation events.

The improved mesh resolution enables a more precise estimation of water levels, flow velocities, and the interaction between the thalweg and adjacent areas (M. V. Bilskie, Hagen, et al., 2012). It helps to capture flow acceleration, deceleration, and direction changes, ensuring a more realistic simulation of storm surge dynamics. Furthermore, the resolution facilitates the modeling of channel constrictions and the effects of flow restrictions, such as bridges or culverts, on flow behavior. These factors contribute to a better understanding of flow dynamics and water movement within the channel (M. V. Bilskie, Hagen, et al., 2012; Roberts et al., 2019). Thalwegs, similar to that of VFs, can be derived using *TauDEM* tools in ArcMap (Tarboton, 2005).

Automated mesh generation technology developed by Roberts (2019) included methods by which a user can input thalwegs in the form of polylines and VFs in the form of fixed coordinates, which elements will generate around (Heinzer et al., 2012; Roberts et al., 2019). The improved mesh resolution around these features will allow for improved risk mitigation from improved real-time storm surge modeling.

VFs can also be optimized in mesh development through the use of a *size function*. In the context of an ADCIRC mesh, a size function refers to a mathematical function that determines the grid spacing or resolution within the mesh. It is used to control the spatial distribution of mesh elements and refine the grid in areas of interest (Groom et al., 2018).

The size function assigns different cell sizes or element lengths to different parts of the computational domain based on predefined criteria. These criteria can include factors such as the proximity to the coastline, the presence of complex coastal features, or specific regions of interest within the domain.

The size function is typically designed to ensure that the grid resolution is higher in areas where more accurate representation is needed. For example, near the coastline, where detailed modeling of wave propagation, sediment transport, or inundation is crucial, the size function would prescribe smaller grid elements. In contrast, in offshore areas or regions with relatively uniform bathymetry, larger grid elements may be assigned to reduce computational costs.

The specific form of the size function can vary depending on the requirements of the modeling study and the desired resolution. Common approaches include linear or polynomial functions, step functions, or adaptive techniques that refine the mesh based on predefined criteria.

By utilizing size functions in ADCIRC mesh generation, researchers and modelers can optimize the grid resolution and allocate computational resources efficiently (Gao, 2021; Groom et al., 2018). This allows for more accurate and efficient simulations of storm surge events, coastal processes, and other hydrodynamic phenomena, improving the reliability of model predictions and aiding in coastal planning and hazard assessment.

3.0 | METHODOLOGY

3.1 | Model Overview

The process detailed in this report automatically generates an ADCIRC-compatible *fort.14* finite element unstructured two-dimensional mesh with using the OM2D mesh generation software (Roberts et al., 2019). OM2D uses a series of MATLAB scripts to achieve Delaunay triangulation across a user-specified meshing domain, and allows the user to specify certain meshing constraints, such as resolution and floodplains (Roberts et al., 2019). The mesh focuses on highest resolution over coastal Georgia, while also holding high resolution across the South Atlantic Bight, and merges the remainder of the western North Atlantic basin with the existing *53K* mesh developed by S.C. Hagen, shown in Figure 3.1 (Hagen et al., 2006).

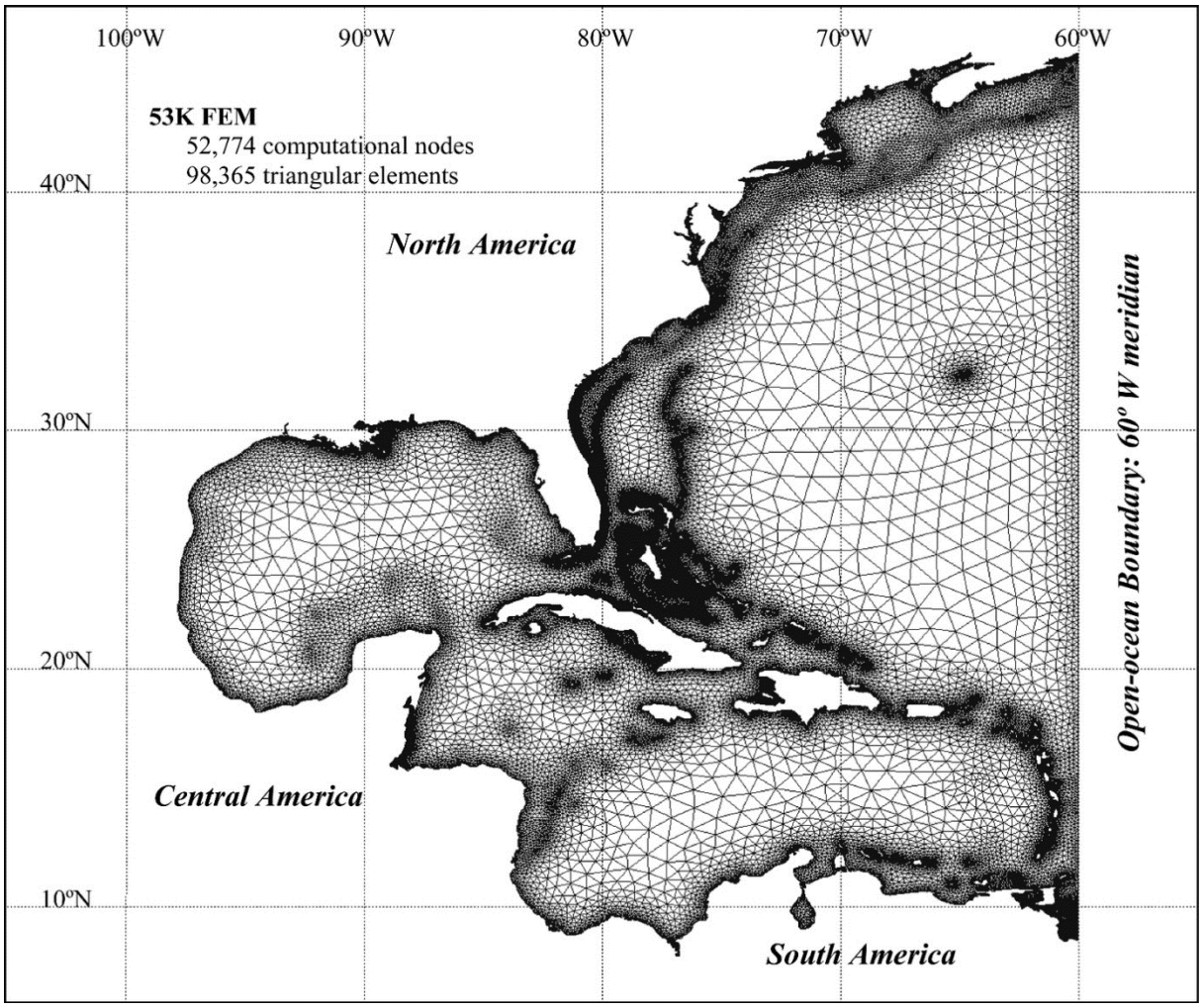

Figure 3.1 The 53K Unstructured Mesh, focused on large domain modeling for the North Atlantic Hurricane Basin (Hagen et al., 2006)

The 53*K* however does not include overland areas within its meshing domain, whereas coastal Georgia and the South Atlantic Bight include overland floodplain meshes as well (Hagen et al., 2006).

The mesh developed for this report aimed to develop a mesh that incorporated several different geographic factors into the mesh generation in order to achieve an ADCIRC-compatible mesh that could be used for both synthetic storm modeling as well as real-time storm surge prediction during a tropical storm landfalling scenario. The incorporated geographic features aimed to improve upon existing meshes developed for real-time storm surge scenarios such as that of the South Atlantic Coastal Study mesh developed by the U.S. Army Corps of Engineers (Roberts et al., 2019; *South Atlantic Coastal Study (SACS)*, 2021).

One of the most significant geographic datum inputs is that of the coastline shapefile, as through a variety of user set parameters, triangulation occurs based on the coastline. Additionally, the user can set higher levels of element resolution along the coastline (Roberts et al., 2019). In this model, the mesh will have high resolution surrounding the coastline's wet/dry boundaries, while also holding mesh node points along the coastline using a size function.

The unique geographic datasets included in the model that had not been used in previous automatically generated meshes include that of both a high-resolution Digital Elevation Model (DEM) and a coastline polygon, representing the wet/dry boundary, as well as significant high and low points along the topography and bathymetry in the forms of VFs and thalwegs (Roberts et al., 2019). The DEM incorporated into the mesh generation was developed via LiDAR collection as a part of the Coastal National Elevation Database (CoNED) Applications Project, and features a 1 square meter resolution, meaning that elevation in coastal Georgia is represented across each square meter (*Coastal National Elevation Database (CoNED) Applications Project | U.S. Geological Survey*, n.d.). OM2D develops elements based on both the *DEM* and the coastline through user set parameters, allowing for node placement based on elevation grade and increased resolution surrounding the wet/dry coastline boundary (Roberts et al., 2019).

The CoNED DEM that was used does not just include elevation values in the water, but also on overland. This allowed for a meshing domain that is both underwater and overland. Having DEM values overland allowed for the collection of geographic significant points such as that of VFs and thalwegs. Similar to how meshing is performed in wet regions, OM2D allows the user to set mesh optimization parameters overland such as minimum resolution and grading, as well as channel resolutions (Roberts et al., 2019).

VFs are the statistically significant elevated points within a certain diameter of the surrounding environment, such as dunes, levees, and highways (M. V. Bilskie et al., 2015; Gao, 2021). Each of the features have been used before in a mesh generation, but not yet before within automated mesh generation software such as OM2D (M. V. Bilskie et al., 2015; M. V. Bilskie, Hagen, et al., 2012). The incorporation of VFs within the mesh involved the holding of nodal points of the mesh along the VFs. Through holding the nodes along the VFs, linear topographic and bathymetric interpolation would not parse over heightened geographic elements that would affect how coastal inundation would be modeled, and rather would include the elevation values of the VFs within the mesh (M. V. Bilskie et al., 2015; Gao, 2021).

The model also includes the incorporation of thalwegs, which are the low points along rivers, creeks, and other channels. Thalwegs represent the point of lowest flow within a channel, rather than just the center of the channel. Through incorporating thalwegs into the mesh generation, there will be higher mesh resolution surrounding the thalwegs, in order to allow ADCIRC to better model how floodwaters will propagate up channels during storm surge scenarios (M. V. Bilskie, Hagen, et al., 2012).

3.2 | Digital Elevation Model (DEM) and Coastline

Prior to beginning an automatically generated unstructured ADCIRC mesh, certain geographic data sets must first be acquired: the coastline polygon and the digital elevation model (DEM) (Roberts et al., 2019). The mesh generation in this model incorporated a DEM sourced from the Coastal National Elevation Database (CoNED) Applications Project, which utilized LiDAR collection techniques (*Coastal National Elevation Database (CoNED) Applications Project | U.S. Geological Survey*, n.d.). The CoNED Georgia DEM encompasses both underwater and overland regions, which is pertinent for a mesh that will be modeling overland flood inundation in a storm surge scenario (Figure 3.2) (*Coastal National Elevation Database (CoNED) Applications Project | U.S. Geological Survey*, n.d.). The DEM captures elevation information for coastal Georgia at a resolution of 1 square meter, ensuring precise representation of elevation across each square meter, which results in a very specific computerized visualization of topographic and bathymetric data, as can be seen in Figure 3.3 (*Coastal National Elevation Database (CoNED) Applications Project | U.S. Geological Survey, n.d*.).

The CoNED Georgia DEM was chosen because of its very fine resolution and due to the DEM's compiling having been completed in 2022, one year prior to this model's development (*Coastal National Elevation Database (CoNED) Applications Project | U.S. Geological Survey*, n.d.). Utilizing this DEM, certain geographic features were able to be extracted to optimize the mesh for a more accurate ADCIRC modeling scenario (M. V. Bilskie et al., 2015).

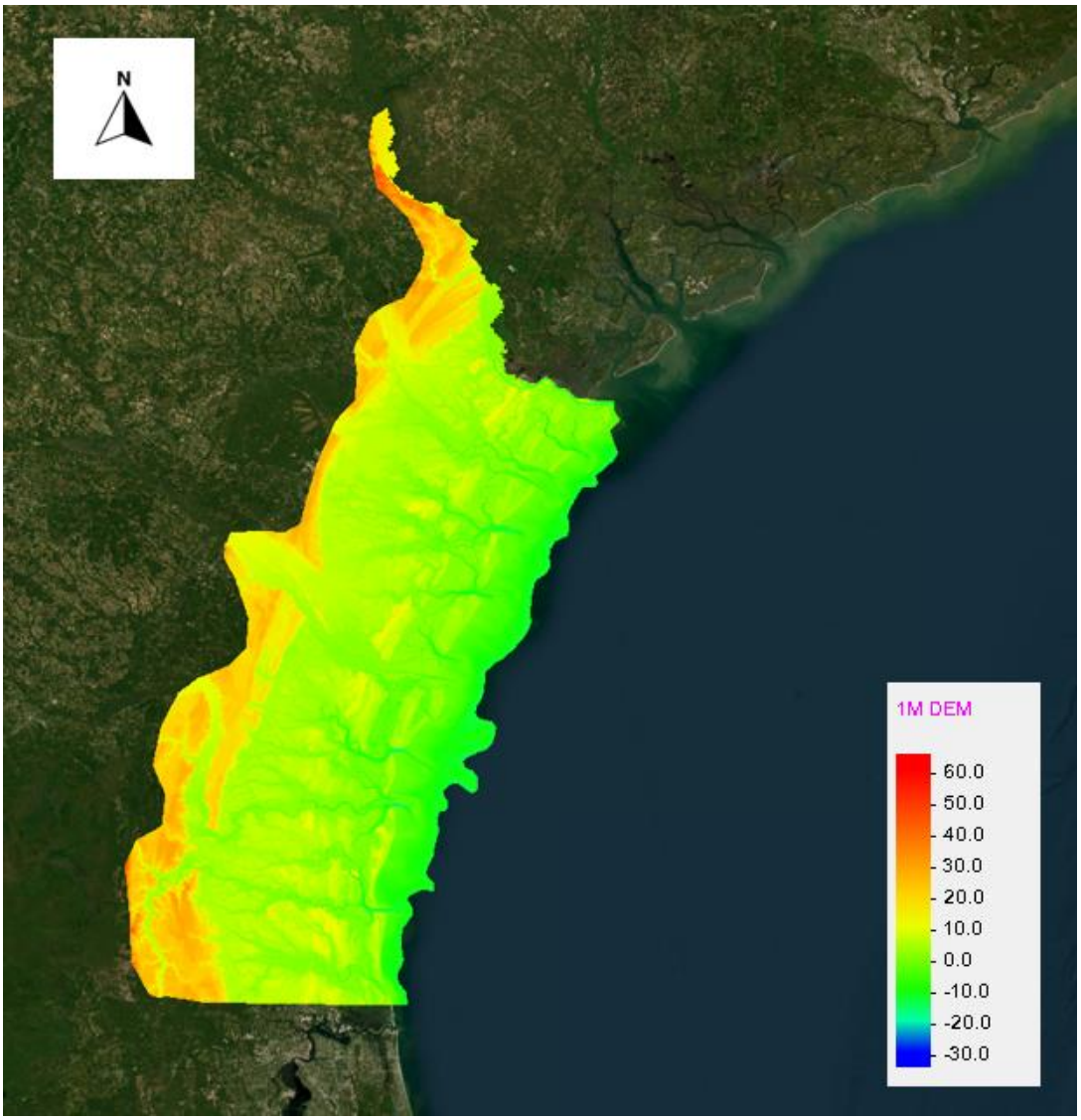

Figure 3.2 1-meter CoNED Georgia DEM visualized over the SAB

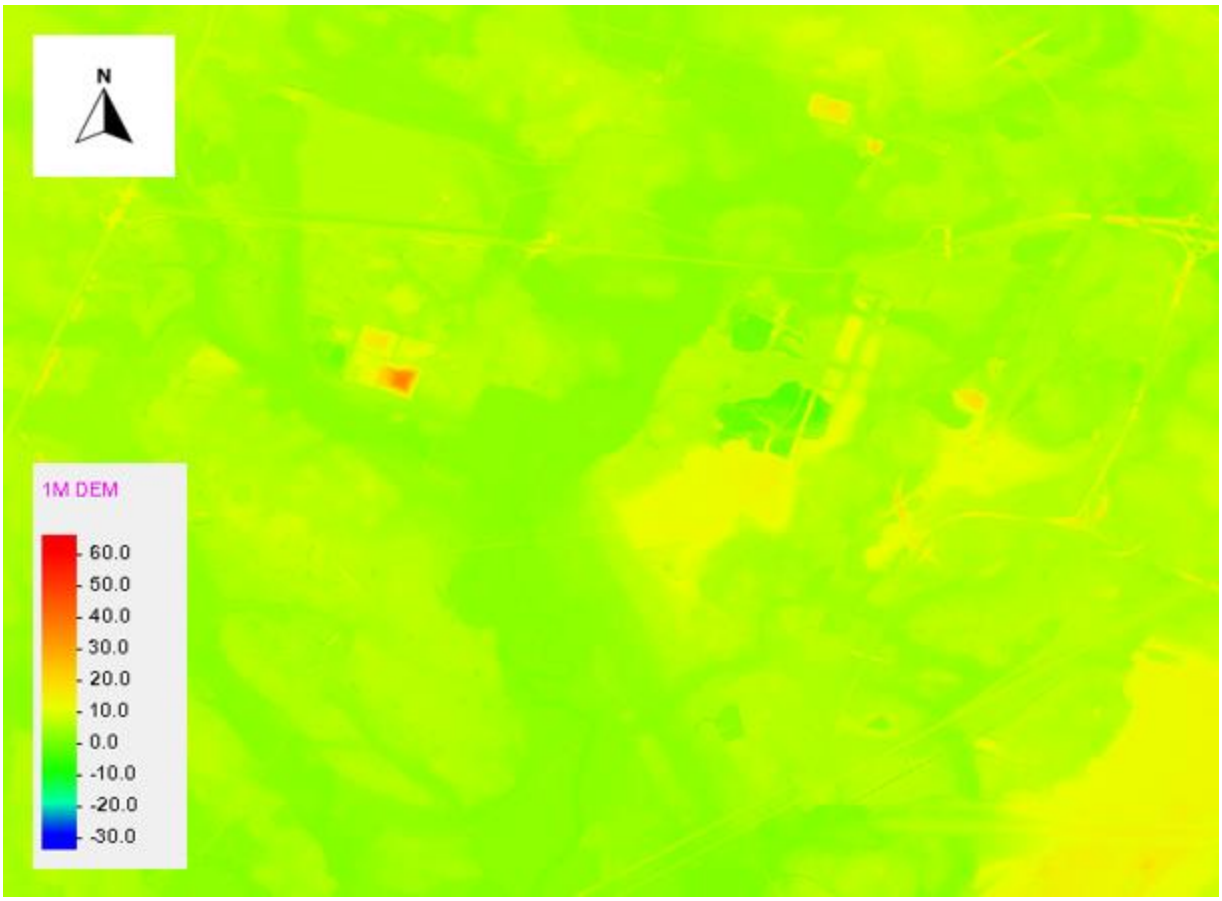

Figure 3.3 1-meter CoNED Georgia DEM, zoomed in on industrial area of Georgia

The CoNED Georgia DEM however was not used for the topographic interpolation. The particular software used for the bathymetric interpolation conserves the most computational cost when the DEM used is split into tiles. The DEM utilized in the topographic interpolation is the 2019 LiDAR data collected for UGA. There are hundreds of tiles, rather than one large DEM, which helps with computational cost and for the software to run efficiently. The difference between the DEMs for the purpose of triangulation and geographic data extrapolation is negligible. The process of the interpolation will be discussed in Chapter 3.6. The CoNED DEM was utilized for the underwater bathymetric interpolation.

Beyond the Georgia DEM, supplemental DEMs were used for topography and bathymetric interpolation for the surrounding regions in Florida, South Carolina, and North Carolina, as well as the outer ocean. The Continuously Updated Digital Elevation Model (CUDEM), similar to the CoNED, is made up of newly updates DEMs across the US, which are continuously updated as new data is developed (*Continuously Updated Digital Elevation Model (CUDEM) - 1/3 Arc-Second Resolution Bathymetric-Topographic Tiles*, n.d.). Comparatively to the CoNED Georgia DEM which have a 1-meter resolution, the CUDEM DEMs used have a 3-meter resolution. The mesh model being developed is only looking at Georgia, and therefore did not include thalwegs or VFs for regions outside of Georgia. It was important however to still mesh the outer regions so that any water forcing as a result of geography in other features that could affect flood heights in Georgia was resolved.

As for the open ocean, the 53K file was reutilized, and along with it the same bathymetric values used in the 53K, which focuses on a large domain underwater mesh with increased resolution along important aspects such as the coast and the shelves (Hagen et al., 2006). This

developed DEM however was not used for the triangulation, as all regions within the mesh domain beyond the Georgia DEM used the commonly used SRTM15+ DEM.

The coastline serves as a critical geographical data input in this study (Roberts et al., 2019). Delaunay triangulation for the mesh is performed based on the coastline, thus it was important to select a coastline that represented the wet/dry boundary in Georgia precisely (Roberts et al., 2019). In order to develop a mesh in OM2D, the coastline must be in shapefile format, and must be an enclosed polygon, as visualized in Figure 3.4 (Roberts et al., 2019). The coastline utilized in the model was developed as a part of the South Atlantic Coastal Study (SACS) by the U.S. Army Corps of Engineers, and illustrated the coastline in a comprehensive manner, with small creeks and marsh channels being resolved, as can be seen in Figure 3.5 (*South Atlantic Coastal Study (SACS)*, 2021).

Figure 3.4 South Atlantic Bight coastline shapefile,

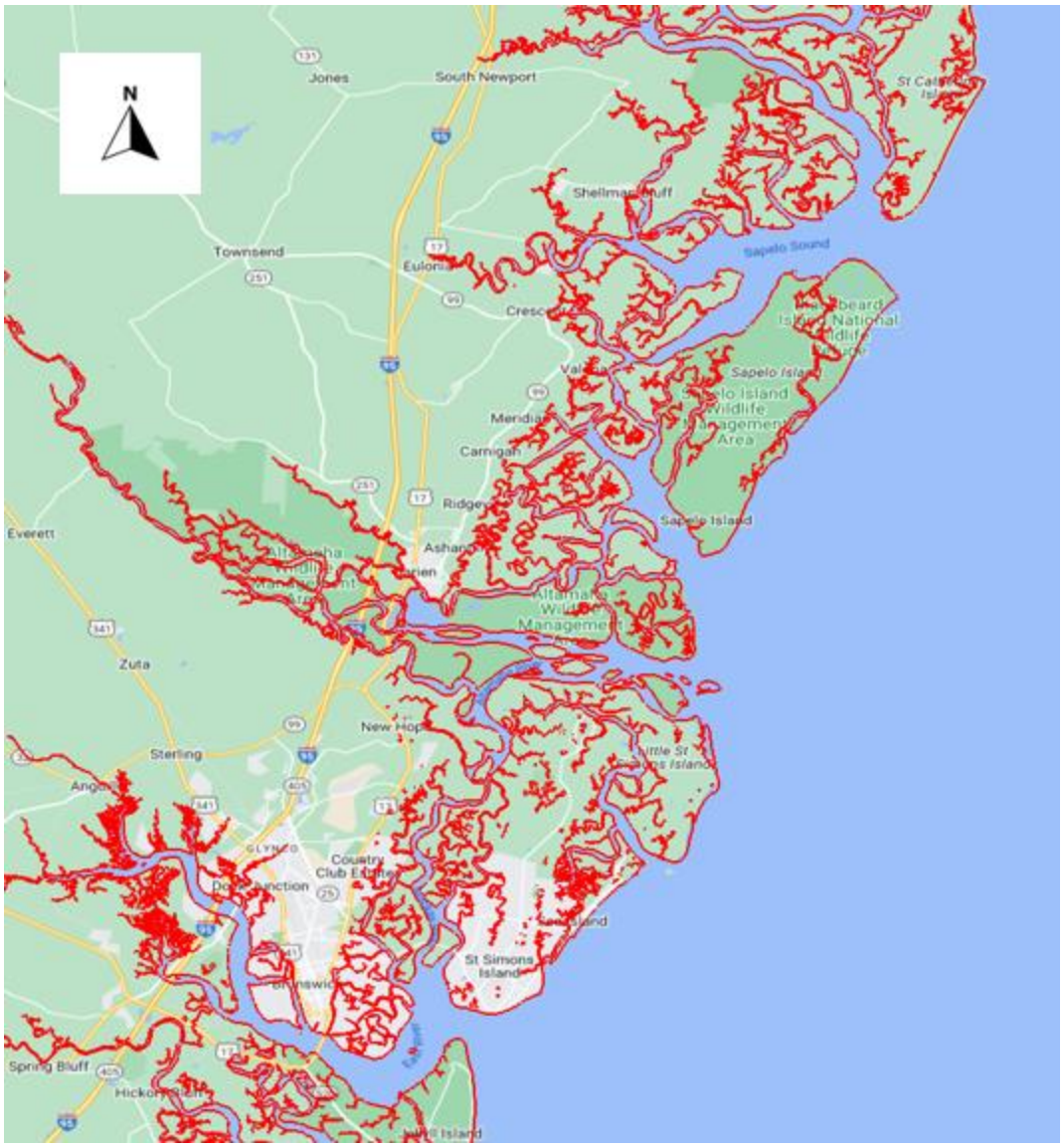

Figure 3.5 South Atlantic Bight coastline shapefile, zoomed in on central coastal Georgia

In order to develop a mesh that encompasses a floodplain however, the model must also include an inner coastline boundary, indicating the extent of the that the user wishes to resolve the floodplain. In this model, the line used was from the Coastal Relief Model, which comes as a part of the OM2D example documentation, as is visualize in Figure 3.6 (Roberts et al., 2019). Similar to the wet/dry coastline, the floodplain line also must be an enclosed polyline in the form of a shapefile. The Coastal Relief Model's polyline indicates a 10-meter averaged elevation line for all of the U.S., meaning that the floodplains are meshed up to an average of a 10-meter elevation. The highest storm surge recorded in U.S. history was during Hurricane Katrina, at just under 28 feet, which is still below a 10 meter elevation line that was used in this model (*Historic Storm Surge Records | Coastal Processes, Hazards, and Society*, n.d.).

Figure 3.6 10-meter SACS coastline shapefile overlaying the SAB

3.3 | Thalweg Extraction (TauDEM) and Python Process

OM2D allows for the user input of certain geographical parameters that affect how the mesh triangulation occurs (Roberts et al., 2019). In this model, one of the inputs is that of *thalwegs*. Thalwegs are the line that follows the lowest points of channels, rivers, or creeks, as shown in Figure 3.7 (M. V. Bilskie, Hagen, et al., 2012; Roberts et al., 2019). OM2D uses a *size function* to determine how the mesh is triangulated in respect to the thalwegs that are input by the user in the form of a shapefile polylines, which will be covered in this report in chapter 3.5.3 (Roberts et al., 2019).

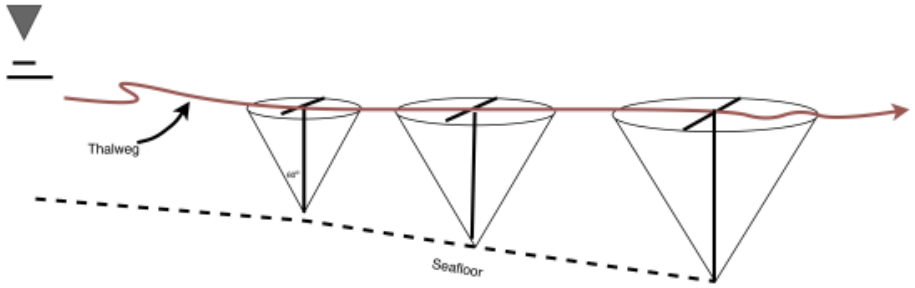

Figure 3.7 Thalweg polyline 3-dimensional description (Roberts et al., 2019)

In this model, thalwegs were delineated using a series of functions in the *TauDEM* toolbox within *ArcMap*. The tools within TauDEM allows a user to input a DEM in the form of a *geotiff*, and then to extract out a watershed from the DEM (Tarboton, 2005). Within several tools in TauDEM, a watershed is delineated from a DEM by parsing over the DEM looking for the low points and the high points across the datum, as shown in Table 3.1.

Step	Description
Pit Remove	Removal of pits or depressions in the terrain
D8 Flow Direction	Calculation of flow direction based on the D8 algorithm
D8 Contributing Area	Calculation of contributing area for each cell
Stream Definition by Threshold	Identification of streams based on a defined threshold
Stream Reach and Watershed	Determination of stream reach and watershed boundaries
Watershed Grid to Shapefile	Changing grid to a polyline shapefile with watershed in it

Table 3.1 TauDEM Tool Steps to creating a Watershed (Gao, 2021; Tarboton, 2005)

In step 4 in Table 3.1, streams are identified by using a defined threshold. The model uses a threshold of 100,000 in its thalweg determination. A threshold value of 100,000 in the context of stream definition by threshold means that only cells with a flow accumulation value equal to or above 100,000 will be considered as part of the stream network.

Flow accumulation represents the accumulated flow from upstream cells in a digital elevation model (DEM). Higher flow accumulation values indicate areas with a larger number of contributing cells and are often associated with larger rivers or streams. By setting a threshold of 100,000, the amount of streams delineated is limited, helping to maintain a lower computational cost (Tarboton, 2005). Cells with flow accumulation values equal to or above 100,000 will be considered as stream cells, while cells with lower flow accumulation values will be excluded from the identified stream network (Tarboton, 2005). The choosing of 100,000 as the flow accumulation threshold was due to data limits within ArcMap. Due to the large extent of the DEM, a threshold of 100,000 allowed for the most optimized stream network in a computer model.

TauDEM outputs the identified streams in the form of a single polyline. These streams are effectively thalwegs, as they are not identifying the borders of streams with the dry land boundary, but rather they indicate the lowest points within a watershed. For improved compilation efficiency, only the thalwegs that had channels that were within the underwater boundary defined by the wet/dry coastline boundary were used, as can be seen in Figure 3.8. Then, using a series of *arcpy* functions in python, the single polyline was looped through and separated into individual streams with coordinate points, so that it could be read into OM2D (Roberts et al., 2019).

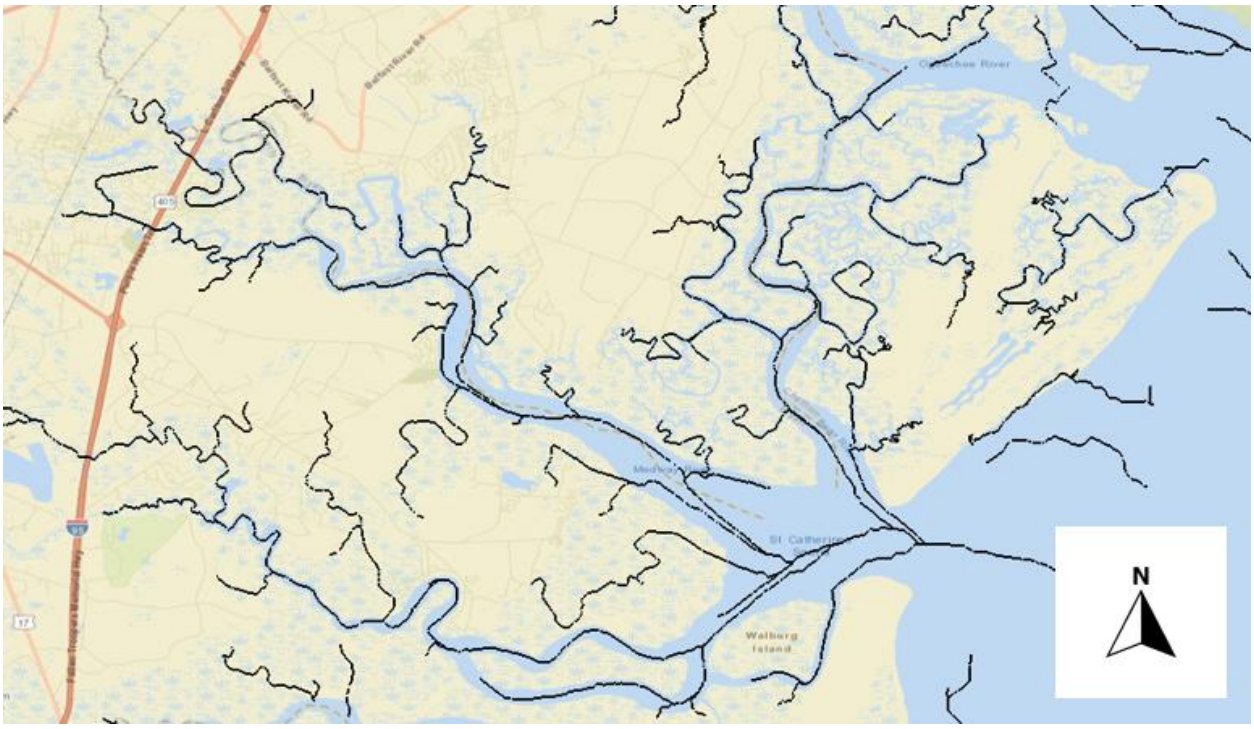

Figure 3.8 Delineated thalweg lines in coastal Georgia

It is important to note however that the GIS functions used to extract the thalwegs are not foolproof. There are certain areas where thalwegs were determined by GIS to be channels when they were in fact not. In order to avoid these, only underwater thalwegs were included. Additionally, certain thalwegs may not have been identified due to their proportional angles. This

was particularly notable in larger channels, where the angle at which the elevation decreased from the bank to the bottom of the channel was smaller. For example, if a channel is more U shaped than V shaped, thalwegs were not extracted, as can be seen in the upper right corner of Figure 3.8.

3.4 | Vertical Feature Extraction (PyVF)

The model utilized a python software for its VF delineation and extraction so that they could be used in the mesh generation. The particular software used is called “PyVF”. PyVF is a Python program developed by Shu Gao that focuses on extracting VFs from LiDAR-DEMs. The program provides functionality for analyzing LiDAR data and identifying VFs such as cliffs, dunes, and ridges. VFs are defined as the significant elevated points within a certain diameter of a surrounding environment, representing features such as dunes, levees, and highways.

By utilizing LiDAR-DEM data from the CoNED 1m Georgia DEM, visualized in Figure 3.9, highly accurate elevation information is provided to PyVF. This enables the extraction of valuable VF information for various applications in geosciences and terrain analysis (*Coastal National Elevation Database (CoNED) Applications Project | U.S. Geological Survey*, n.d.; Gao, 2021).

The program employs advanced algorithms and techniques to detect and delineate the VFs within the LiDAR-DEM dataset. It considers the elevation variations and gradient changes to identify prominent vertical structures present in the terrain. Additionally, PyVF offers options for setting specific thresholds and parameters to customize the extraction process based on the characteristics of the LiDAR-DEM data and the desired features to be extracted (Gao, 2021). For this model, a *dh* value of 1.5 meters was set with a radius, *r*, of 3 meters. These values indicate any DEM grids that protruded 1.5 meters above a surrounding cell with a radius of 3 meters. PyVF then will output *Potential Vertical Features* (PVF) as a shapefile (Gao, 2021).

These VFs were then cleaned using a series of post-processing functions by researchers at Louisiana State University (LSU). The post-processing functions included a size function, where the mesh developed without the VFs was measured for grid spacing across the mesh. This grid

spacing was then utilized to determine if a VF polyline expanded the distance of at least 2 nodes. There were several other processes run, including ones that deleted any VFs that water still would run through, in instances where weirs or bridges may have been misconstrued by LiDAR (Figure 3.10). The functions however that were used are undisclosed due to proprietary concerns with LSU. The total process is illustrated in Figure 3.11 (Gao, 2021).

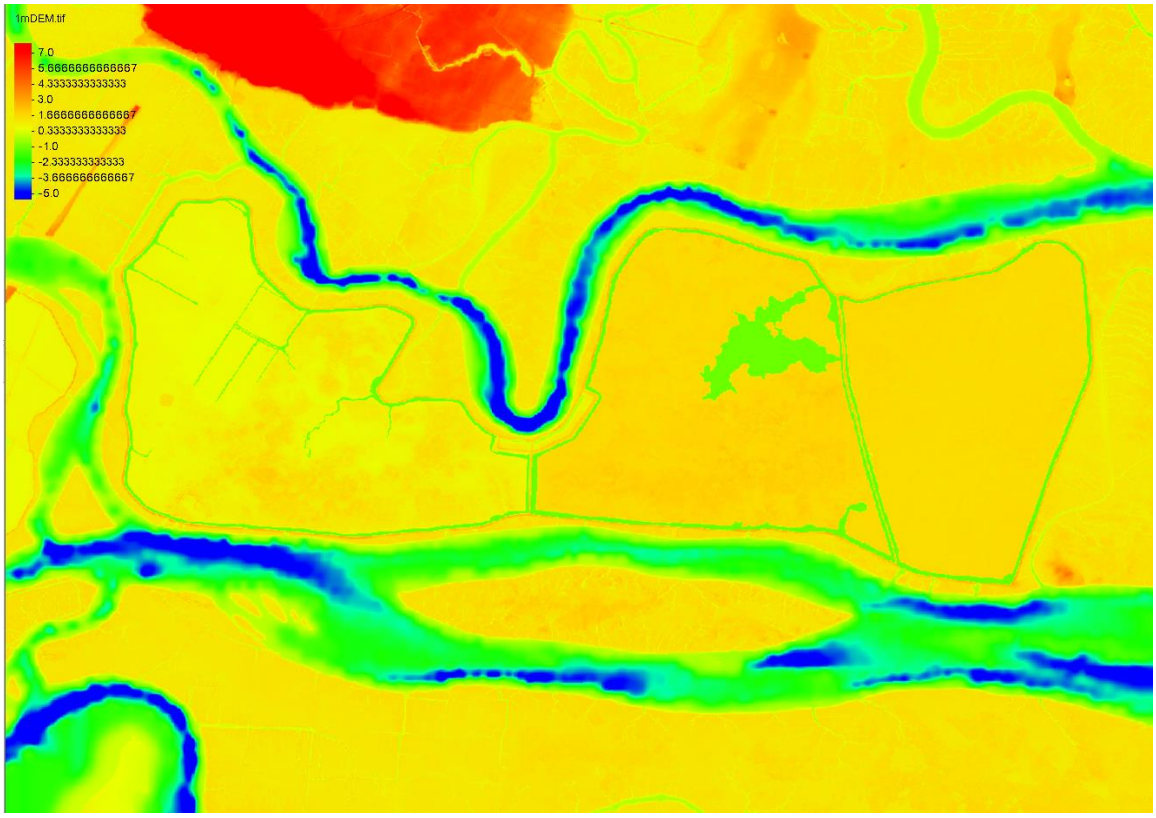

Figure 3.9 CoNED 1m DEM without illustrated VFs

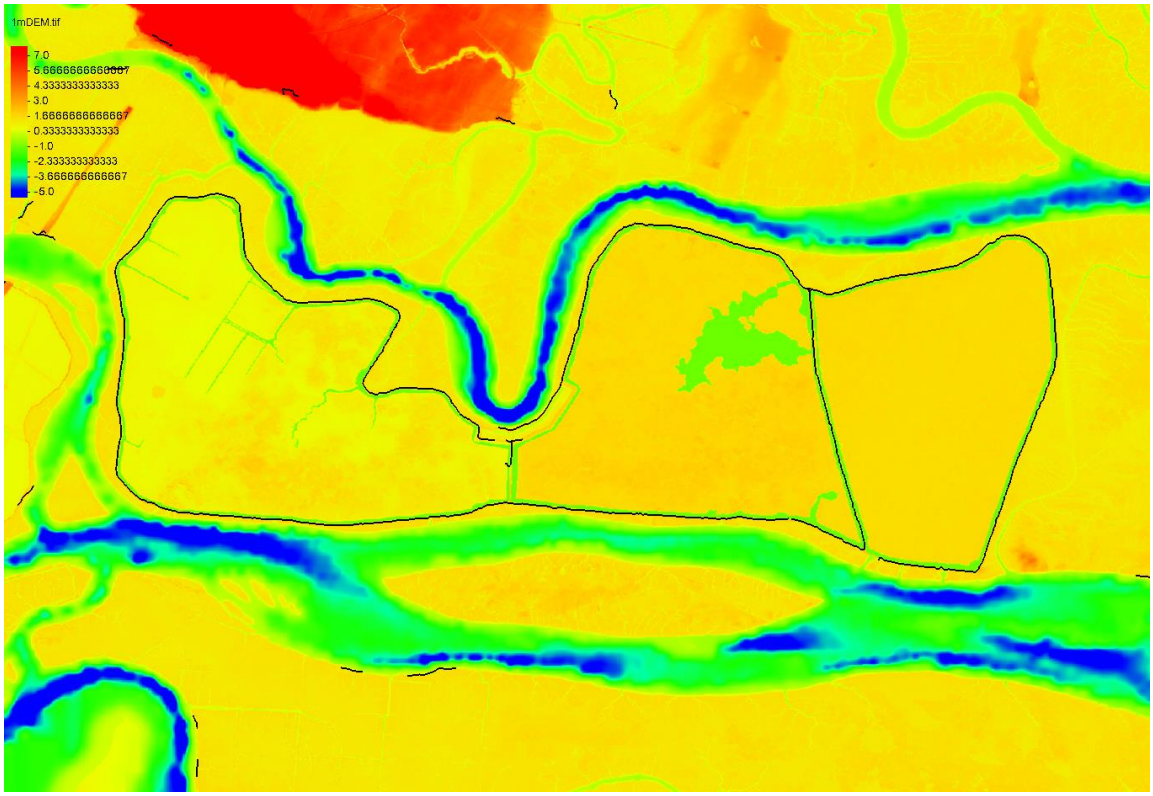

Figure 3.10 CoNED 1m DEM with VF polylines after post-processing

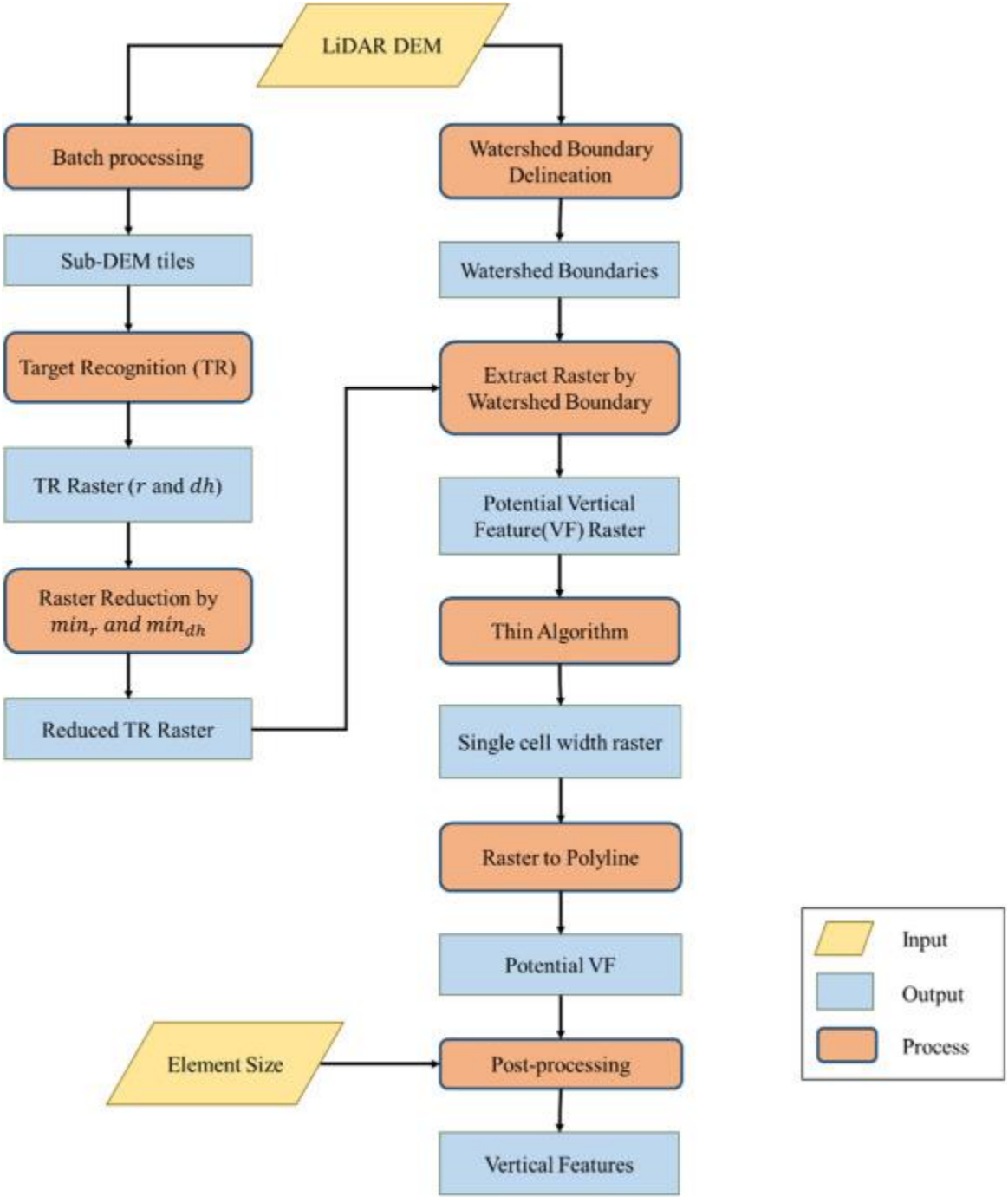

Figure 3.11 PyVF Flowchart (Gao, 2021)

Once the post-processing was completed by LSU, the VFs were then optimized further for the final mesh creation. Utilizing the same python loop as that of the thalweg delineation, the VFs that were output as a single polyline shapefile were split into individual segments, and then utilizing the same size function sent to LSU, the VF polylines were then turned into a scatter of coordinate points based on the grid spacing, as visualized in Figure 3.12.

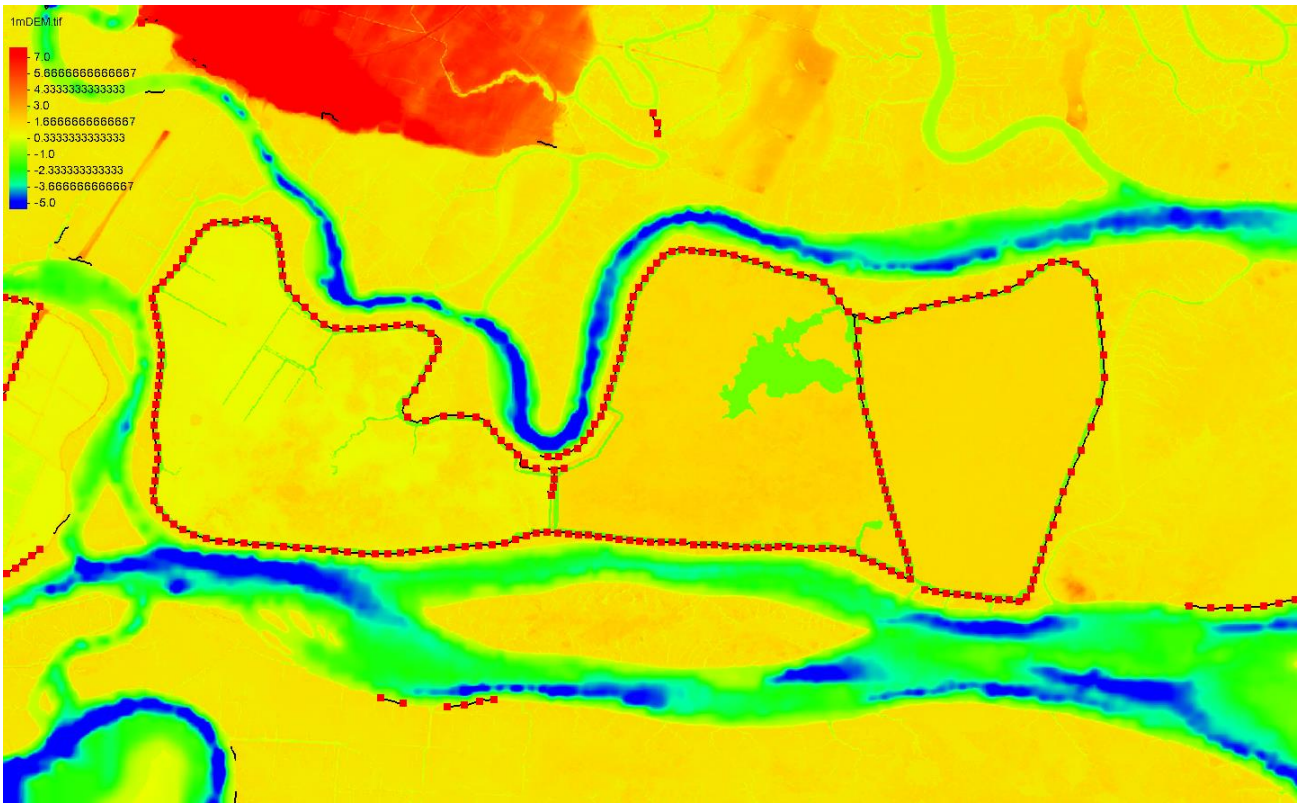

Figure 3.12 VFs as coordinates after size function

These VF coordinates were then able to be utilized in OM2D as fixed nodal coordinates, which will be explained further in Chapter 3.5.

3.5 | OceanMesh2D

This study utilizes OM2D for its mesh generation. OM2D is a user-friendly software tool specifically designed for coastal and oceanographic modeling, focusing on automatically generating high-quality two-dimensional unstructured meshes. Developed by researchers Keith Roberts and William Pringle, its advanced algorithms, including Delaunay triangulation, ensure accurate representation of coastal features such as shorelines, islands, and estuaries within a mesh (Roberts et al., 2019).

This software supports adaptive mesh refinement, allowing users to refine the resolution in areas of interest and maintain computational efficiency. It handles both small and large-scale coastal domains effectively, making it suitable for regional and global-scale modeling applications, combining them in what is known as a *multiscale* mesh generation (Roberts et al., 2019). The multiscale method allows a user to develop a large-domain, lower resolution mesh with user-specified areas within the mesh having higher resolution. This is helpful from a computational cost perspective as it allows for more efficient modeling, due to having larger element sizes in areas that aren't as pertinent to the mesh (M. V. Bilskie et al., 2020).

The multiscale method was implemented in the mesh developed as a part of this study, in order to develop a mesh with highest resolution in coastal Georgia with resolution then tapering off throughout the surrounding regions in Florida, South Carolina, and North Carolina. will be expanded on further in the chapter. OM2D accepts diverse input data formats like topographic data and coastline information, facilitating seamless integration with other modeling tools (Roberts et al., 2019).

OM2D offers comprehensive features including data preprocessing, intuitive visualization of the generated mesh, and export capabilities to popular numerical modeling software, such as

ADCIRC (Roberts et al., 2019; Westerink et al., 2008). The mesh generated as a part of this model were developed using OM2D due to its much faster efficiency and lower computational cost, comparatively to other mesh generation techniques used prior.

The mesh developed as a part of this study specifically focused on optimizing many of the optional inputs built into OM2D. How those parameters and geographical data affect the mesh will be expanded upon further in this chapter.

OM2D follows an order of operations that can be visualized in Table 3.2 (Roberts et al., 2019). However, it is important to note that this order of operations is generalized, and an order of operations changes based on what the user wishes to achieve with the mesh.

Order of Operations	Description
1. Domain Definition	Define the computational domain for the oceanographic or atmospheric simulation, specifying geographical boundaries, coastlines, islands, and other relevant features. This domain is known as the ***boubox,*** or ***BBOX***, and is user specified.
2. Bathymetry and Topography	Incorporate bathymetry data (ocean floor depth) and topography data (land surface elevation) to accurately represent the domain's geometry, in the form of user input ***DEM***.
3. Mesh Initialization	Initialize an unstructured initial mesh over the domain, covering the entire domain or subdividing it into smaller regions.
4. Mesh Adaptation and Refinement	Apply mesh adaptation and refinement techniques to improve mesh quality and resolution in specific regions of interest, such as coastlines or boundary layers.
5. Smoothing and Optimization	Perform operations to smooth and optimize the mesh, eliminating irregularities, removing distortions, and enhancing computational efficiency, using Delaunay triangulation to achieve best triangulation, avoiding thin triangles.
6. Boundary Condition Specification	Define appropriate boundary conditions for the simulation, including boundary types (ocean, land, island, etc.).

Table 3.2 OM2D Order of Operations

3.5.1 | Mesh Optimization Parameters and Governing Equations of OM2D

As mentioned in previous chapters, one of the biggest benefits to using OM2D is the software's ease of mesh optimization. The code workflow is visualized in Figure 3.13 (Roberts et al., 2019). Within the *geodata* object, geographic data and the mesh optimization parameters are stored. This is where geographic feature objects such as the coastline, DEM, and the meshing domain are held (Roberts et al., 2019). The model created in this study uses an array of parameters that control how the input geographic data stored in the *geodata* object is interpreted by OM2D. To be able to create the best possible mesh for accurate storm surge modeling while trying to total data to conserve computation cost involved the use of different parameters in different regions of the mesh.

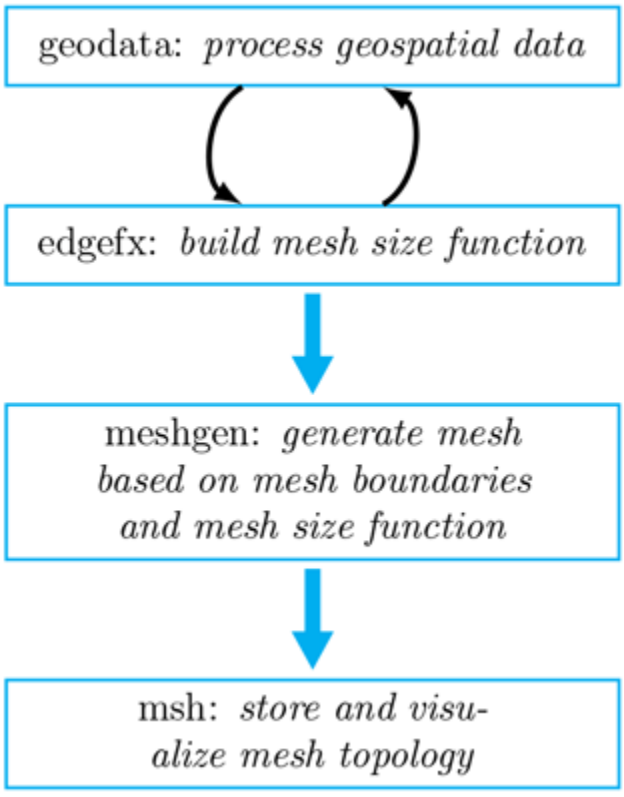

Figure 3.13 OM2D Code Workflow (Roberts et al., 2019)

The model was able to achieve both a finite mesh while maintaining a lower level of computation cost through the use of the *multiscale* technique, where coastal Georgia used a lower minimum resolution than the surrounding regions and open ocean. The multiscale technique creates two meshes while developing, a "*parent mesh*" and a "*child mesh*". This thesis aimed to create a child mesh whose domain ranged just over coastal Georgia and its nearshore underwater regions. The parent mesh in this model's scenario is the open ocean of the North Atlantic and the surrounding states. Additionally, OM2D allows the user to set different resolution parameters for both overland and underwater regions (Roberts et al., 2019).

The parameter *min_el* represents the minimum mesh resolution in meters, which is the circumradius around an element (Roberts et al., 2019). This parameter makes a significant difference in the total data size of the mesh. The higher the resolution, the less elements and thus a lower data. Reduction in total amount of data in a mesh improves the speed at which ADCIRC can run a storm surge simulation, which can be beneficial during the real-time tracking of a storm (M. V. Bilskie et al., 2020). Comparatively, the parameter *max_el* sets the upper limit of how large an element can be within the meshing domain.

OM2D then requires parameters regarding *grade*, which uses the variable *g*. Grade is the percent gradient between element edge length, using a marching algorithm (Persson, 2006; Roberts et al., 2019). For example, if one element had an edge length, of 100, and there was *g* value of .1, then bordering triangles could not have an edge length larger than 110 meters or less than 90 meters. Where elements are places is also based upon user parameters such as *max_el_ns*, which indicates the highest resolution that an element attached to the input shoreline can be. The use of this parameter helps OM2D to maintain very fine resolution close to the shore and within floodplains.

Additionally, other parameters are used in the model to better resolve geographic features. These include *angleOfReslope, ch, min_el_ch*, which are used to crease channel resolution and *fs,* which is used to establish how many elements will be placed along shoreline feature. OM2D uses the input DEM to dictate how the channel parameters are used. All of the utilized parameters can be visualized in Table 3.3, for the child and parent meshes respectively.

Variable	**Parent Mesh Value**	**Child Mesh Value**	**Description**
min_el	100	50	Minimum resolution in meters
max_el	10,000 wet and dry	1000 wet, 250 dry	Maximum resolution in meters
g	.1	.1	Mesh grade in decimal percent
angleOfReslope	60	60	Angle at which a channel is graded, and the extent at which it will be resolved as a channel
ch	.328	.328	Scale of resolution proportional to the depth of the thalweg
min_el_ch	100	50	Minimum resolution for a channel to be resolved
max_el_ns	240	N/A	Maximum resolution nearshore in meters
fs	10	10	Number of elements per width of shoreline

Table 3.3 OM2D Parameters Utilized (Roberts et al., 2019)

3.5.2 | Geographical Data Input (DEM, BBOX, Coastlines) and Multiscale Technique

OM2D allows for a user input of specific geographic data that will help dictate how the triangulation of the mesh occurs (Roberts et al., 2019). As discussed in **Chapter 3.2**, the model developed as a part of this thesis utilizes the CoNED 1-meter DEM and the SACS coastline to guide its mesh generation. The DEM is required in the mesh development for the use of the channel-related parameters that are used within the mesh, that are discussed in **Chapter 3.5.1**. The DEM has elevation data both on land and underwater, which is known as a "topobathic DEM". Because the DEM has both above and below sea level vertical data, OM2D is able to set different resolution parameters for wet versus dry regions.

The DEM was also used to set the child mesh BBOX. Utilizing manual mesh generation and visualization software, SMS, a boundary surrounding the Georgia DEM was created. This boundary was then used within the multiscale technique. The boundary is visualized in Figure 3.14 by the pink polygon. Then within SMS, the polygon was transformed into a set of coordinates. OM2D then will read in the coordinates as a BBOX, and develop a mesh within those set boundaries.

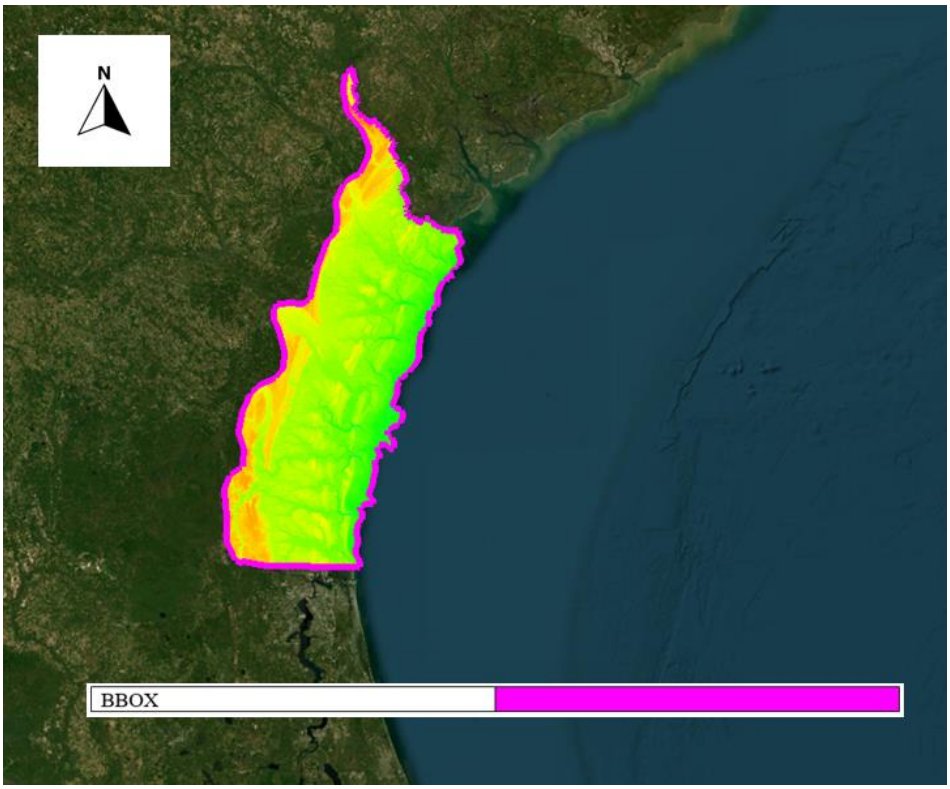

Figure 3.14 Georgia BBOX used in Multiscale

The multiscale technique is a method within OM2D that allows the user to create a single large domain mesh with specified areas of high refinement (Roberts et al., 2019). Regions of interest or areas with fine-scale features are represented with smaller elements. In contrast, regions of lower importance or areas where coarser representation is sufficient are assigned larger elements, reducing computational effort. By dynamically adjusting the mesh resolution across the computational domain, multiscale meshes allow for the allocation of computational resources in a more efficient manner, enabling simulations of larger and more complex systems that would be computationally prohibitive with a uniform fine mesh (M. V. Bilskie et al., 2020; Hagen et al., 2006; Roberts et al., 2019). The regions are defined as child and parent meshes, and OM2D seamlessly merges them together while maintaining a certain set mesh quality.

OM2D achieves a multiscale mesh without poor quality stitching between the meshes through allowing the development of multiple *meshgen* and *edgefx* classes which is discussed in Figure 3.13 in **Chapter 3.5.1**. This way, differing parameters can be set for each mesh, and then when the final mesh optimization is completed and the mesh object is built, it is all in one (Roberts et al., 2019). For the mesh developed for this thesis, the parent mesh was set as the SAB while the child covered just coastal Georgia. The multiscale technique can be visualized in Figure 3.15 below.

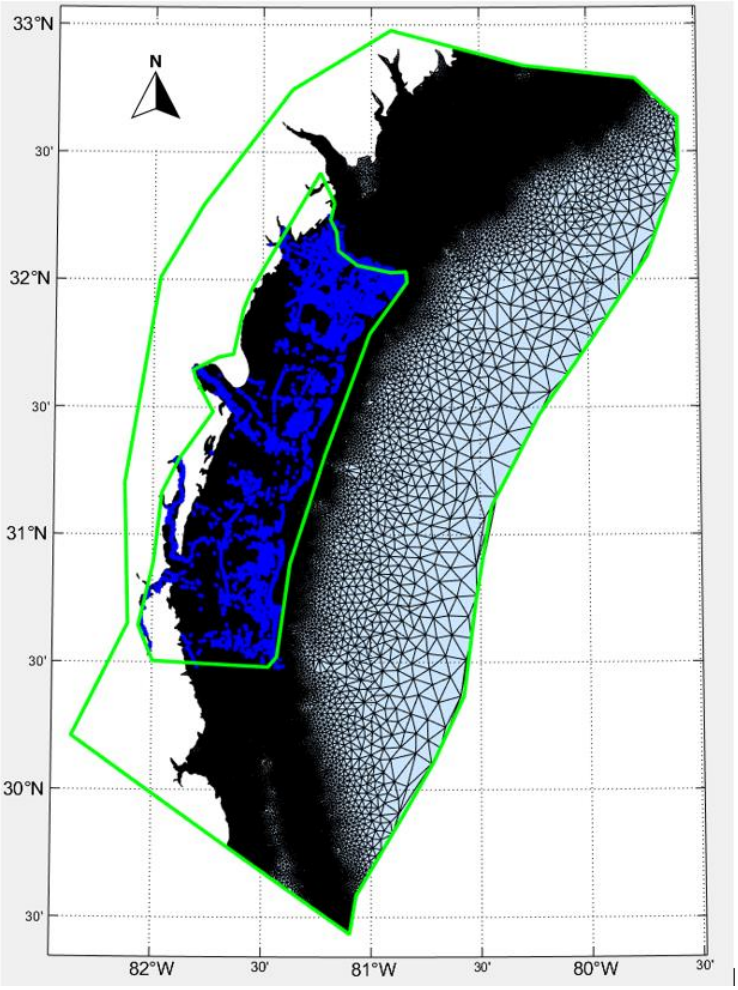

Figure 3.15 BBOXs used for both the child (inner polygon) and parent (outer polygon) meshes

Then again in SMS, a separate BBOX was drawn for the surrounding SAB to set the outer parent mesh. This parent mesh used the SRTM15+ DEM for its channel and wet/dry boundary identification to coordinate with set mesh optimization parameters detailed in **Chapter 3.5.1**. The BBOX drawn set the parent domain to include the SAB and the open-water region reaching out to the Atlantic shelf, and the two meshing domains can be visualized in Figure 3.15 above.

The coastlines shapefiles utilized were the SACS coastline and the Coastal Relief Model 10-meter line. The Coastal Relief Model 10-meter line was used as the inner meshing domain boundary for both the child and the parent meshes. This line is used to set the edge of the floodplain at a 10-meter elevation contour. OM2D generates a mesh for a floodplain similar to how it would in the open-ocean, through meshing a set polygon. The 10-meter line serves as the inner side of the polygon, while the 0-meter elevation line is set through the respective DEMs for both the parent and the child meshes (Roberts et al., 2019).

The SACS coastline is then used to better establish resolution surrounding the wet/dry boundary. Using the parameter *max_el_ns*, OM2D sets a maximum resolution that can exist along the shoreline. It is desirable to have a higher level of resolution nearshore to be able to better resolve coastal morphology, channels, dunes, and other man-made features (Greenberg et al., 2007; Roberts et al., 2019).

As mentioned in **Chapter 3.1**, one of the additional goals of the thesis was to determine if there is a benefit to holding node points along the wet/dry boundary. OM2D features a built-in size function, which will distribute vertices along the SACS coastline (Roberts et al., 2019). This size function comes from developing a separate mesh using a separate structure from the multiscale technique. The separate mesh uses a function, *extractFixedConstraints*, which first develops a

mesh for the underwater only boundary using the SACS shoreline as the inner boundary and the drawn BBOX as the outer. Then, prior to developing the inner floodplain mesh, *extractFixedConstraints* parses over the SACS shoreline and determines average grid size along the shoreline, in what is known as a size function. These vertices are then saved into a separate file and entered into the multiscale model as held points, where mesh nodes will be placed along the shoreline. The resulting final mesh with held points is visualized in Figure 3.16.

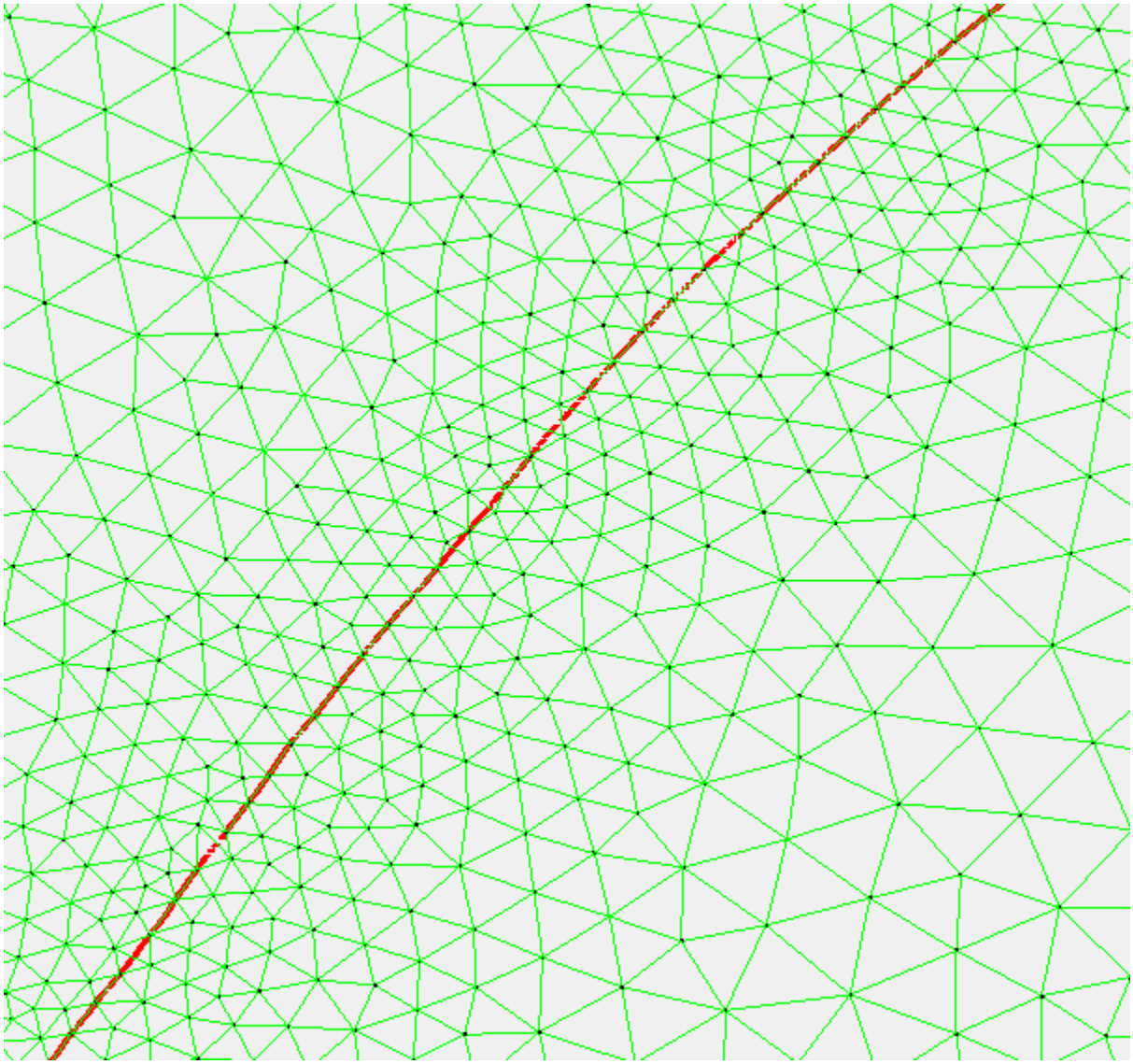

Figure 3.16 Mesh with node points held to coastline. Red line indicates SACS coastline.

3.5.3 | Thalweg Input and Thalweg Size Function

OM2D allows for the user-input of thalwegs (Roberts et al., 2019). Thalweg lines were extracted using a function detailed in **Chapter 3.3**. Once the thalwegs were identified and transformed into polylines, a series of python codes broke the polylines into individual lines each representing single creeks or channels. The polylines were then broken into coordinate points, which are read into OM2D. OM2D then utilizes a thalweg size function to be able to determine how the mesh will be resolved around the thalwegs. Utilizing parameters detailed in **Chapter 3.5.1**, the size function determines how far in each direction from the thalweg that the mesh should be resolved. It is advantageous to have higher mesh resolution along thalwegs, as thalwegs dictate the locations where water propagates up and down channels (M. V. Bilskie, Hagen, et al., 2012). The mesh developed for this model aims to have well resolved channels using thalwegs, resulting in what is visualized in Figure 3.17 (Roberts et al., 2019)

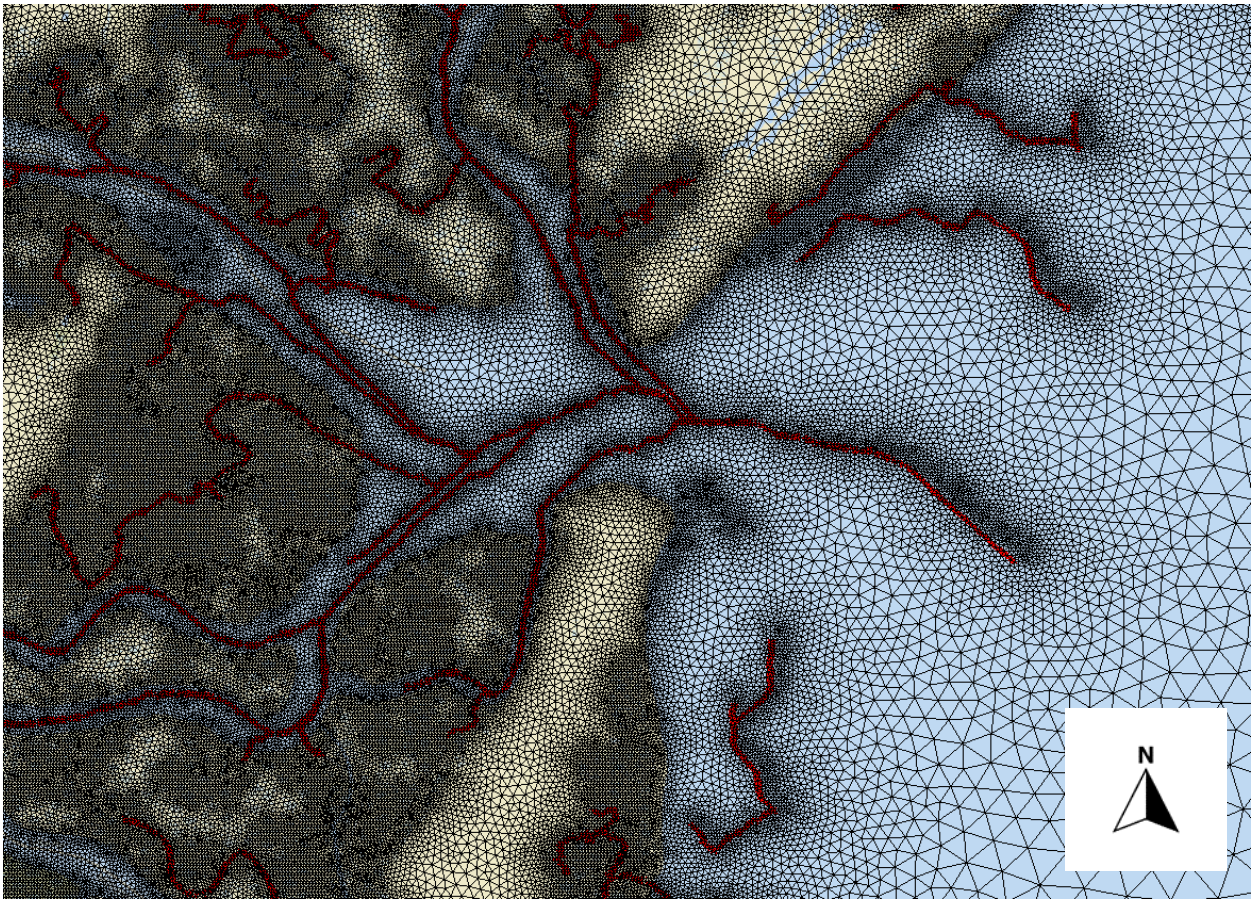

Figure 3.17 Thalwegs as resolved in final meshes. Red lines indicate extracted thalweg polylines.

OM2D develops a size function that utilizes parameter *angleOfReslope* to set the V-styled angle from the thalweg to develop a circular region around each thalweg point. Compared to other size functions, this one uses depths from the DEM to determine how wide a channel is. Then using the other channel parameters, resolution around the thalweg points are set based on the depth of the thalweg (Roberts et al., 2019). The deeper the thalweg, the wider the channel cone, which increases the amount of channel nodes, as is visualized in Figure 3.18.

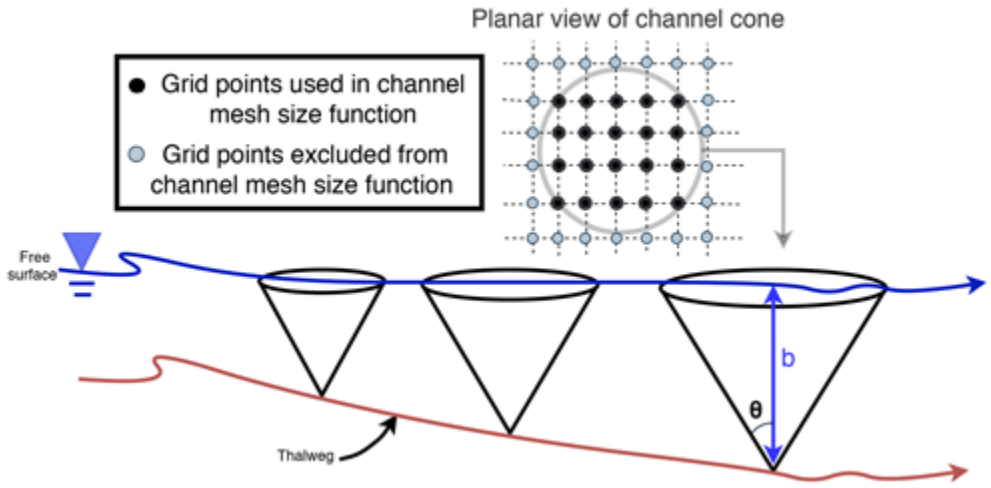

Figure 3.18 Illustration of thalweg size function implementation (Roberts et al., 2019)

3.5.4 | Vertical Feature Input

The VFs were input utilizing an OM2D variable, *pfix*. *Pfix* represents the permanently fixed points that nodes must be placed on within the mesh (Roberts et al., 2019). The process where the VFs were extracted is detailed in **Chapter 3.4**. Once the VFs had been extracted and then cleaned, a size function was developed to be able to transform the vertical polylines into points. Once in the form of points in WGS84, they then are placed into a two-column MATLAB array, which is named *pfix*. It should be noted that if the point spacing of the VFs significantly differs from the desired mesh size function, it can lead to poorly formed triangulations in the vicinity of these constraints, as *pfix* is held at a higher priority than the triangle optimization. In other words, if there are *pfix* points that are too close together or too close to other resolved features, such as the coastline, the resulting elements could cause instabilities (Kojima, 2005; Roberts et al., 2019). Compared to thalwegs, the node points are held to the exact coordinate that is input, whereas the thalwegs develop high resolution around the thalweg points but do not hold nodes tight to the thalweg.

In order to avoid poor triangulation, the mesh size function is developed in order to ensure that no two VF nodes are too close together and rather they are distributed based on the mesh resolution of the area they are places in. However, this size function does not consider other held points such as the coastline, in the case of the mesh with held coastline points. Triangulation problems occur with this scenario in areas where there are dunes close to the shoreline, as well as other man-made features (Roberts et al., 2019). To avoid this, the *pfix* file was merged to include both the coastline points and the VF points. Then, any coastline points that fell within 50 meters of the VF points were deleted. The points all together in the final coastline-held mesh can be visualized in Figure 3.19.

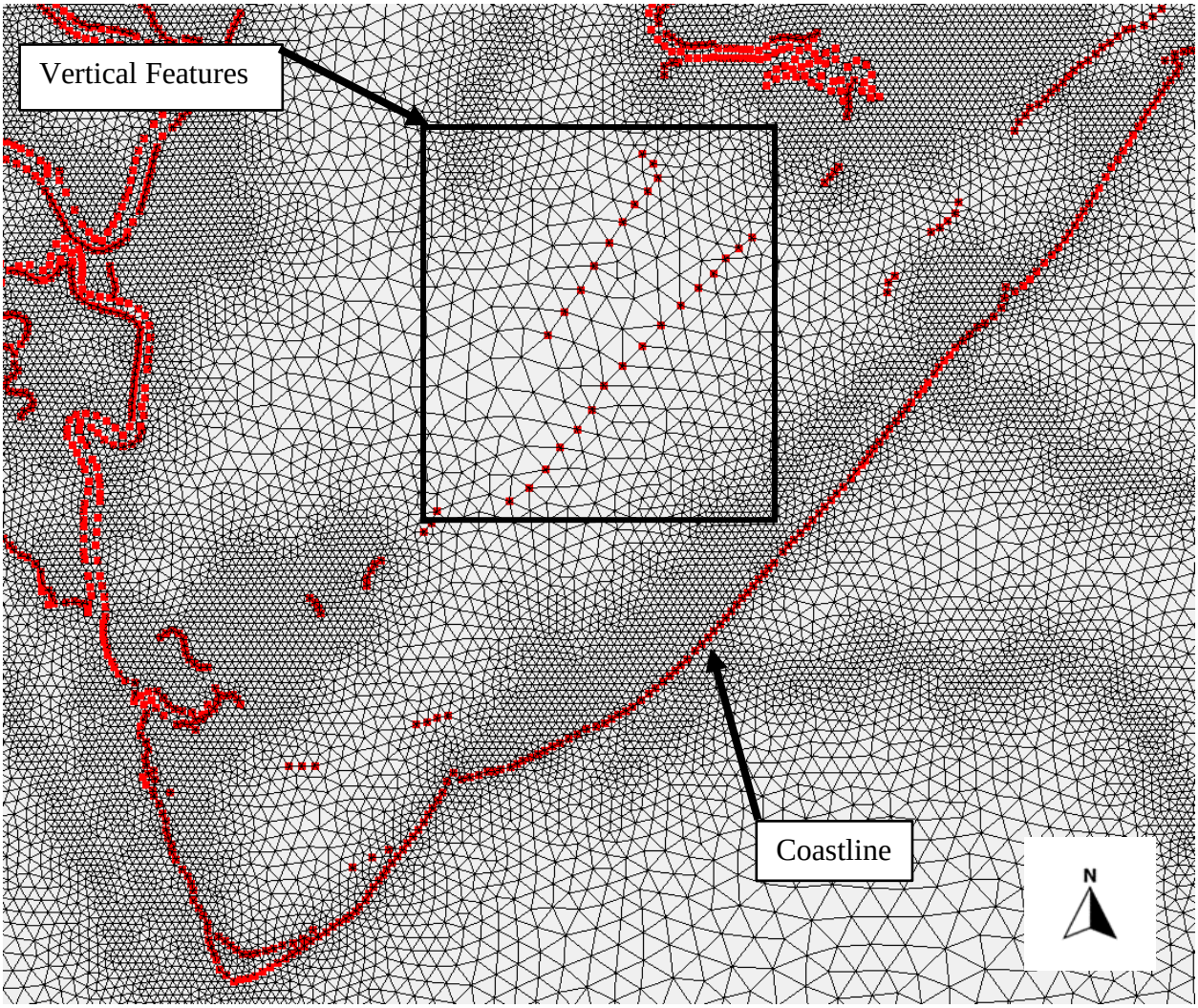

Figure 3.19 Finalized mesh with both VF nodes and coastline nodes displayed

3.5.5 | Mesh Merge

The parent and child meshes were then merged together using SMS. The mesh merging process preserves constraints from each of the *msh* objects being merged. This includes items such as *pfix*, so that as the plus function progresses, previously held points are not lost, such as the VFs and the coastline (Roberts et al., 2019). The 53K file developed by Hagen was merged with the multiscale mesh developed within OM2D (Hagen et al., 2006). Hagen's 53K mesh was chosen due to its finer resolution around important marine features such as the shelves, while also maintaining a lot computational cost (Hagen et al., 2006). The resulting merge can be visualized in Figures 3.20 and Figure 3.21.

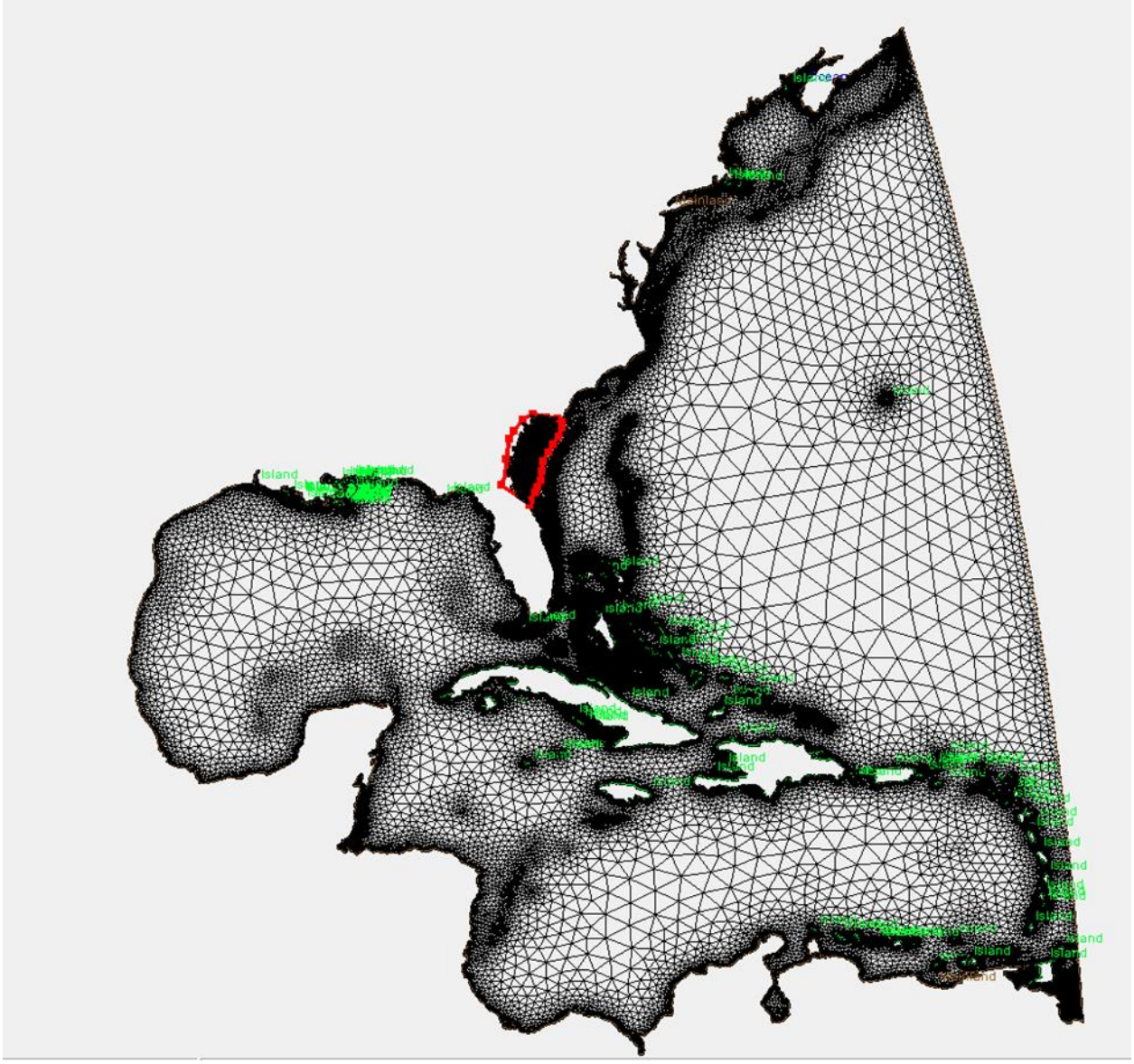

Figure 3.20 Merged 53K mesh with red boundary indicating multiscale mesh

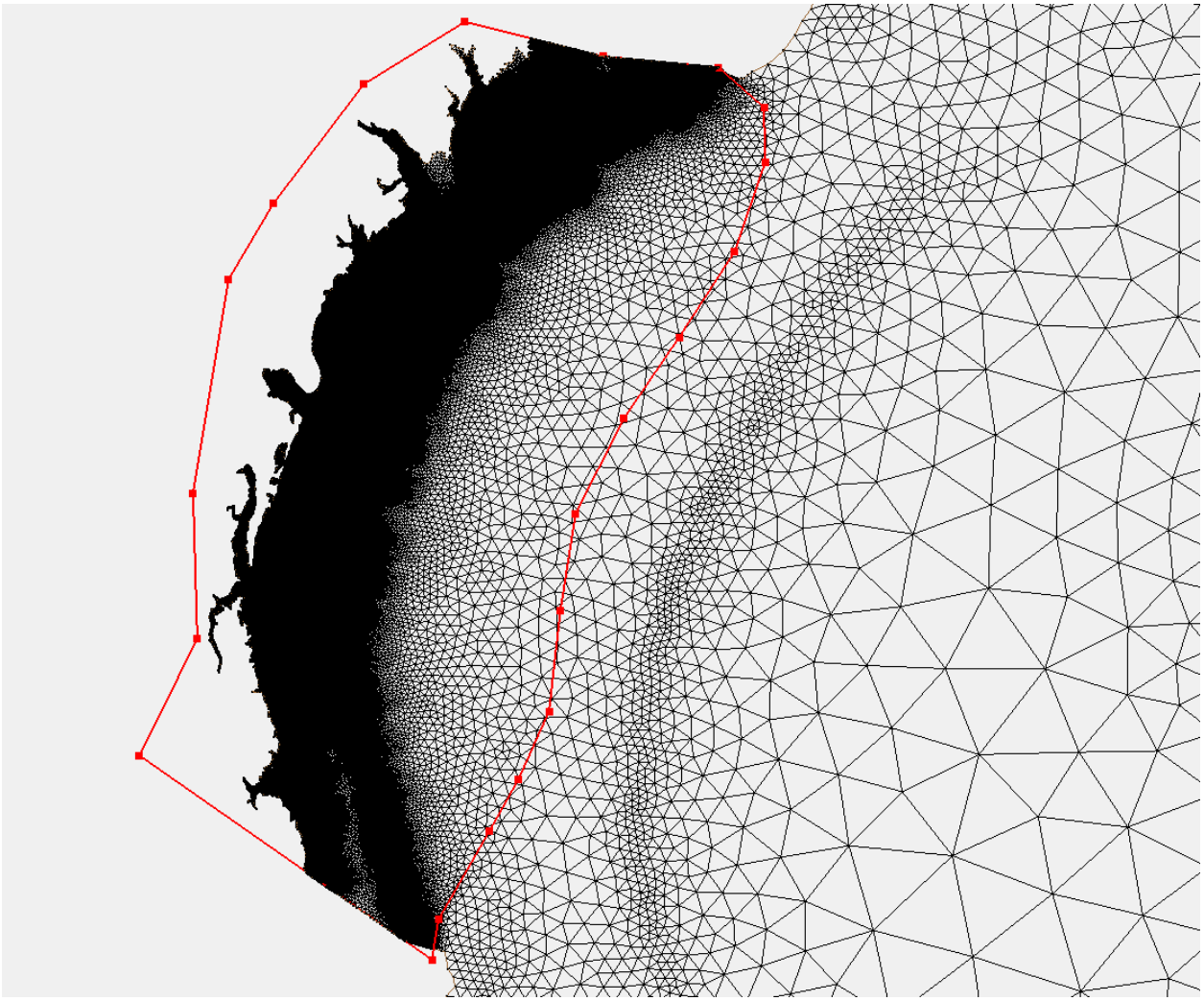

Figure 3.21 Zoomed in 53K and multiscale mesh merge, with red line indicating the border between the two meshes

3.5.6 | Cleaning (RemoveKites.m and msh.clean)

Prior to the merging of the meshes, OM2D cleans the mesh after it has been generated through the *msh.clean* function. The *msh.clean* function allows the user to set certain parameters, such as mesh quality and maintaining *pfix.* Mesh quality is a variable that is based on angles of the triangles (Roberts et al., 2019). For the mesh developed as a part of this model, a "medium" cleaning level was utilized, which deletes any triangles that contain angles that are above 150 degrees or below 10 degrees. The medium cleaning level is a predetermined default within OM2D, and is applicable to both border and inner elements (Roberts et al., 2019). However, since *pfix* is entered in as a parameter to the cleaning, any triangles that are determined to be bad quality but the deletion would interfere with the *pfix* points are ignored.

Once the final mesh had been developed from the plus function, cleaning was then performed on the mesh. Again, a medium cleaning level was applied, as the plus function affects the existing triangulation. It is important however to perform the cleaning before the plus function as well as irregularities in the triangulation of the child mesh can cause OM2D to fail to merge the two meshes. The resulting post-merge cleaned meshes were then run through an additional cleaning code within MATLAB, *RemoveKites.m*. *RemoveKites.m* parses over the meshes for any nodes that have connected to 4 or 8 other nodes. When a node is connected to 4 or 8 nodes, the entailing elements are known as kites, which cause instabilities when ran in ADCIRC.

3.6 | Topographic/Bathymetric Interpolation and Boundary Conditions

Although the topographic and bathymetric interpolation processes can be performed in both SMS and OM2D, a different code was used to maximize the smoothing process of interpolation. This was done using a code developed by Dr. Matthew Bilskie named PyDEM2GRD (M. V. Bilskie & Hagen, 2013). The code works in 3 different steps, with each step including a more intensive smoothing than the one before. The steps proceed as follows: 1) underwater bathymetric interpolation, 2) overland topographic interpolation, and 3) VF interpolation.

PyDEM2GRD performs smoothing based on cell averaging. In the case of a 1-m resolution DEM, PyDEM2GRD will parse over DEM cells surrounding the desired area, and smooth them based on an average of the surrounding cells. This is done in order to avoid any noise from being interpolated into the mesh (M. V. Bilskie & Hagen, 2013)

In order to complete the interpolation however, the DEM must be broken into small tiles. Additionally, the more precise and recent of a DEM, the better. Therefore, the 2019 LiDAR data obtained by the University of Georgia Skidaway Research Institute of Oceanography was utilized for the PyDEM2GRD code. The interpolation function assigned Z-values to the mesh, indicating relative elevation from mean sea level.

PyDEM2GRD was only used for the topographic and bathymetric interpolation over Georgia, due to the computational cost behind running the interpolation function. SMS has its own interpolation function, which was used to interpolate the remaining areas using a combination of the CoNED and CUDEM DEMs, as well as the 53K mesh. The CoNED was used for areas over Georgia not covered by the 2019 LiDAR, CUDEM was used for the surrounding topographic and bathymetric regions of the SAB, and the 53K was used for the surrounding open ocean. Examples

of the SAB mesh after interpolation are visualized in Figure 3.22, and an example of the VFs resolved in the interpolation is visualized in Figure 3.23.

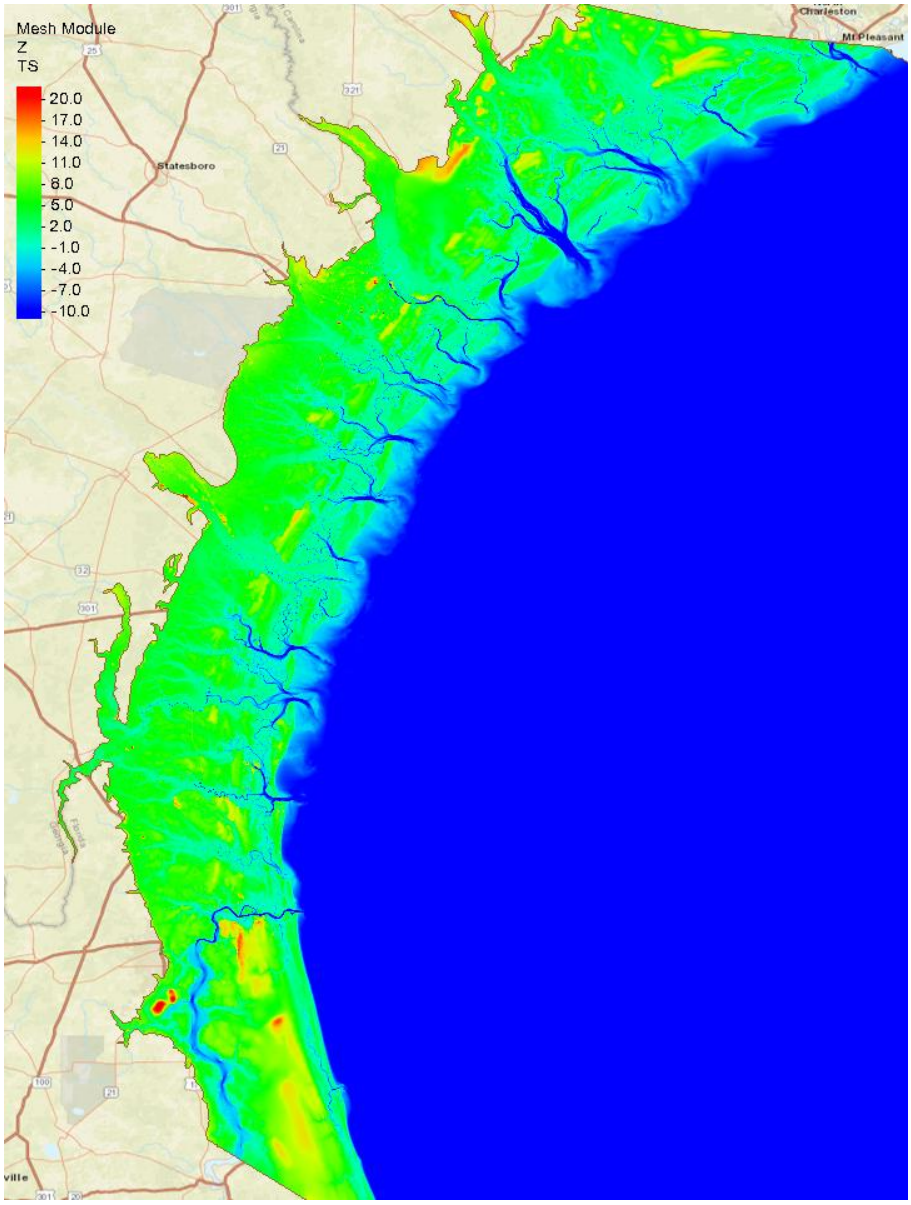

Figure 3.22 Interpolated topography and bathymetry on the SAB

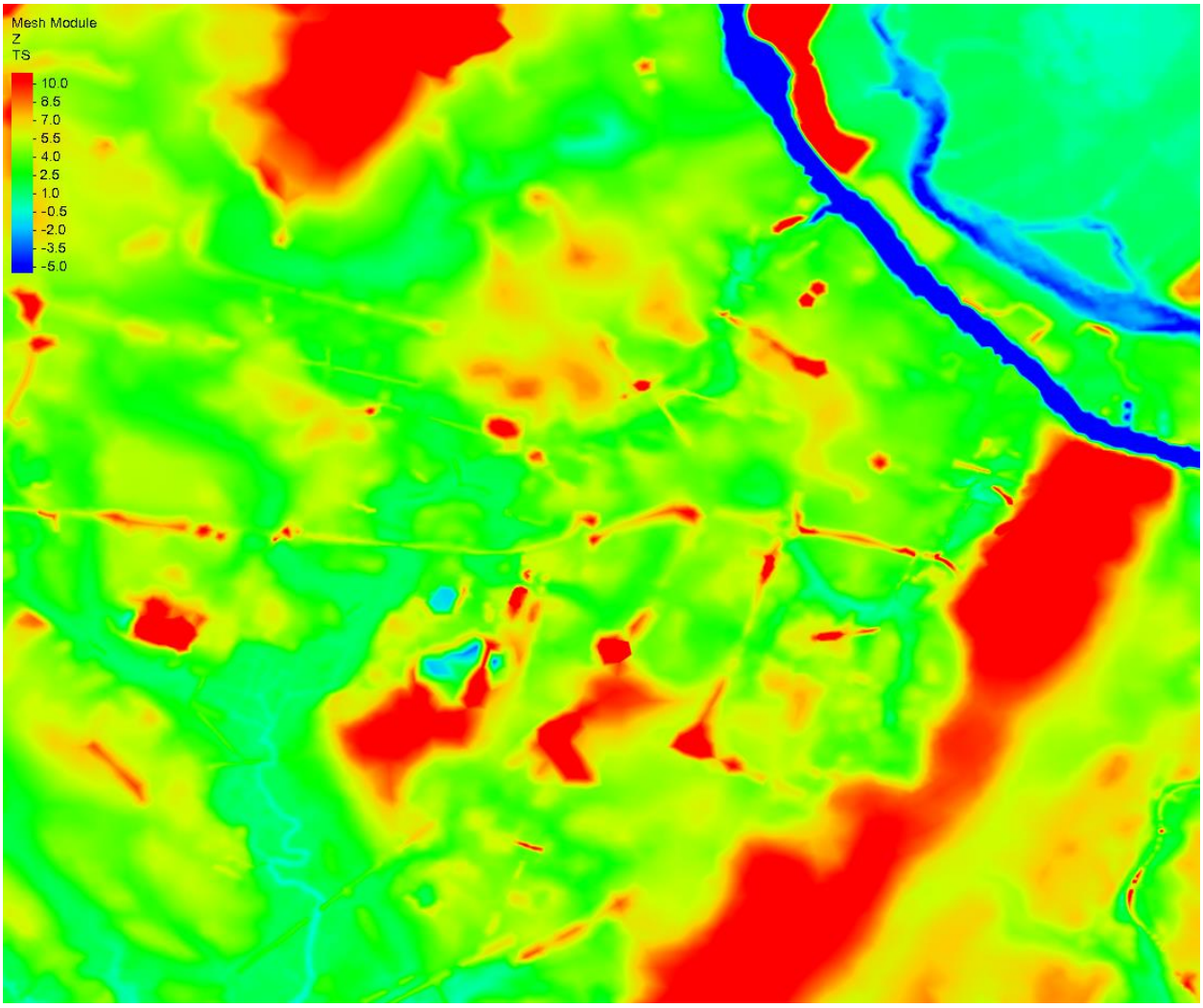

Figure 3.23 Interpolated topography and bathymetry in Savannah, GA, with focused VF smoothing

Once the topographic and bathymetric data has been interpolated to the mesh, boundary conditions were applied using a function in OM2D, *make_bc* (Roberts et al., 2019). The function serves the purpose to apply ADCIRC compatible boundaries to the mesh, which is required to run ADCIRC (Luettich et al., 1992). *Make_bc* develops boundaries using the interpolated elevation data, by setting any mesh border over 0 meters as land, and below as open ocean, using the option *auto_outer, 'depth', 0*. Additionally, another run of *make_bc* using the option *inner* allows for the

appendage of island boundary conditions for all interior polygons (Roberts et al., 2019). The resulting mesh can be visualized in Figure 3.24.

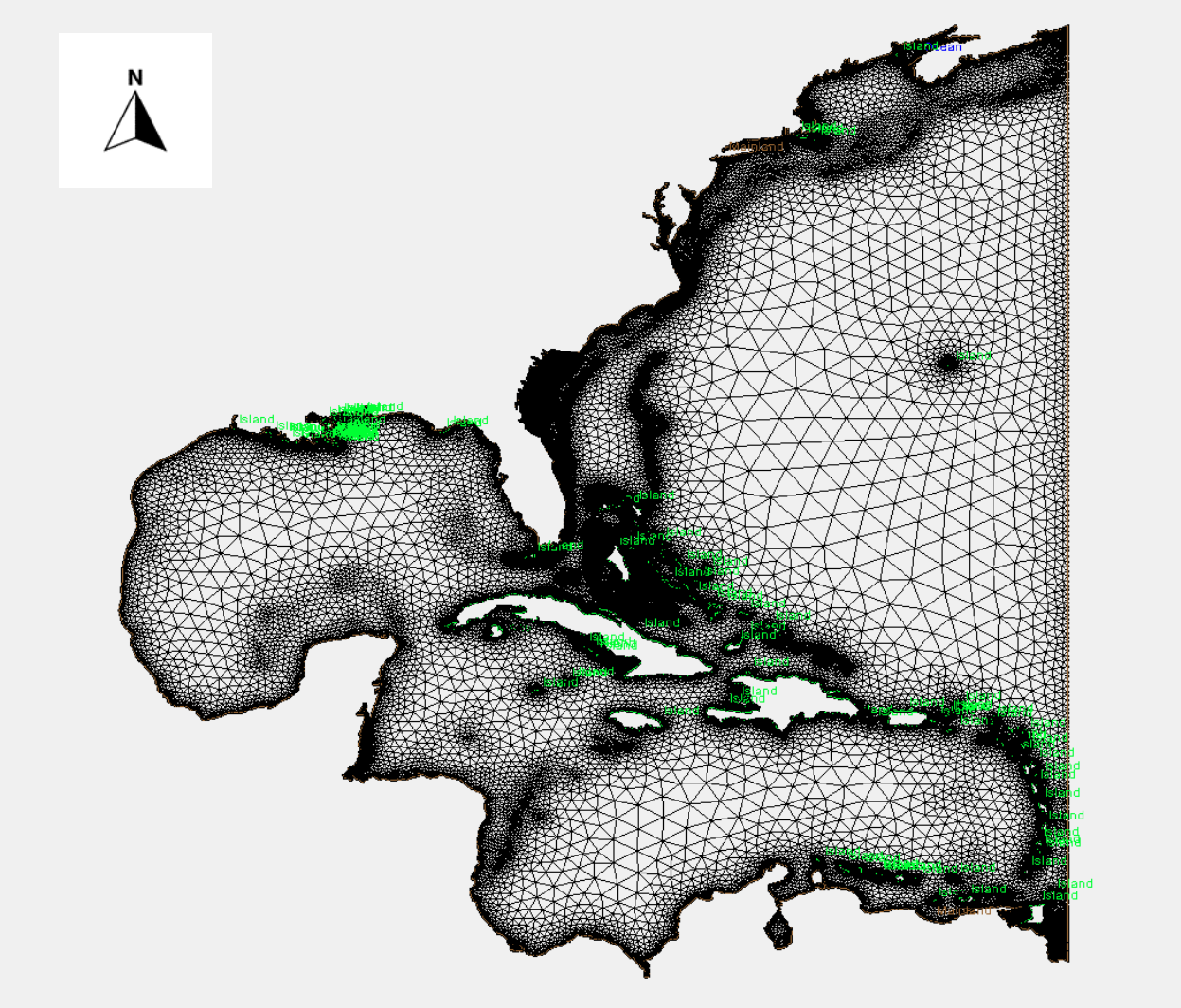

Figure 3.24 Final mesh with appended boundary conditions

3.7 | Nodal Attributes

The *fort.13* is the nodal attributes file, and covers information such as bottom roughness, eddy viscosity, Manning's n, surface roughness, amongst other optional inputs (Luettich et al., 1992). OM2D includes functions that allots users the ability to develop a *fort.13* that corresponds to the *fort.14* mesh file (Roberts et al., 2019). The OM2D functions, *Calc_Mannings_Landcover* and *Calc_Tau0* are utilized in the model to develop the *fort.13*. In order to run these functions however, Manning's n landcover maps had to be retrieved and input into OM2D. The model utilized the C-CAP landcover map in the form of a *netCDF* for the OM2D functions, and can be visualized in Figure 3.25 (*C-CAP Regional Land Cover and Change*, n.d.). Each of the colors in Figure 3.26 dictate a different landcover type, each of which have different levels of water flow and affect how storm surge inundates the land.

Figure 3.25 C-CAP Landcover Map for SAB

Figure 3.26 C-CAP Landcover Legend (*C-CAP Regional Land Cover and Change*, n.d.)

3.8 | ADCIRC Simulation

ADCIRC is a numerical model used for simulating coastal and oceanic hydrodynamics. It is specifically designed to simulate storm surge and tidal dynamics, making it a valuable tool for predicting the behavior of water levels during extreme weather events such as hurricanes (Turan et al., 2018). ADCIRC solves the shallow water equations, which are a set of partial differential equations that govern the flow of water in shallow seas and coastal regions. These equations consider factors such as water depth, velocity, and pressure, and consider various physical processes such as tides, wind forcing, and bottom friction (Dietrich et al., 2012; Luettich et al., 1992). The model uses a finite element method to discretize the governing equations and solve them numerically. It divides the domain of interest into a mesh of interconnected triangles, known as the mesh (Luettich et al., 1992; Roberts et al., 2019). ADCIRC then solves the equations at each node of the mesh, considering the interactions between neighboring nodes to determine the water flow and elevation at each location (Dietrich, Zijlema, et al., 2011). ADCIRC is discussed further in Chapter 3.3.

A hydrodynamic simulation was performed using the numerical model, ADCIRC using the finalized Georgia mesh. The Georgia mesh served as the spatial discretization used in ADCIRC was the completed unstructured, finite element mesh. The simulations conducted in this study employ a time step of 1 second. Wetting and drying effects are activated with a minimum depth of 0.1 meters, and a turbulence closure based on the Smagorinsky method is utilized with a value of 0.20. Manning's n for bottom friction was derived from the Coastal Change Analysis Program (CCAP) land use land cover data (*C-CAP Regional Land Cover and Change*, n.d.; Dietrich, Westerink, et al., 2011).

To validate astronomic tides, a 45-day astronomic tide simulation was performed. ADCIRC simulated tides at six different NOAA tidal gauges to compare against observed data. The stations included: Fort Pulaski, GA; South Ossabaw Island, GA; South Newport River, GA; Saint Simons Island, GA; Kings Bay, GA; and Mayport Basin, FL. At all 6 stations, ADCIRC simulated the tidal range and phase, as well as the 23 highest tidal constituents. The simulated and observed tidal harmonic amplitudes and phases were compared using a tidal resynthesis. The resynthesis was carried out over a course of 14.7 days (M. V. Bilskie et al., 2019). At each gauge, two error metrics were calculated to assess the accuracy of the simulation: mean square error and root mean square error.

A simulation of Hurricane Matthew (2016) was additionally performed in ADCIRC. Wind and pressure fields for Hurricane Matthew were provided by Oceanweather Inc. (OWI). The data-assimilated meteorology is based on observations and the Tropical PBL model (TropPBL) (Thomas et al., 2019; Thompson & Cardone, 1996). Three NOAA tidal gauges were utilized in the hurricane simulation: Fort Pulaski, Georgia; Fernandina Beach, Florida; and Mayport Basin, Florida. The simulated water heights at each gauge location were compared to the observed data at the gauge location during the storm, and a map of the maximum inundation across the duration of the storm was generated.

4.0 | RESULTS

4.1 | Mesh Results

The finalized mesh was developed for the model is displayed below in Figure 4.1. The meshing domain extended over the Western North Atlantic, while maintaining higher levels of resolution in the SAB, especially over Georgia. Georgia was meshed with higher resolution using the multiscale technique built into OM2D, separating the parent and child meshes into BBOXs illustrated in Figure 4.2 (Roberts et al., 2019) The mesh utilized Hagen's 53K mesh to merge with the SAB mesh, utilizing the plus function built into OM2D (Hagen et al., 2006; Roberts et al., 2019). Using this function, the seam between the two meshes was generated to avoid poor triangulation and instabilities when running ADCIRC, as is visualized in Figure 4.3.

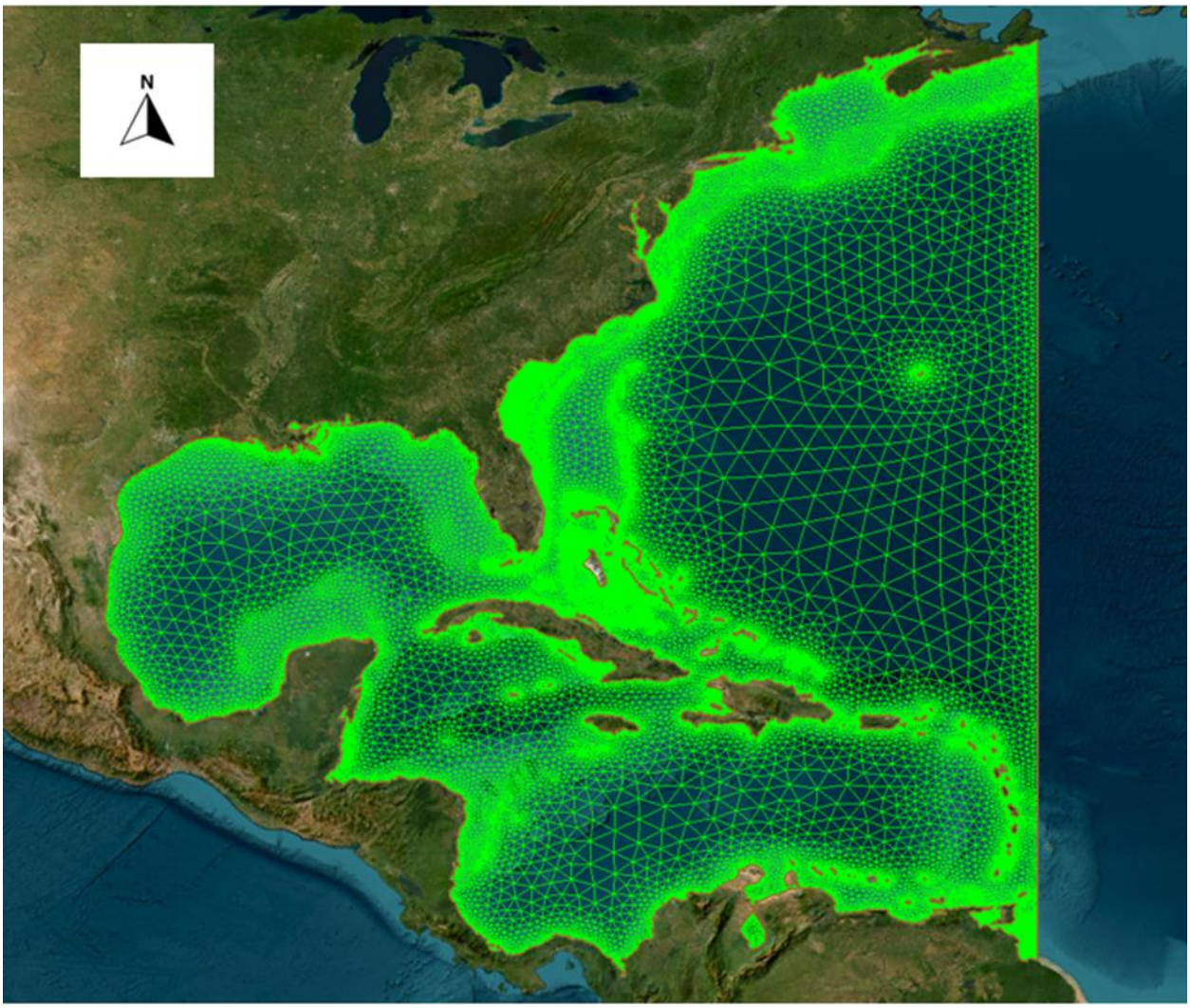

Figure 4.1 Final mesh of western North Atlantic, with focused resolution in the SAB

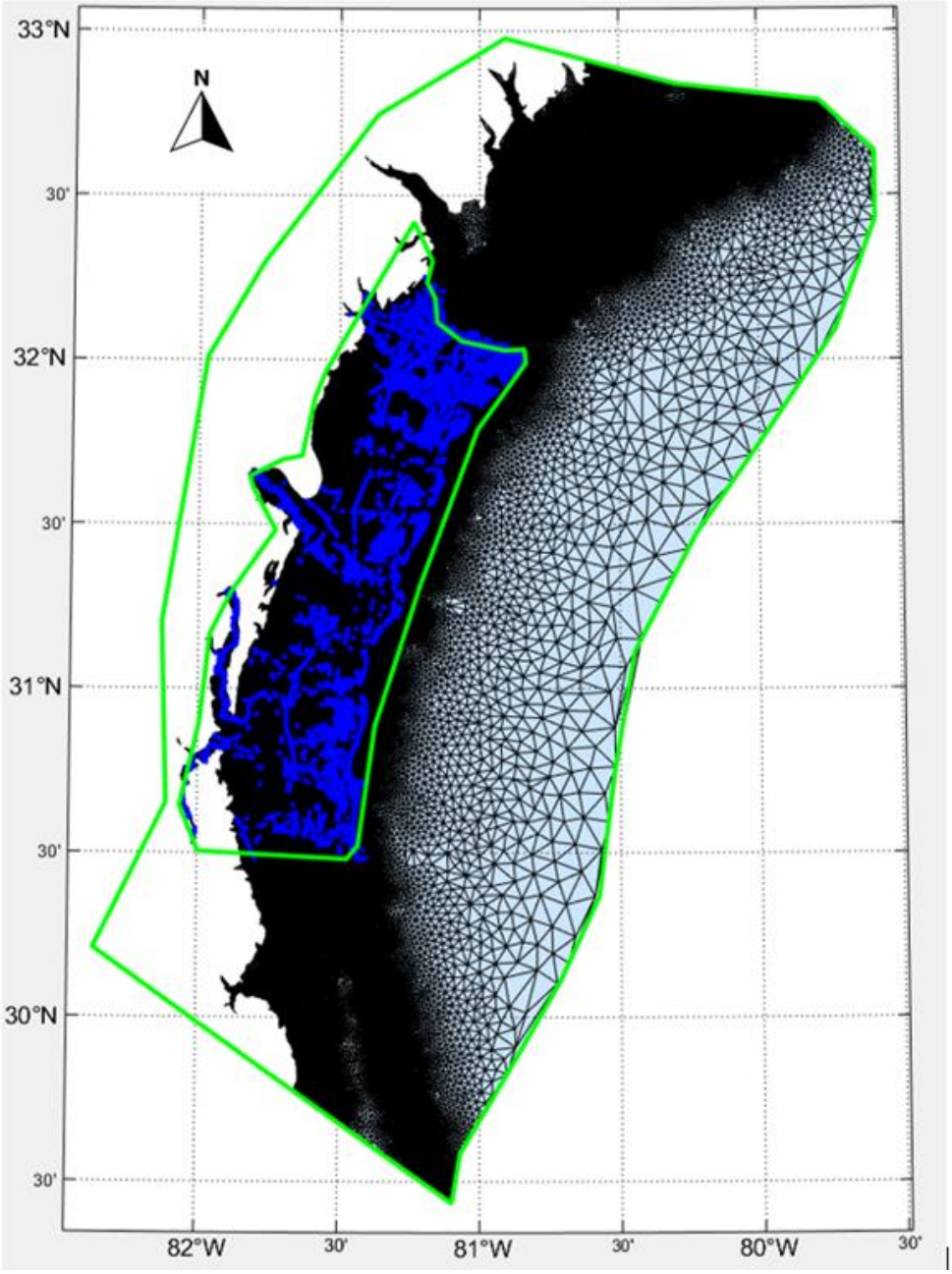

Figure 4.2 SAB mesh, separated into parent and child meshes through BBOXs, illustrated in green, using the multiscale technique

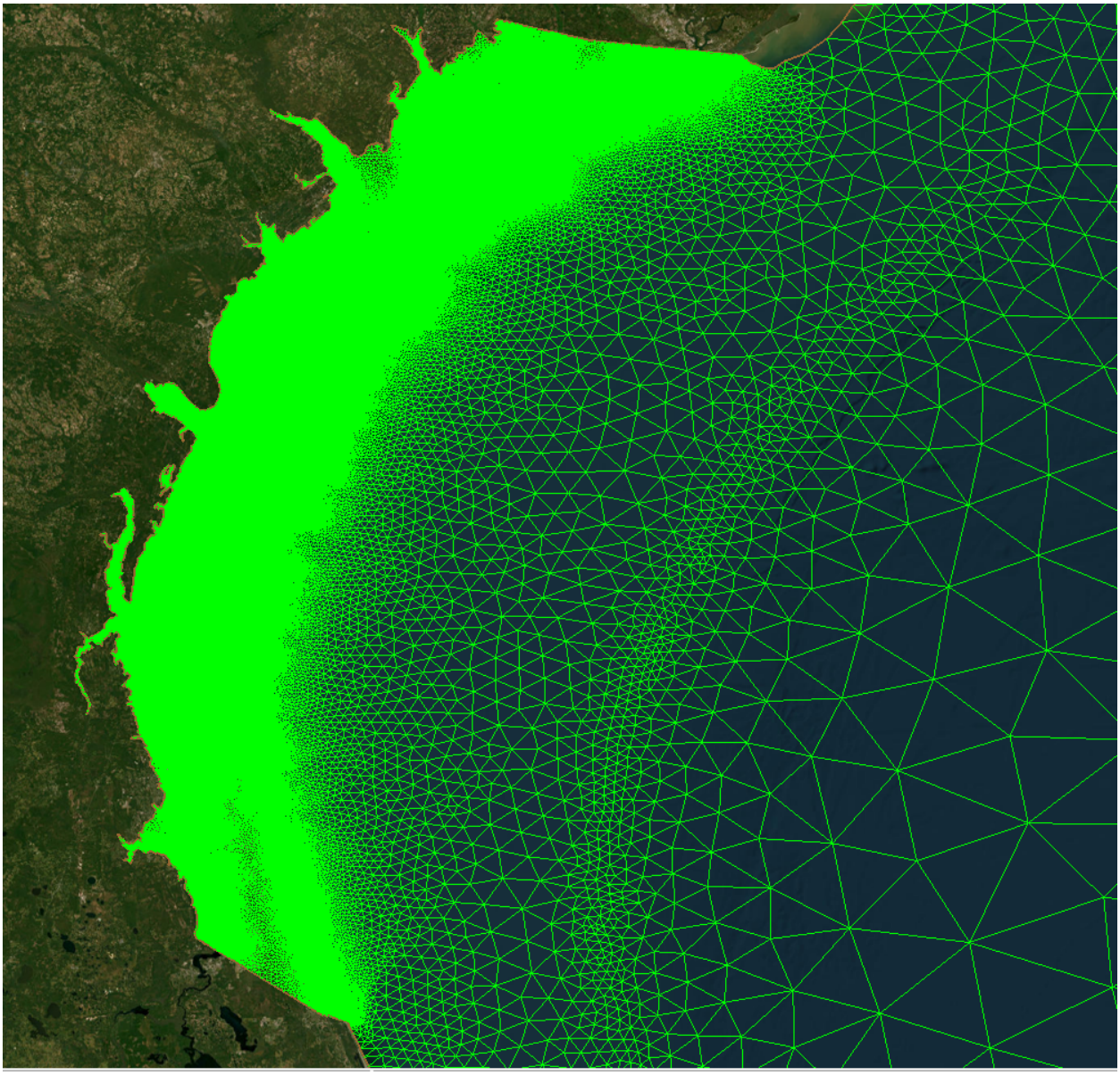

Figure 4.3 Final mesh zoomed into the seam between the SAB mesh and the 53K mesh

The mesh generated additionally included the modeling of the overland floodplain in addition to the oceanic regions. Using parameters in OM2D, higher mesh resolution was placed over marsh regions, while overland regions away from water features were resolved with lower resolution (Figure 4.4).

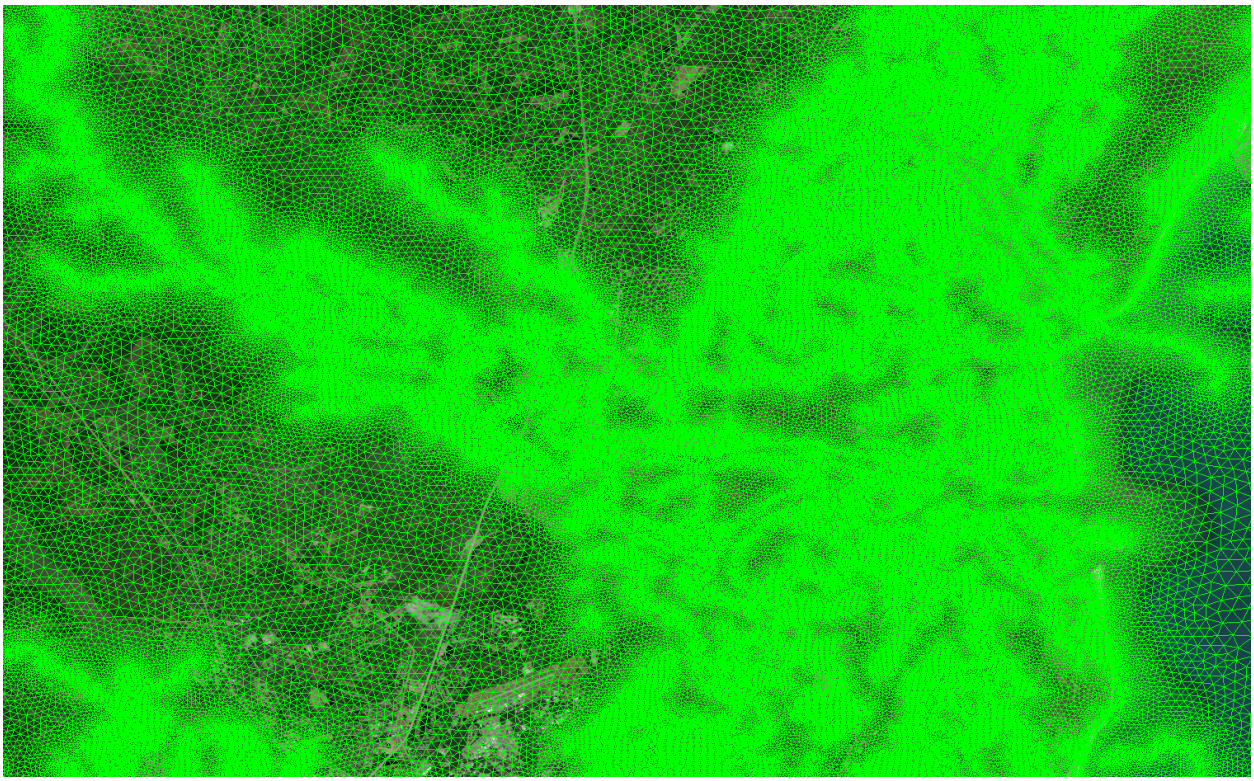

Figure 4.4 Increased mesh resolution surrounding coastal features in Central Coastal Georgia

Similar to the overland regions, oceanic regions further away from coastline features were resolved with lower resolution (Figure 4.5). Increased resolution surrounded coastline and marsh regions using several OM2D parameters. The reduction in resolution in areas further from significant geographic points allows for improved computational cost, which is helpful for real-time storm surge modeling (M. V. Bilskie et al., 2020).

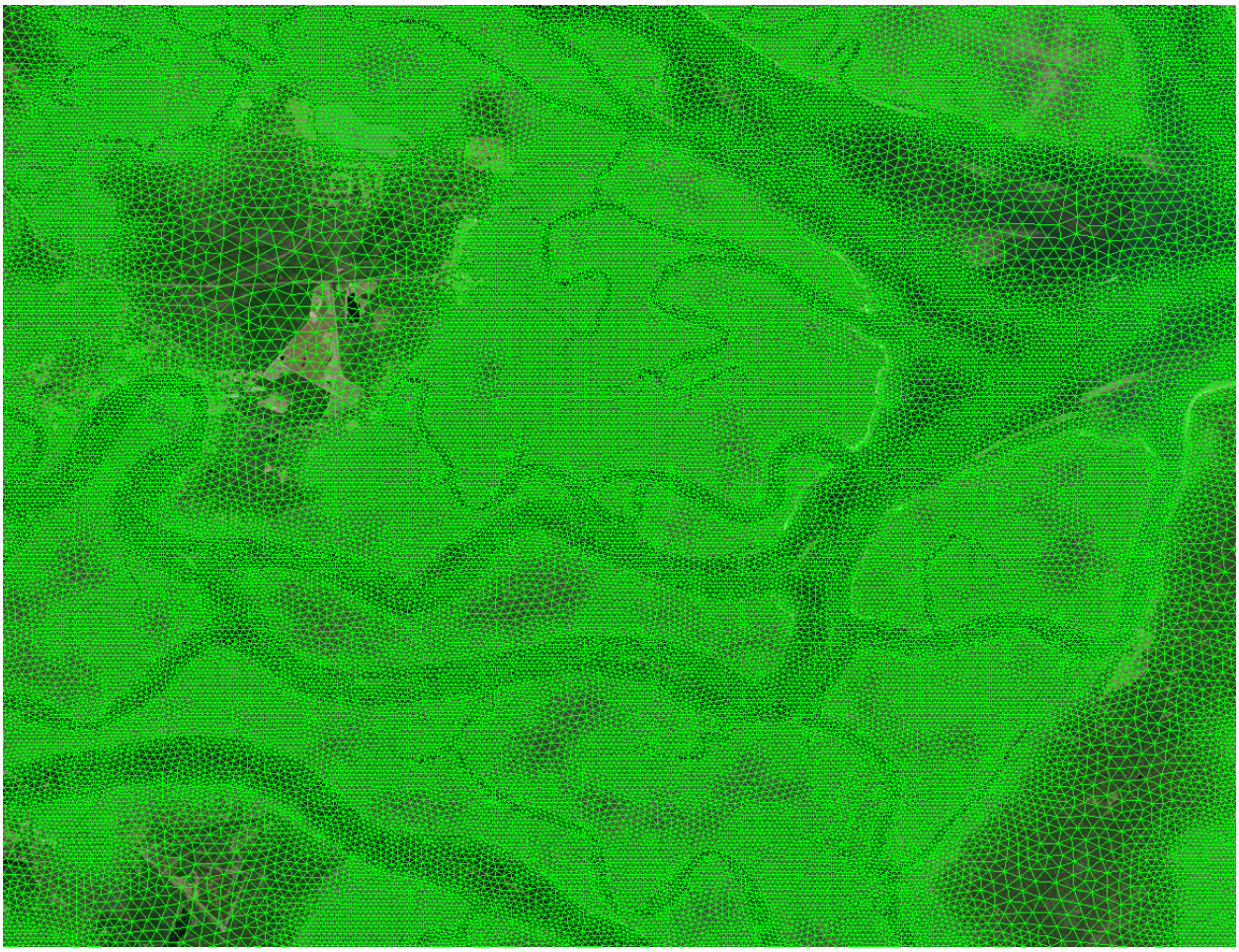

Figure 4.5 Minimum mesh resolution in Georgia marsh regions, with higher resolution achieved in overland and oceanic regions further from wet/dry boundary and thalwegs

In addition to resolving the coastline, thalwegs were also resolved with higher resolution (Figure 4.6). The thalwegs were entered into OM2D as an array of coordinate points, broken up by each individual channel and stream. OM2D established a resolution of 50 meters in the Georgia child mesh, while maintaining a resolution of 100 meters in the parent mesh of the surrounding SAB (Figure 4.7).

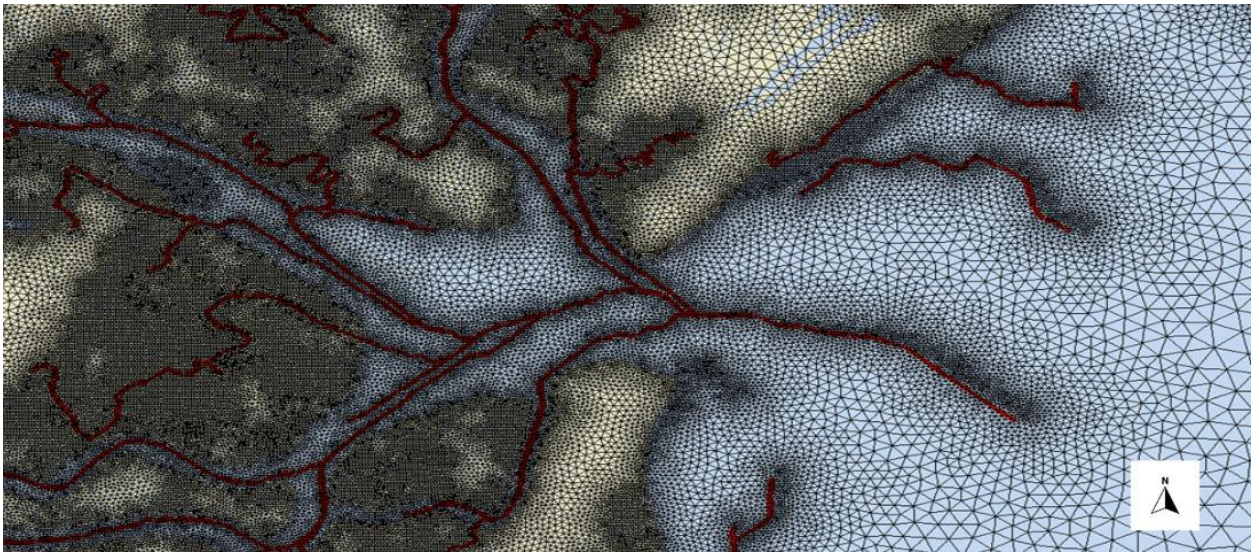

Figure 4.6 Increased mesh resolution surrounding thalwegs, illustrated with a red line

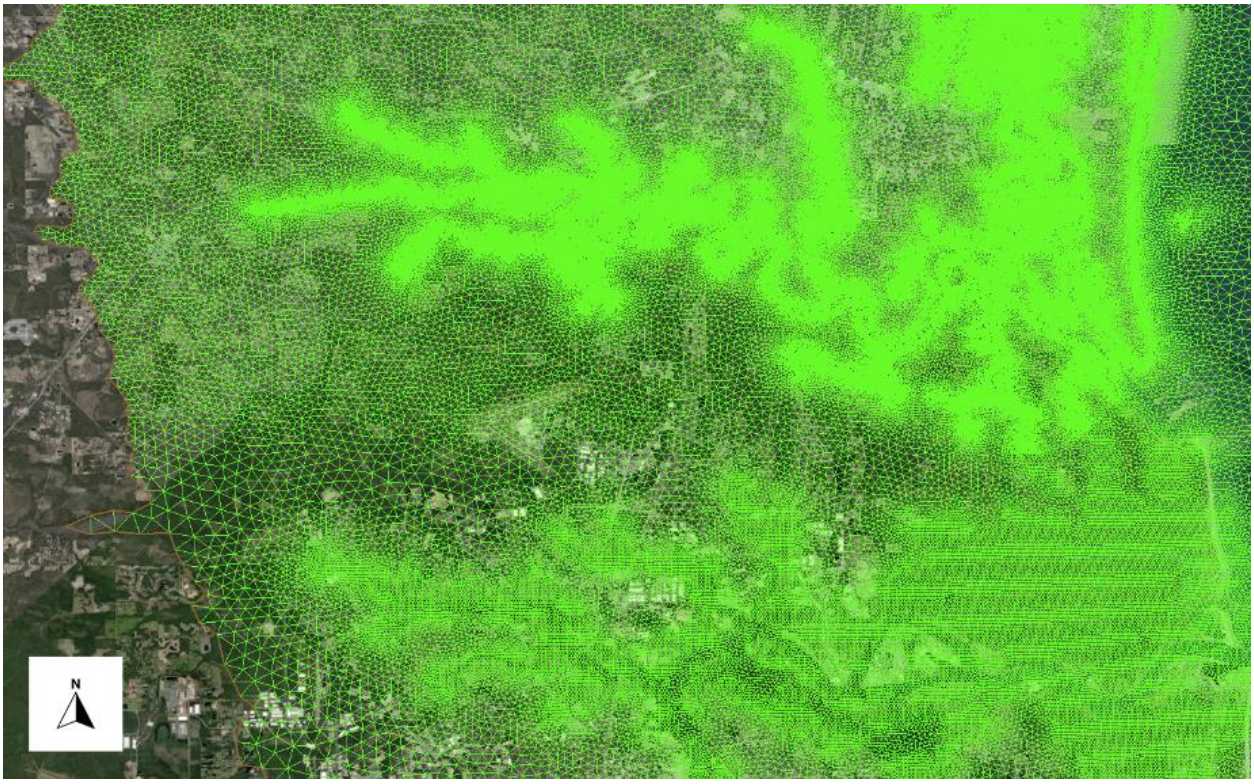

Figure 4.7 Thalweg resolution differences over child and parent meshes, next to one another

The resulting mesh had high resolution surrounding both the coastlines and the thalwegs (Figure 4.8). Mesh resolution differed in oceanic and floodplain regions to optimize computational cost. Mesh node points were held along the coastline, using a built-in size function within OM2D and then entering those points into the *pfix* array (Figure 4.9).

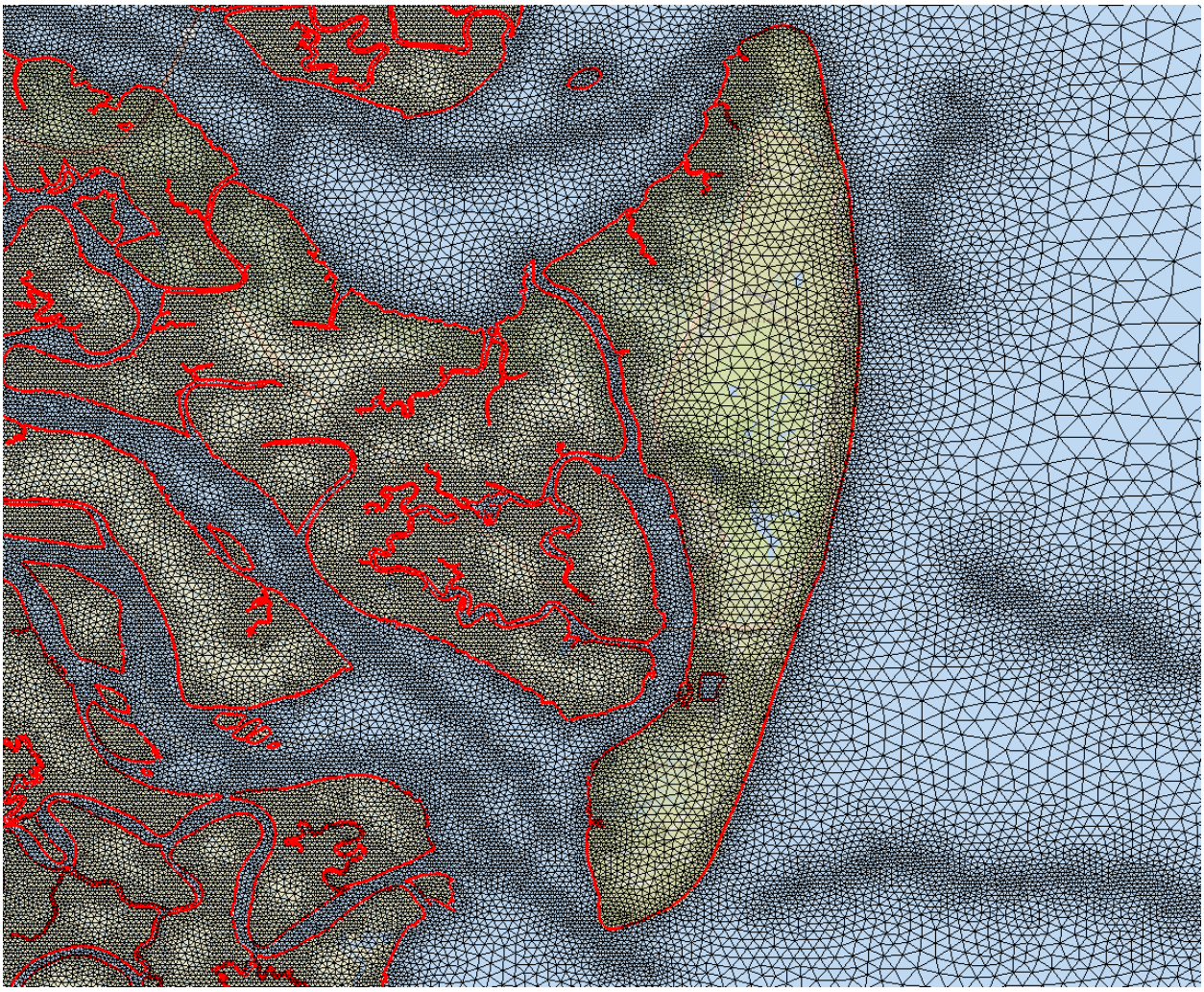

Figure 4.8 Mesh focused on Jekyll Island, GA, with coastline outlines in red

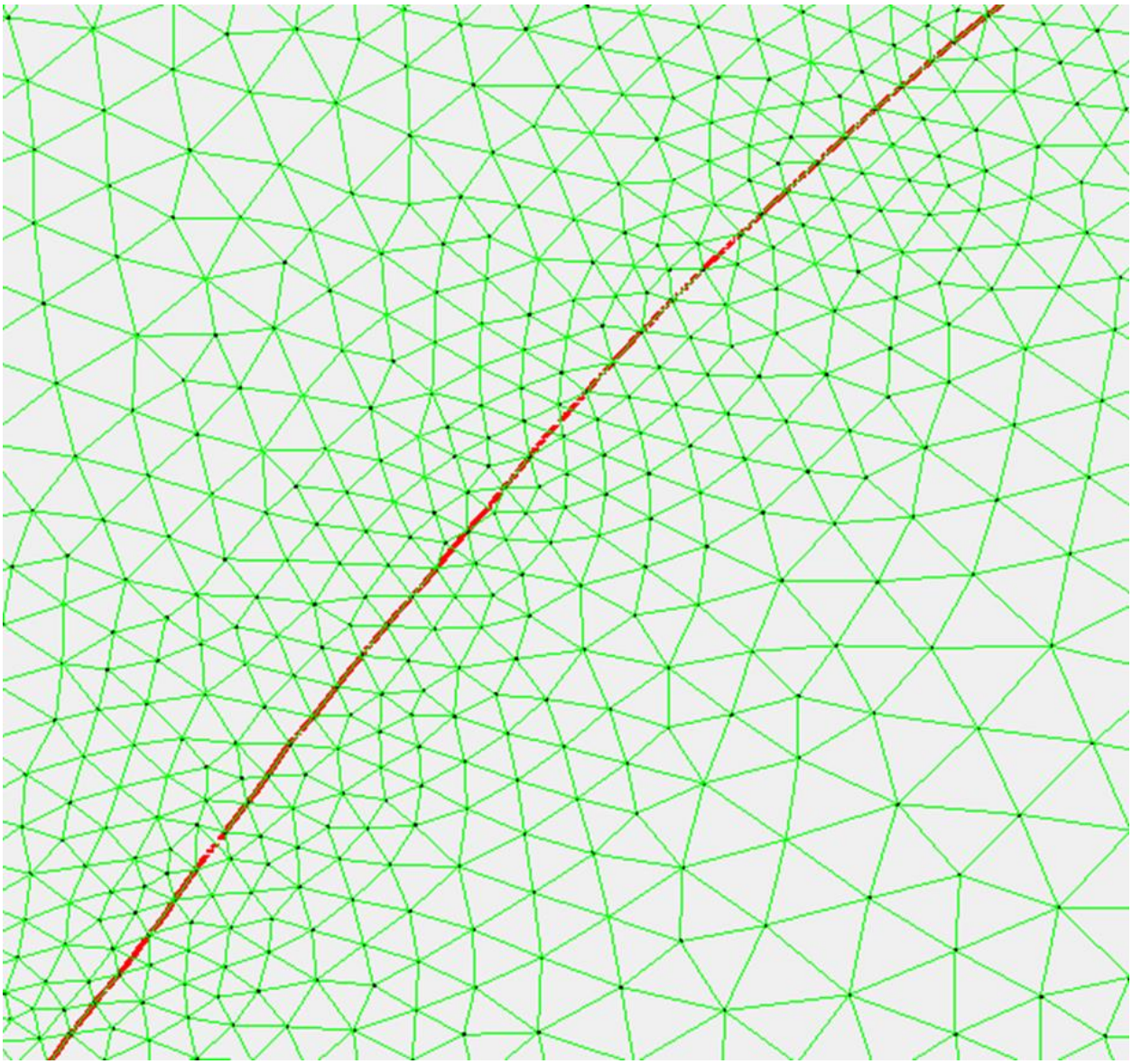

Figure 4.9 Mesh zoomed in on node points appended to the coastline, outlined in red

Lastly, VF points extracted using PyVF were appended to the *pfix* array, and resolved as nodes in the finalized mesh (Figure 4.10). These points were delineated using a size function built in SMS, in order to separate VF nodes from each other based on the grid spacing in each VF's respective location.

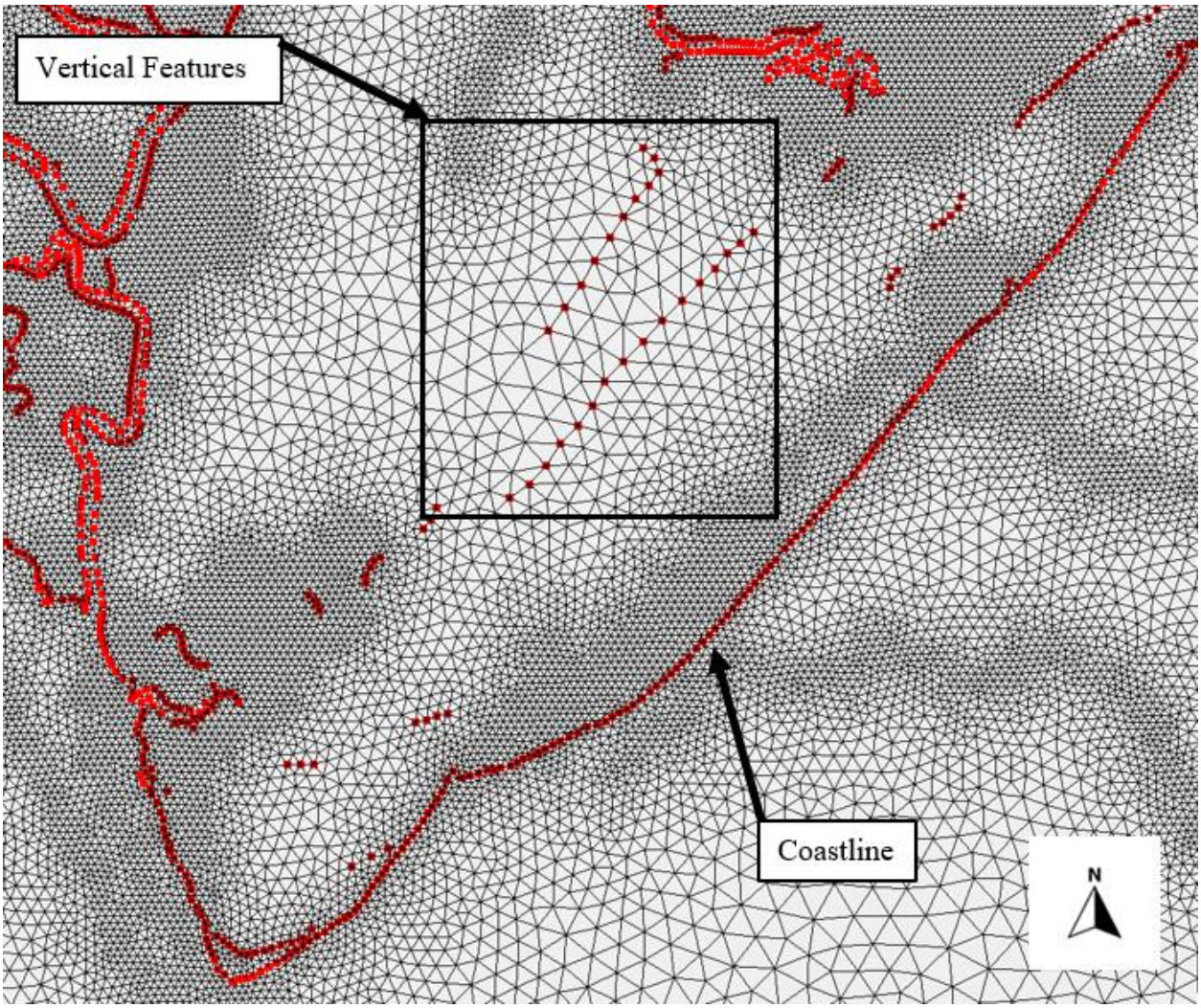

Figure 4.10 VF and coastline points held as node points in the mesh

4.2 | ADCIRC Tidal Run and Validation

A generic ADCIRC tidal simulation was performed using the finalized unstructured mesh. This tidal simulation aimed to see the precision of the mesh when simulated under normal, non-cyclonic conditions. Six different NOAA tidal gauges were utilized for observed data collection to be compared with the ADCIRC simulation: Fort Pulaski, GA; South Ossabaw Island, GA; South Newport River, GA; Saint Simons Island, GA; Kings Bay, GA; and Mayport Basin, FL (Figure 4.11). Each tidal location's observed tidal harmonics were collected from the NOAA Tides and Currents site, and compared to the simulated ADCIRC tides.

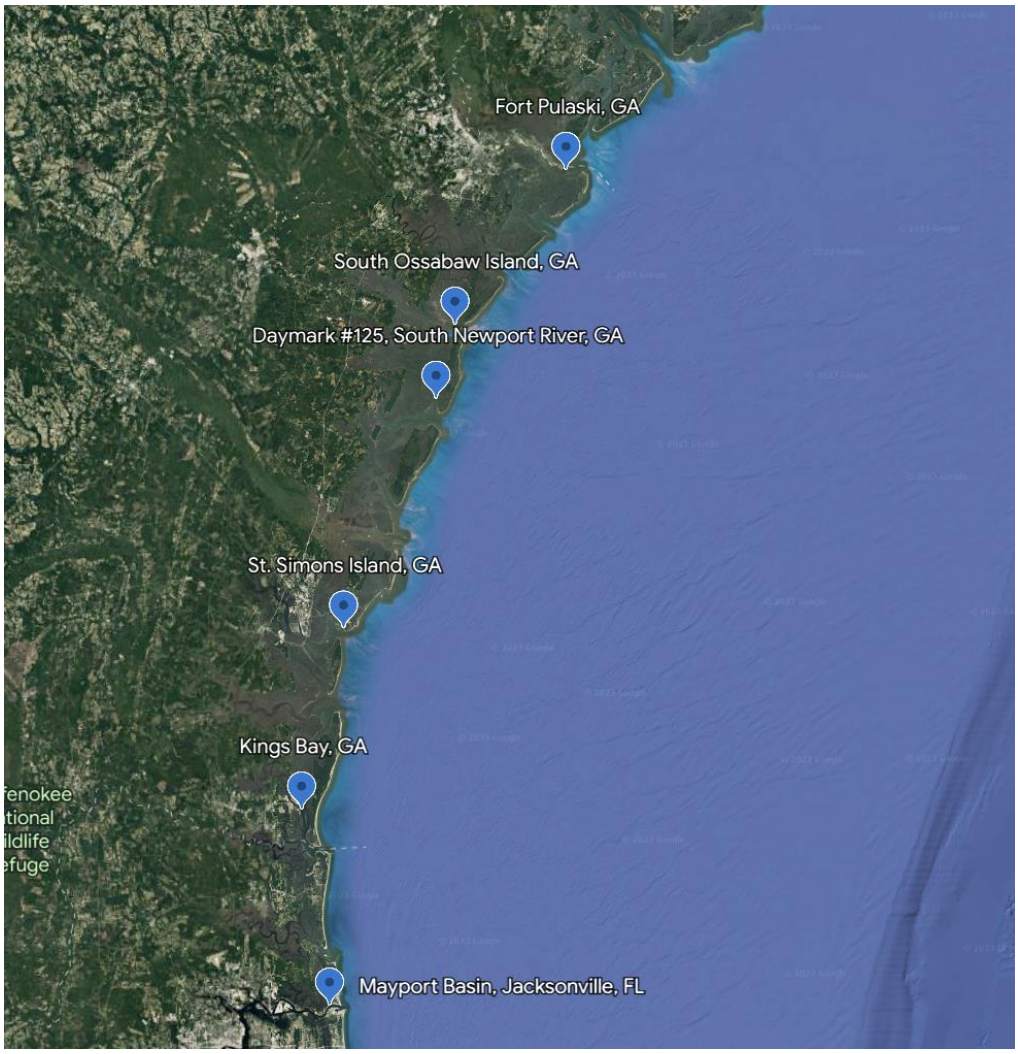

Figure 4.11 NOAA tide gauges utilized for observed data for comparison with ADCIRC tidal simulation

The simulated and observed tidal harmonic amplitudes and phases were utilized in a tidal synthesis. Root mean square error (RMSE) and mean square error (MSE) was measured for each station's ADCIRC comparison. Additionally, a regression analysis was performed and R^2 values were obtained (Figure 4.12 – 4.17). Tide gauges beyond the extent of the Georgia child mesh or along the boundary had higher MSE values, while gauges along the middle Georgia coast had lower MSE values. The Mayport, Jacksonville, FL gauge had the largest deviation between the two lines, and was additionally the only gauge in a region where no VFs were within the mesh.

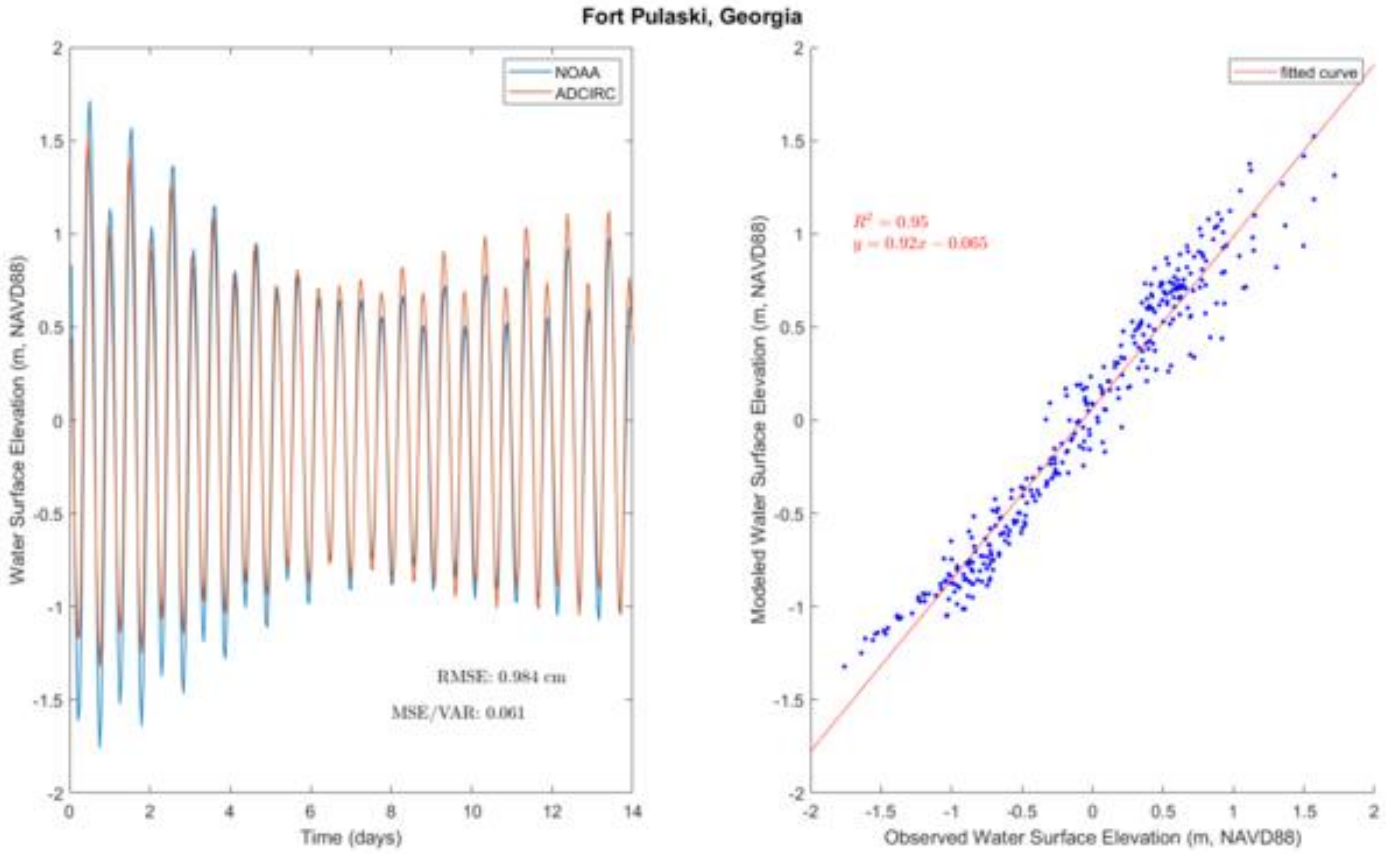

Figure 4.12 Fort Pulaski, Georgia NOAA tidal gauge observed versus simulated results and regression analysis

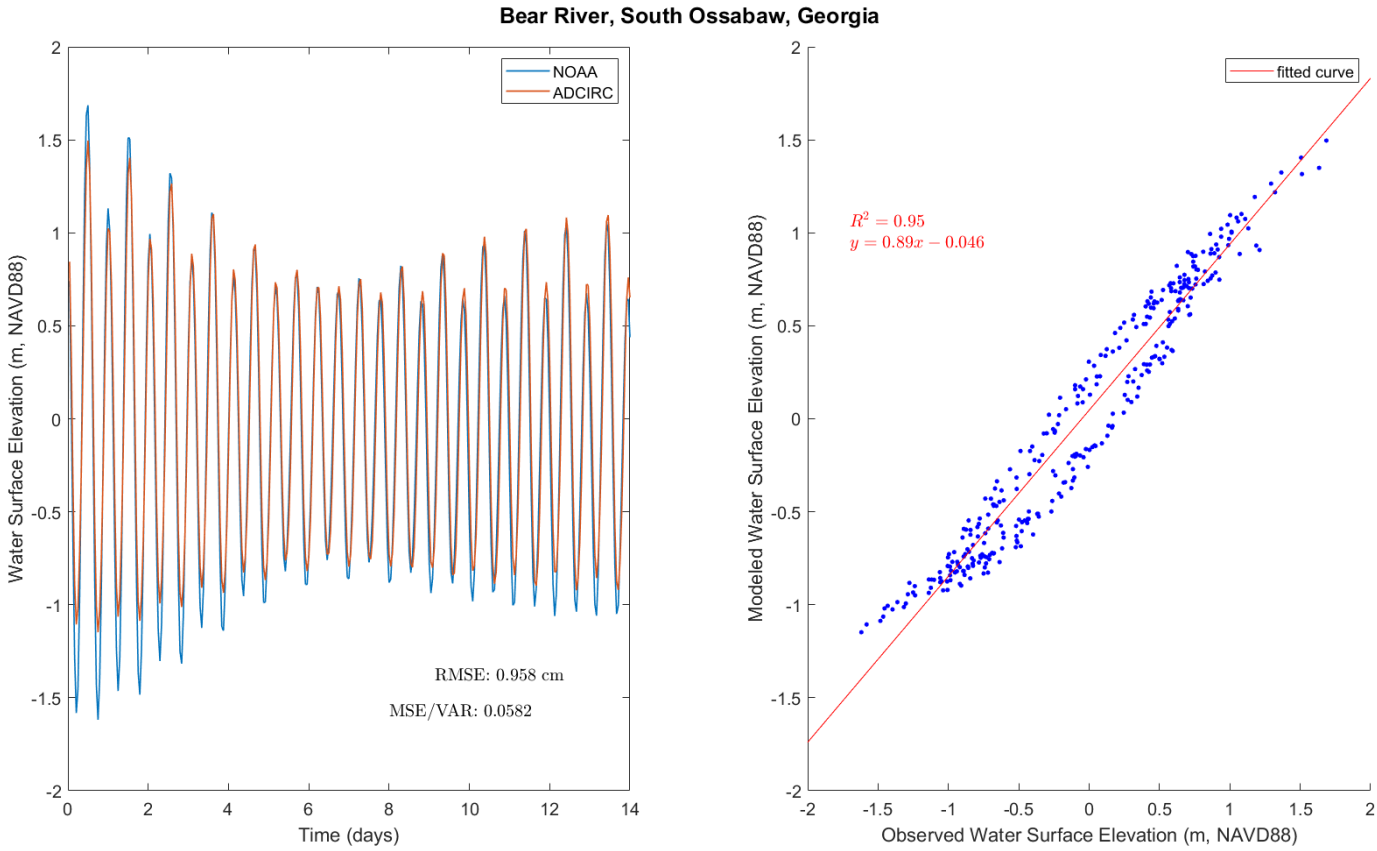

Figure 4.13 Bear River, South Ossabaw, Georgia NOAA tidal gauge observed versus simulated results and regression analysis

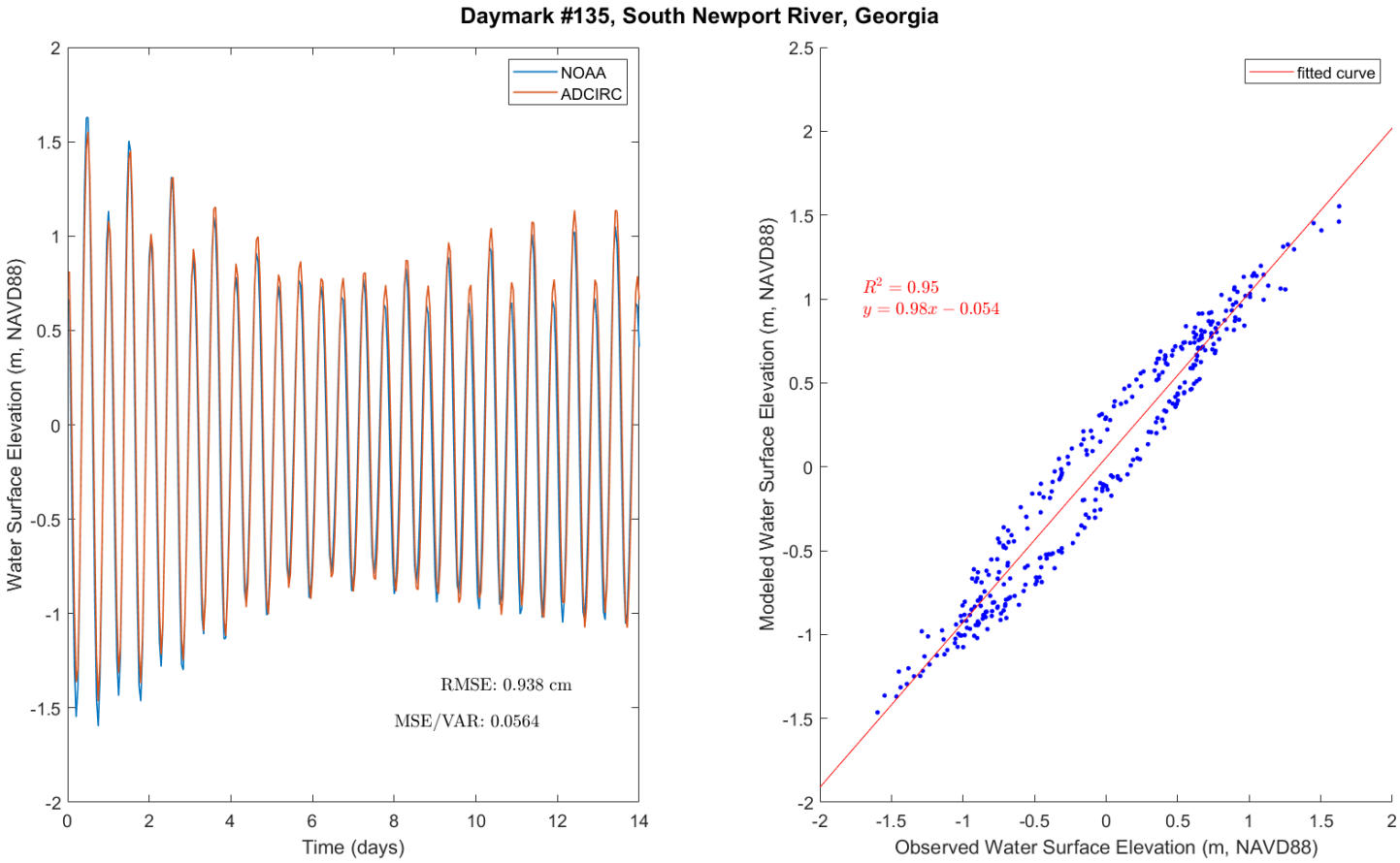

Figure 4.14 Daymark #135, South Newport River, Georgia NOAA tidal gauge observed versus simulated results and regression analysis

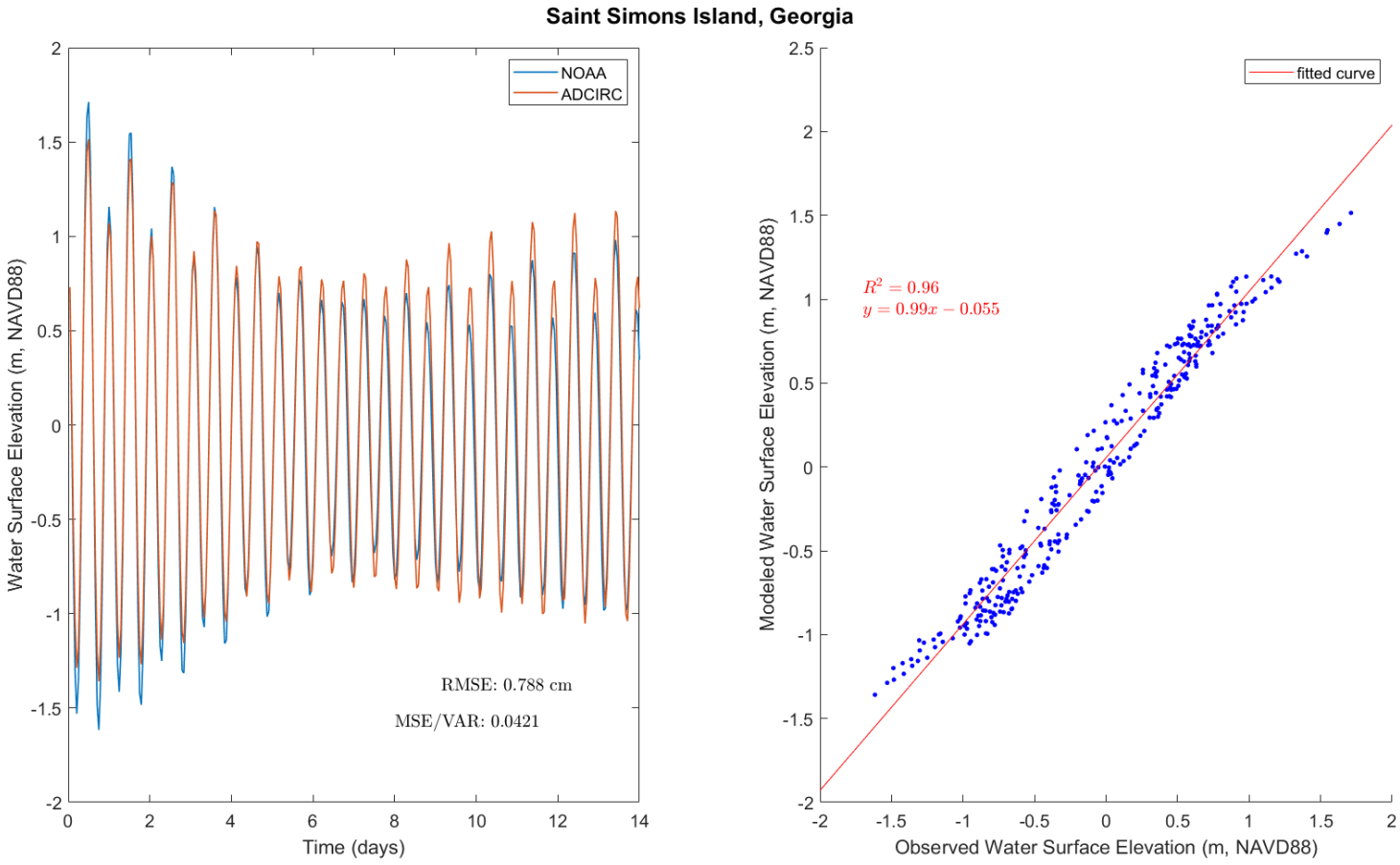

Figure 4.15 Saint Simons Island, Georgia NOAA tidal gauge observed versus simulated results and regression analysis

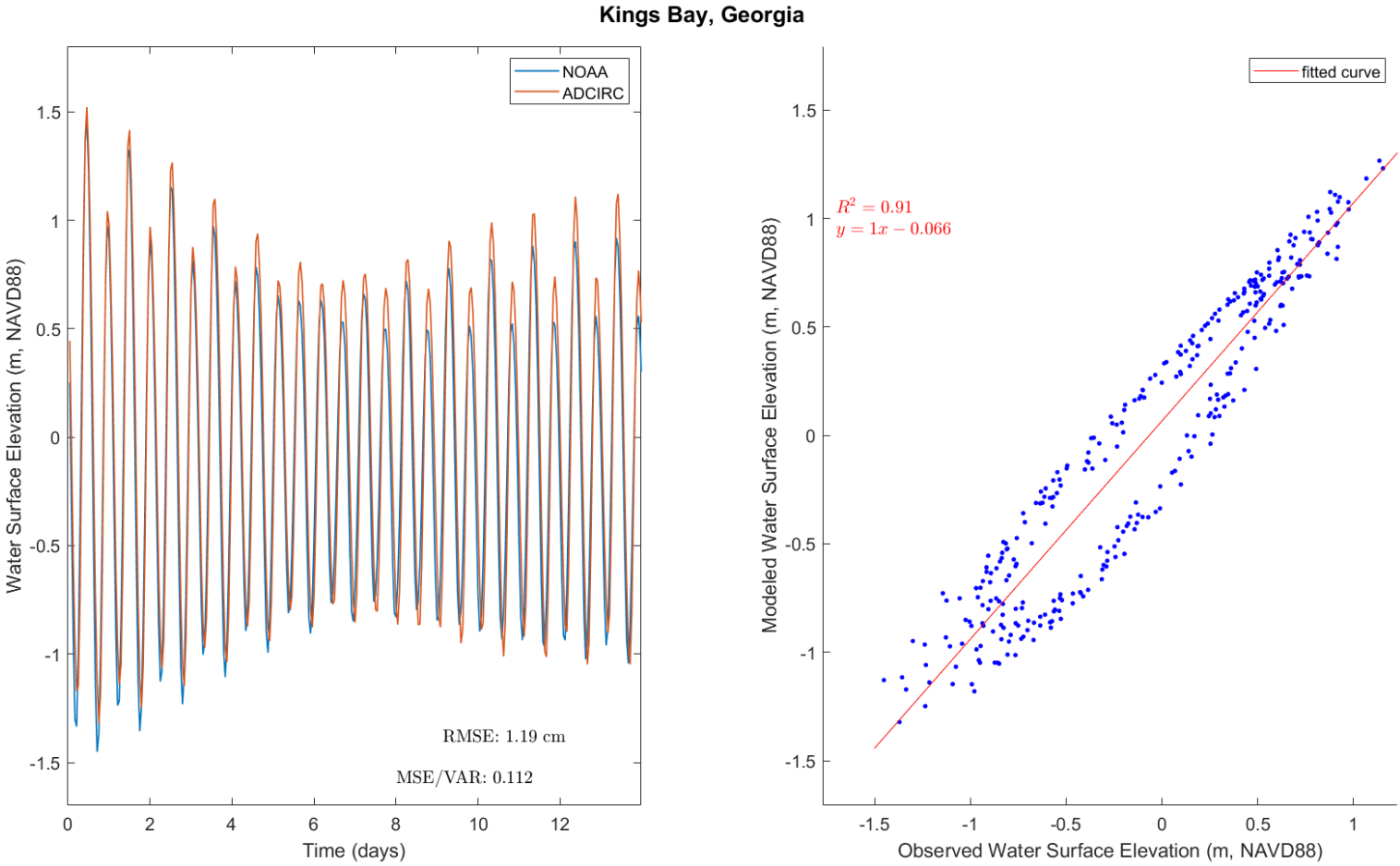

Figure 4.16 Kings Bay, Georgia NOAA tidal gauge observed versus simulated results and regression analysis

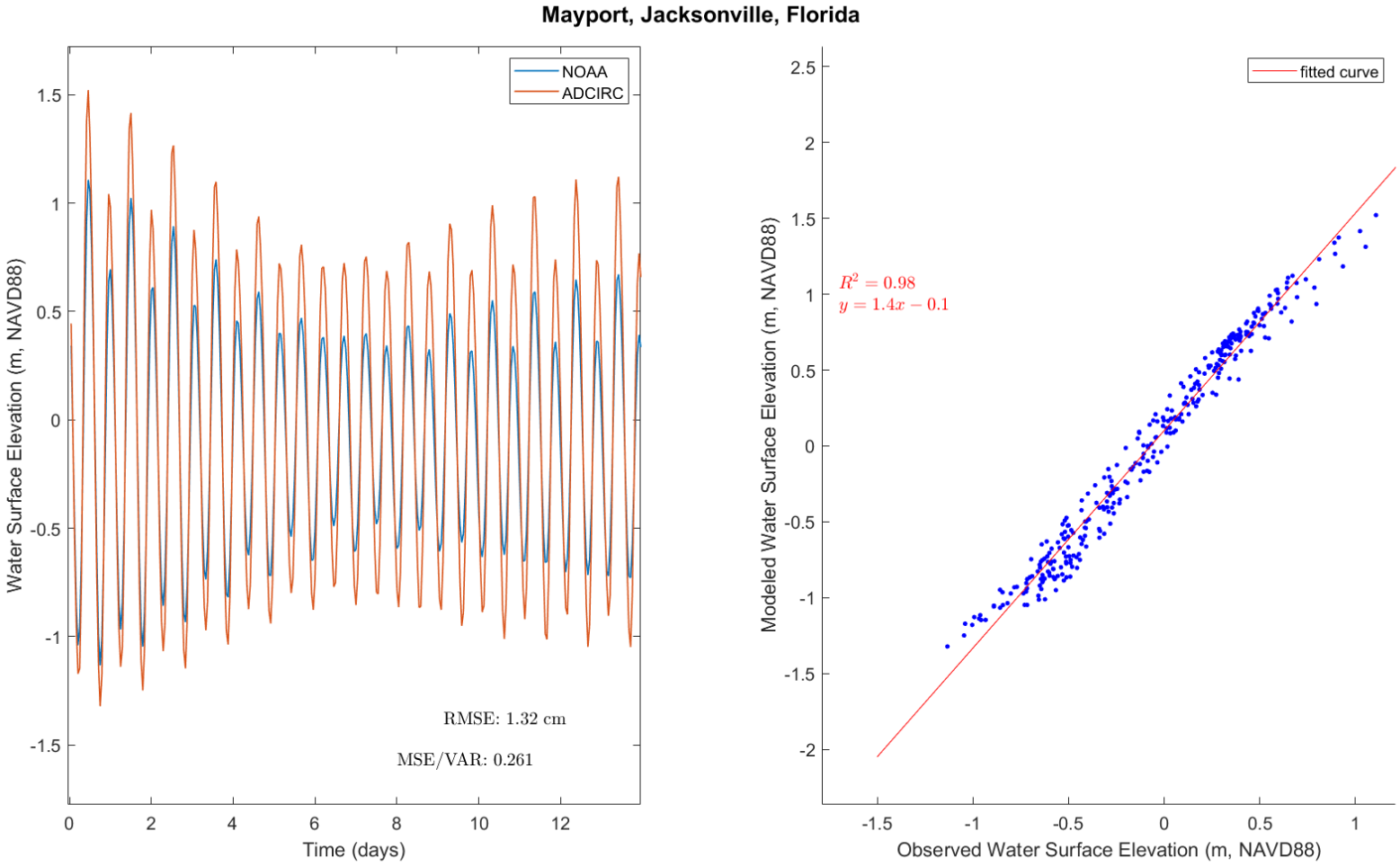

Figure 4.17 Mayport, Jacksonville, Florida NOAA tidal gauge observed versus simulated results and regression analysis

The finalized mesh was then utilized in ADCIRC for a simulation of Hurricane Matthew (2016). In order to run an ADCIRC simulation, required files indicating Hurricane Matthew's path and intensity were acquired and entered into ADCIRC (Figure 4.18). Hurricane Matthew made landfall along the coast of South Carolina, but caused coastal flooding across the SAB (Figure 4.19).

Figure 4.18 Hurricane Matthew (2016) eye path, with strength indicated by color (red being strongest and blue being weakest)

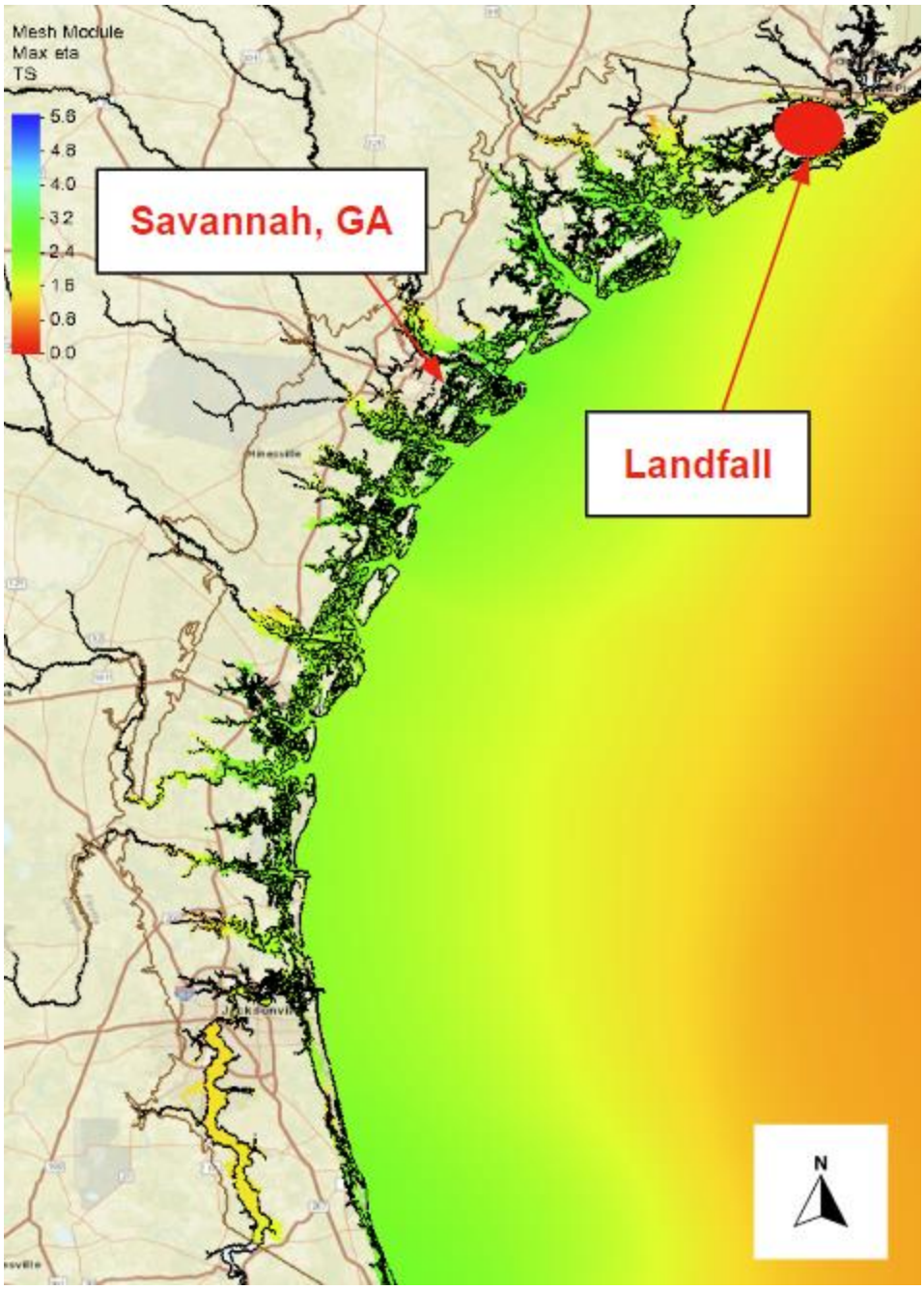

Figure 4.19 Hurricane Matthew coastal inundation map, with landfall location indicated

The Hurricane Matthew simulation modeled the storm surge for the entire SAB, but observed data was only compared to the ADCIRC results in the tidal gauges closest to Georgia. Three NOAA tide gauges chosen to compare against modeled ADCIRC results: the Fort Pulaski, Georgia Tide Gauge; the Fernandina Beach, Florida Tide Gauge; and the Mayport Basin, Florida Tide Gauge (Figure 4.20).

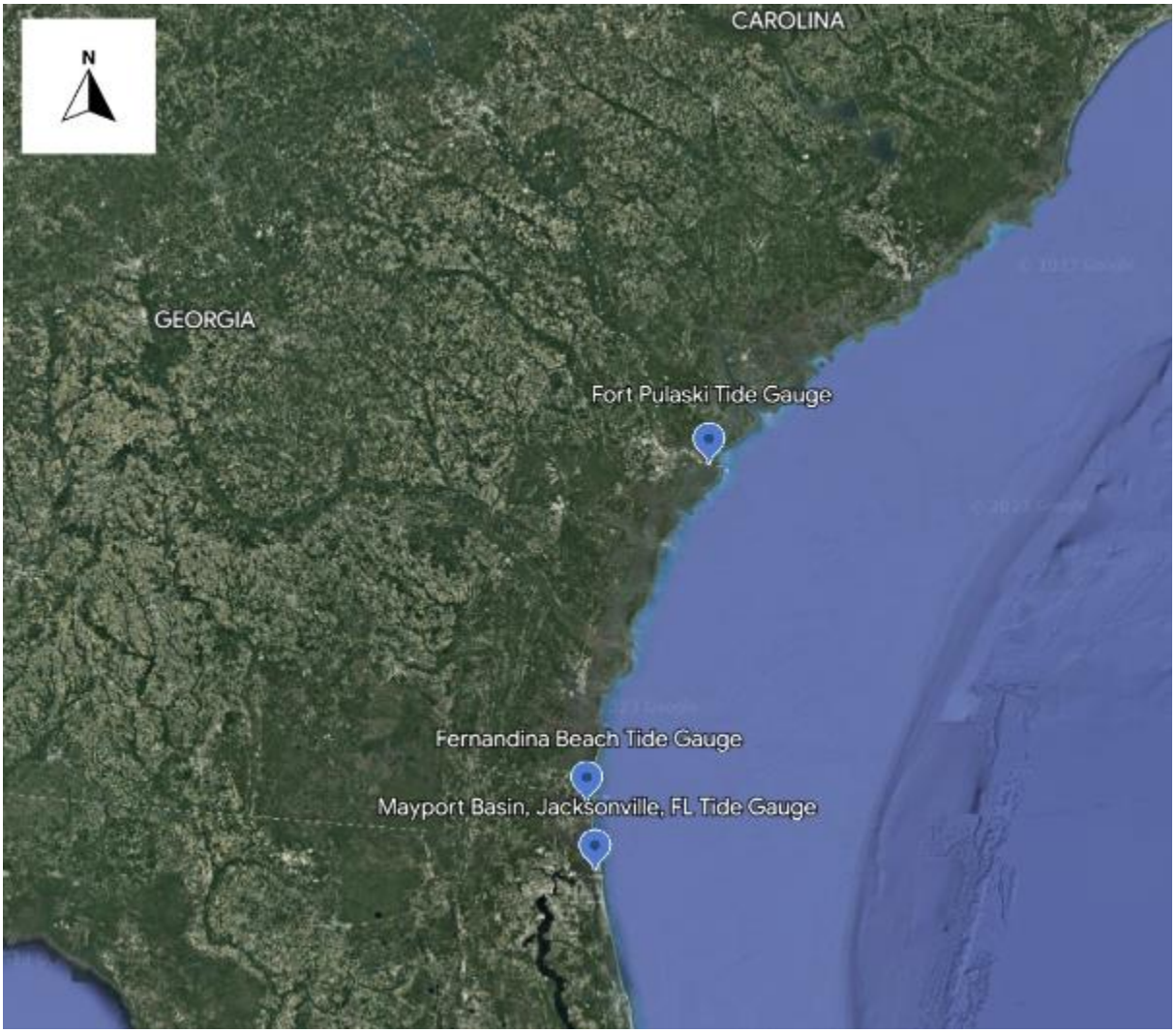

Figure 4.20 NOAA tides and currents gauges used for comparison to ADCIRC simulation

Data from each gauge was extracted for the lifespan of Hurricane Matthew, including days before and after landfall. The data in each circumstance was then compared to the simulated floodwater heights at each gauge point from ADCIRC. The highest storm surge height simulated occurred at the Fort Pulaski tide gauge, which additionally featured the most accurate simulated storm surge value (Figure 4.21). At peak surge, modeled surge was simulated to be 2.6 meters, while the observed value was 2.48 meters, a difference of only 0.12 meters. Additionally, at the first surge peak, modeled surge was only .7m above the observed values.

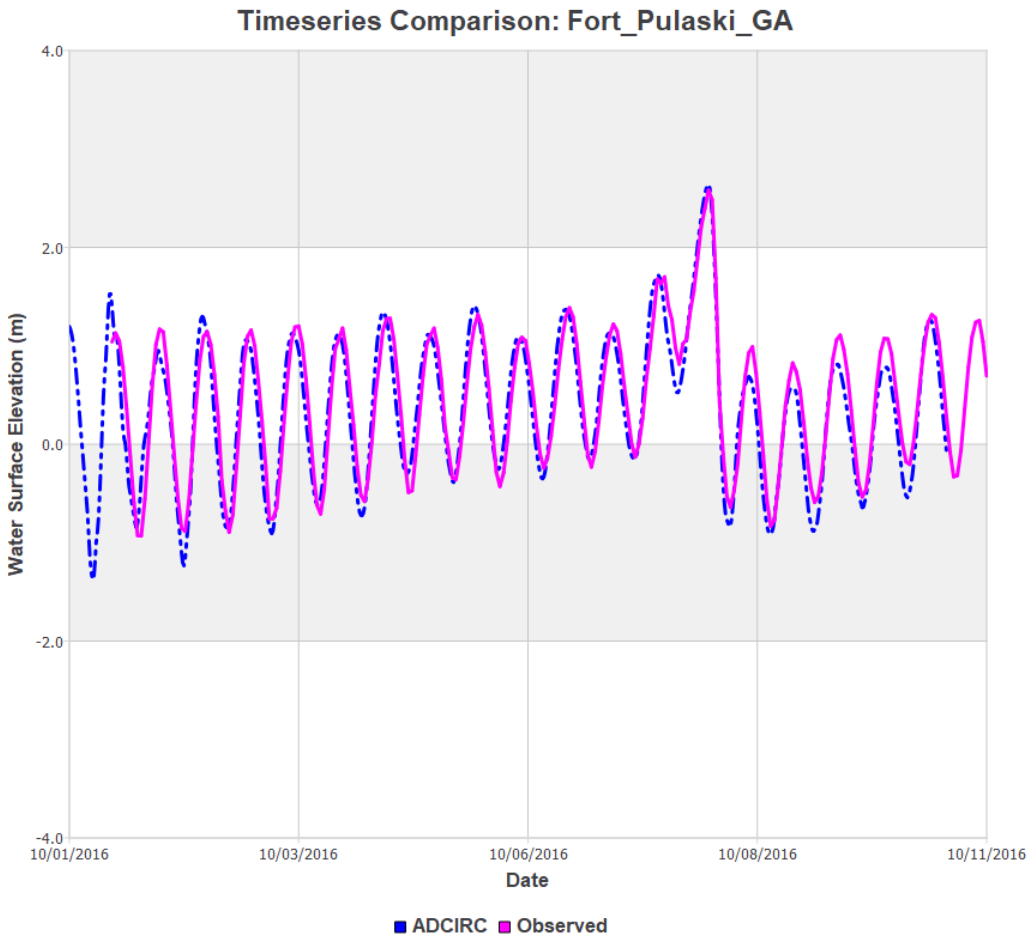

Figure 4.21 Fort Pulaski gauge observed data from Hurricane Matthew (2016) compared to ADCIRC simulated storm surge

At the Fernandina Beach, FL tidal gauge, simulated surges were also highly accurate. Peak surge simulated was estimated at 2.23 meters, whereas measured surge was at 2.06 meters (Figure 4.22). This tidal gauge is just south of the Georgia state border, thus meaning any VFs north of the gauge were resolved, while VFs south were not. Due to the proximity of the gauge to the high-resolution child mesh, mesh resolution remained high in this region.

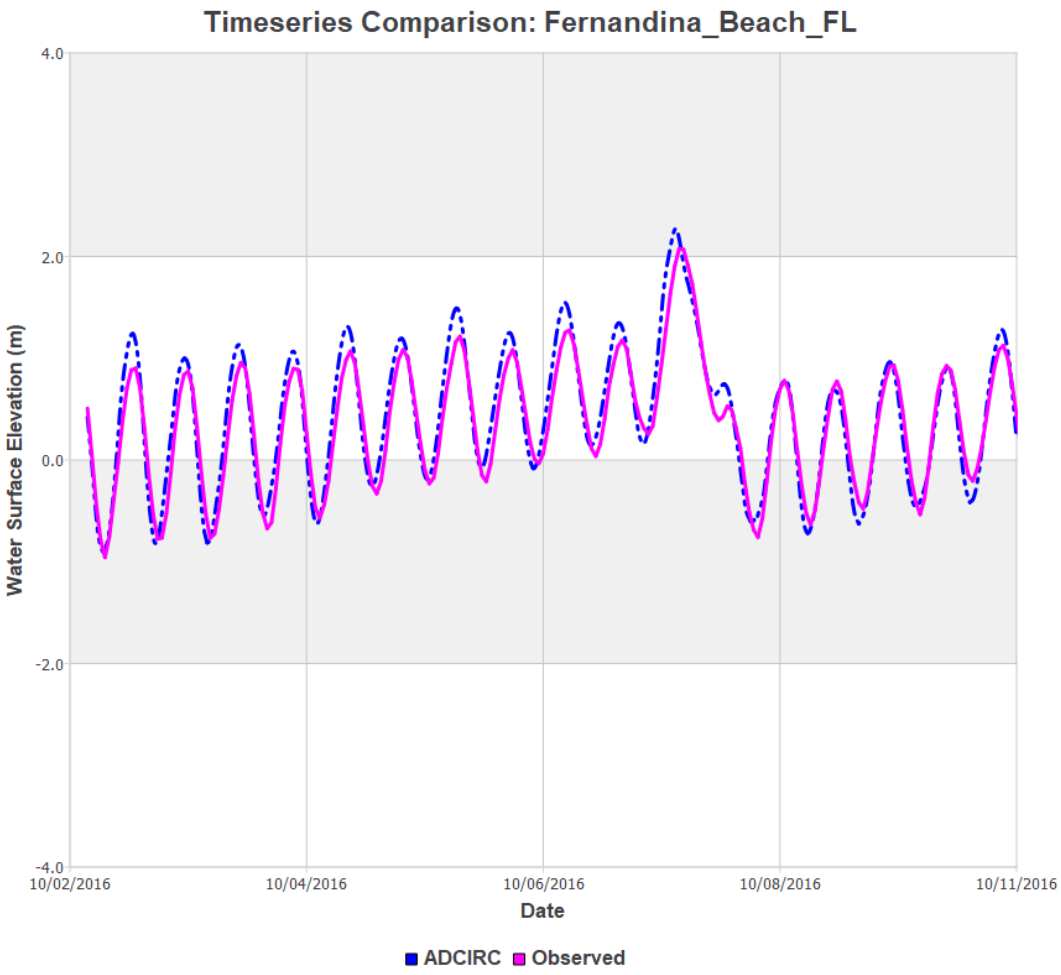

Figure 4.22 Fernandina Beach gauge observed data from Hurricane Matthew (2016) compared to ADCIRC simulated storm surge

At the Mayport, Jacksonville, FL tidal gauge, simulated surges were not as accurate as the other two sites. Peak surge simulated was estimated at 2.01 meters, whereas measured surge was at 1.55 meters (Figure 4.23). This tidal gauge is further south into Florida, thus meaning any VFs both north and south of the gauge were not resolved. Additionally, mesh resolution was lower in this region due to the distance from the high-resolution Georgia child mesh.

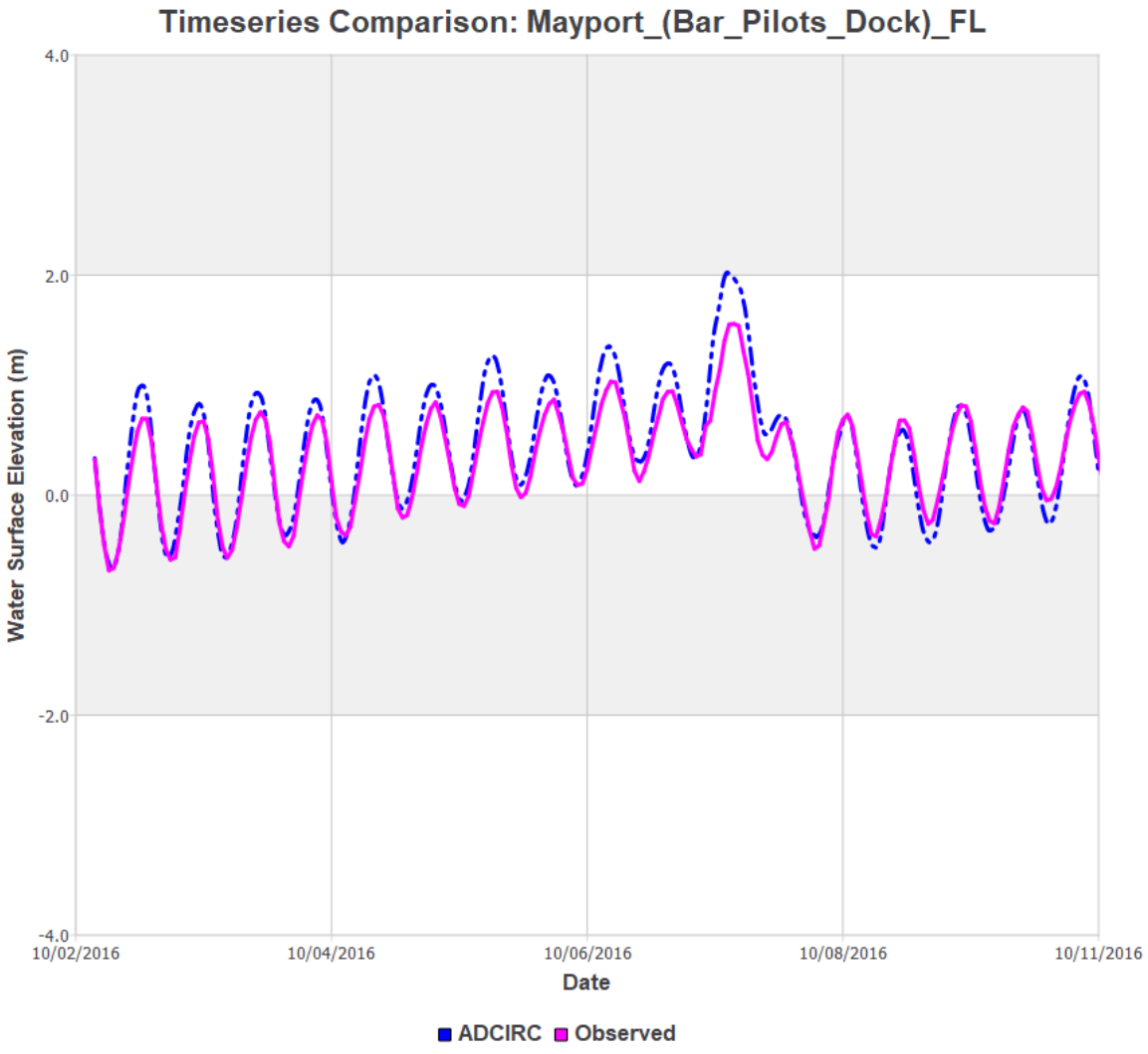

Figure 4.23 Mayport, Florida gauge observed data from Hurricane Matthew (2016) compared to ADCIRC simulated storm surge

The simulated ADCIRC results were additionally overlaid on the mesh domain to visualize extent of storm surge inundation. The mapped flood regions represent the maximum extent of Hurricane Matthew's storm surge across the extent of the storm at each region (Figure 4.24 - 4.27). Due to Hurricane Matthew's landfall in South Carolina, storm surge values were higher in northern coastal Georgia than the southern coast. Additionally, the north ends of the mainland and barrier islands experienced higher storm surge values than other areas of the island. Simulated storm surge inundation maps for northern coastal Georgia and southern coastal Georgia are visualized in Figures 4.24 and 4.26, respectively. Maps of northern coastal Georgia and southern coastal Georgia without overlaid flood inundation are visualized in Figures 4.25 and 4.27, respectively.

In addition, the maximum inundation map was contrasted with a map of the VFs used as a part of the mesh generation process. An example of the maximum flood map with VFs included is visualized in Figure 4.28, with a map of the region without floodwaters visualized in Figure 4.29.

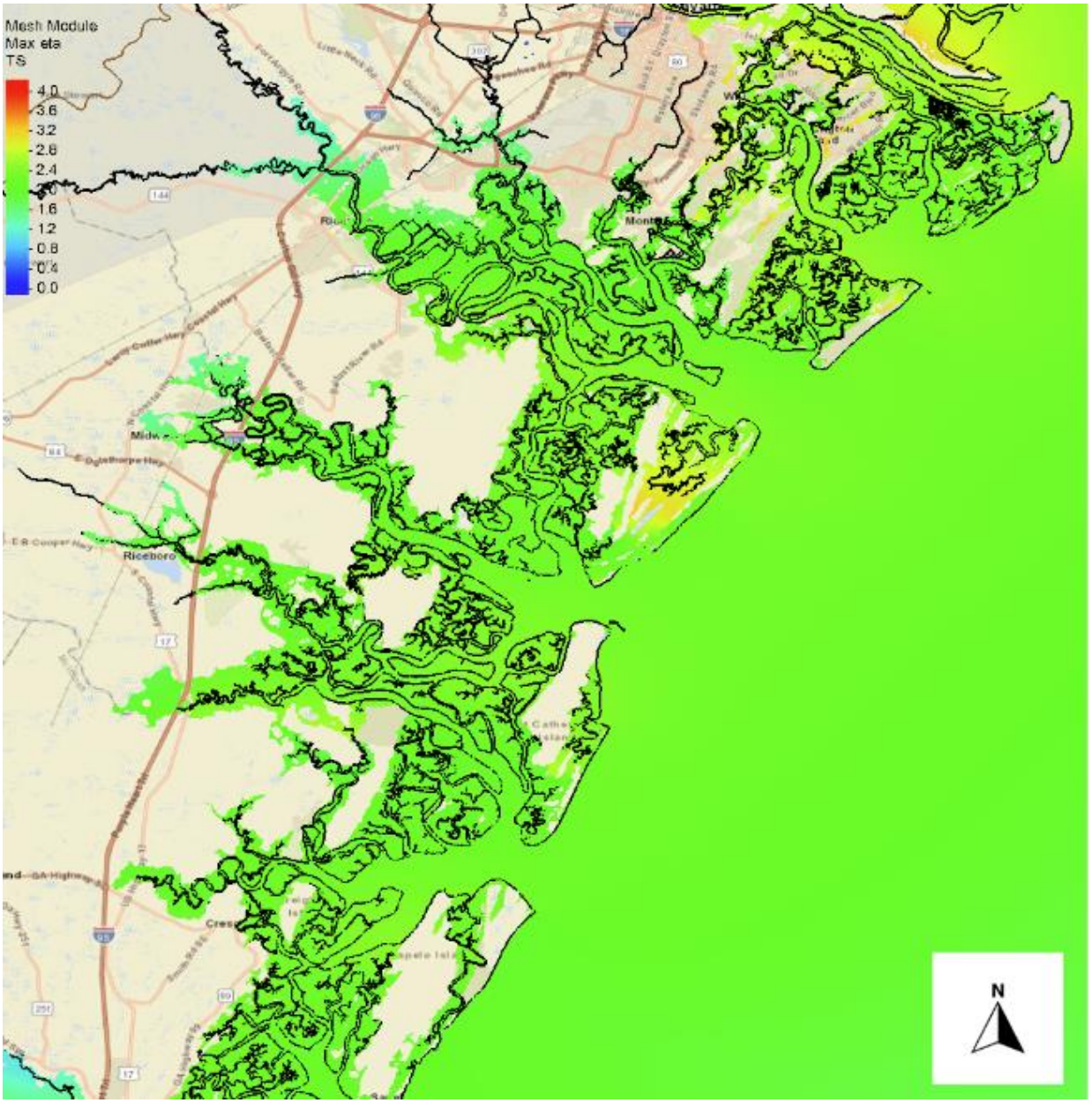

Figure 4.24 Coastal inundation of northern coastal Georgia during Hurricane Matthew (2016) simulated by ADCIRC

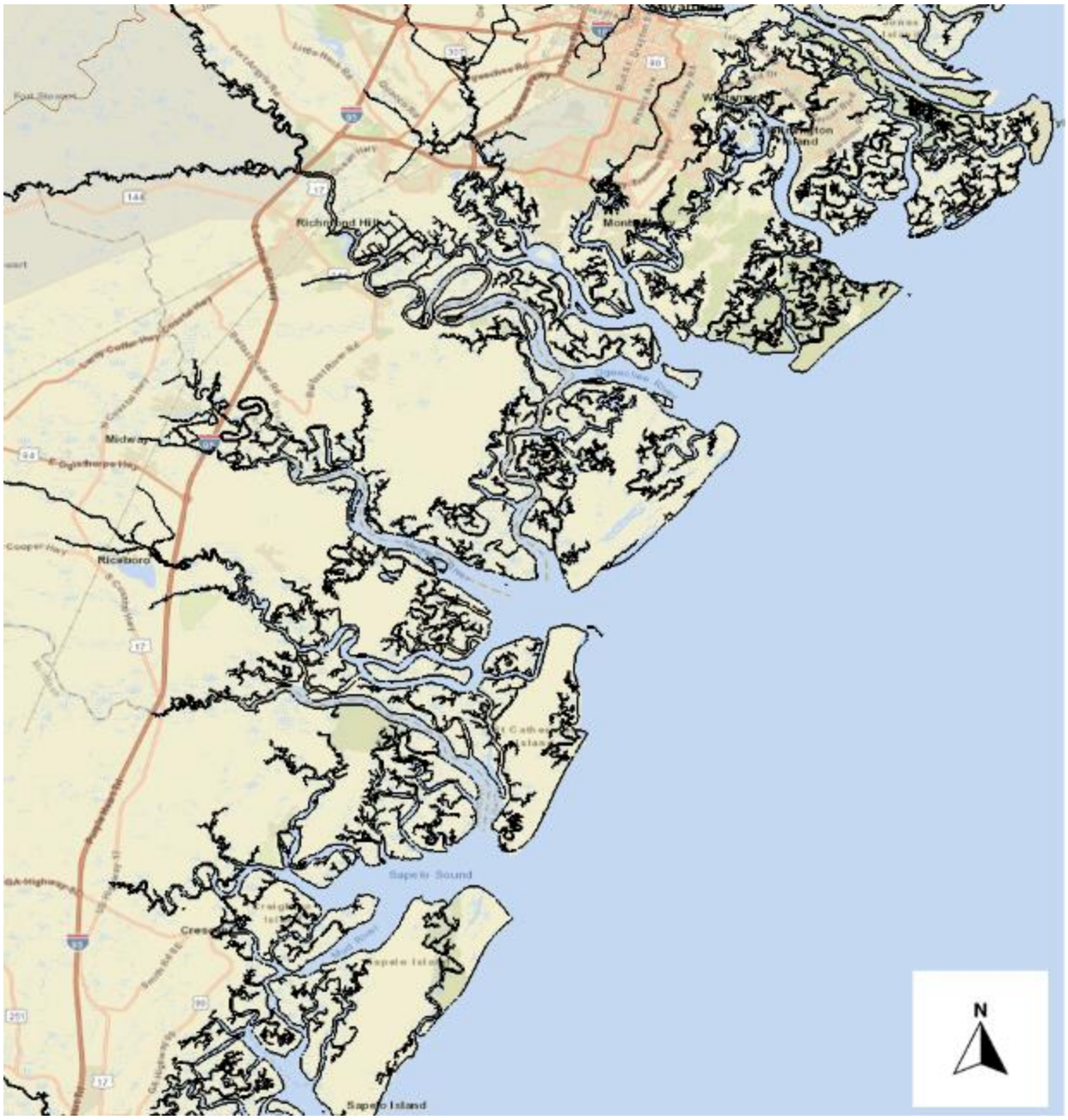

Figure 4.25 Northern coastal Georgia without mapped floodwaters

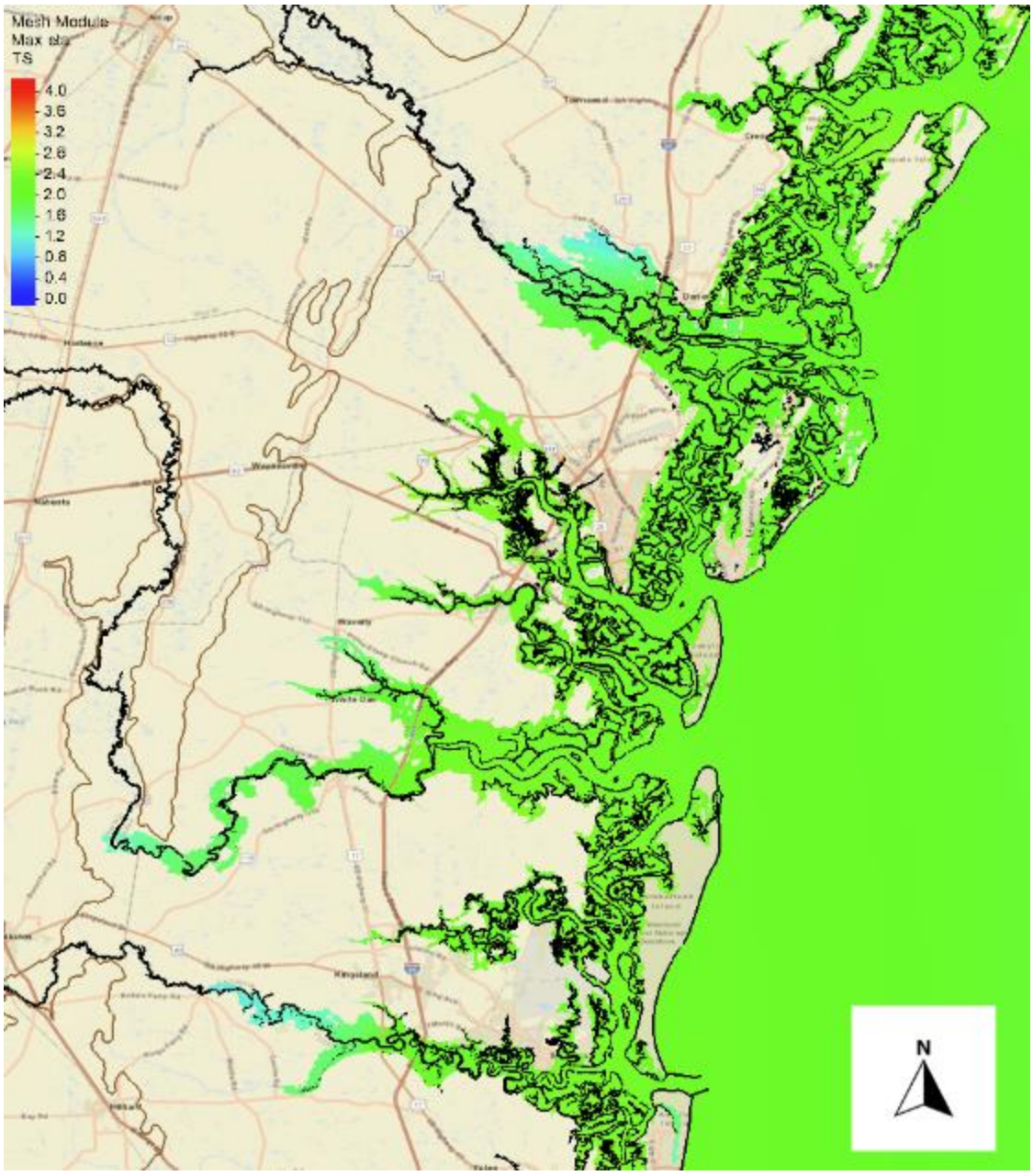

Figure 4.26 Coastal inundation of southern coastal Georgia during Hurricane Matthew (2016) simulated by ADCIRC

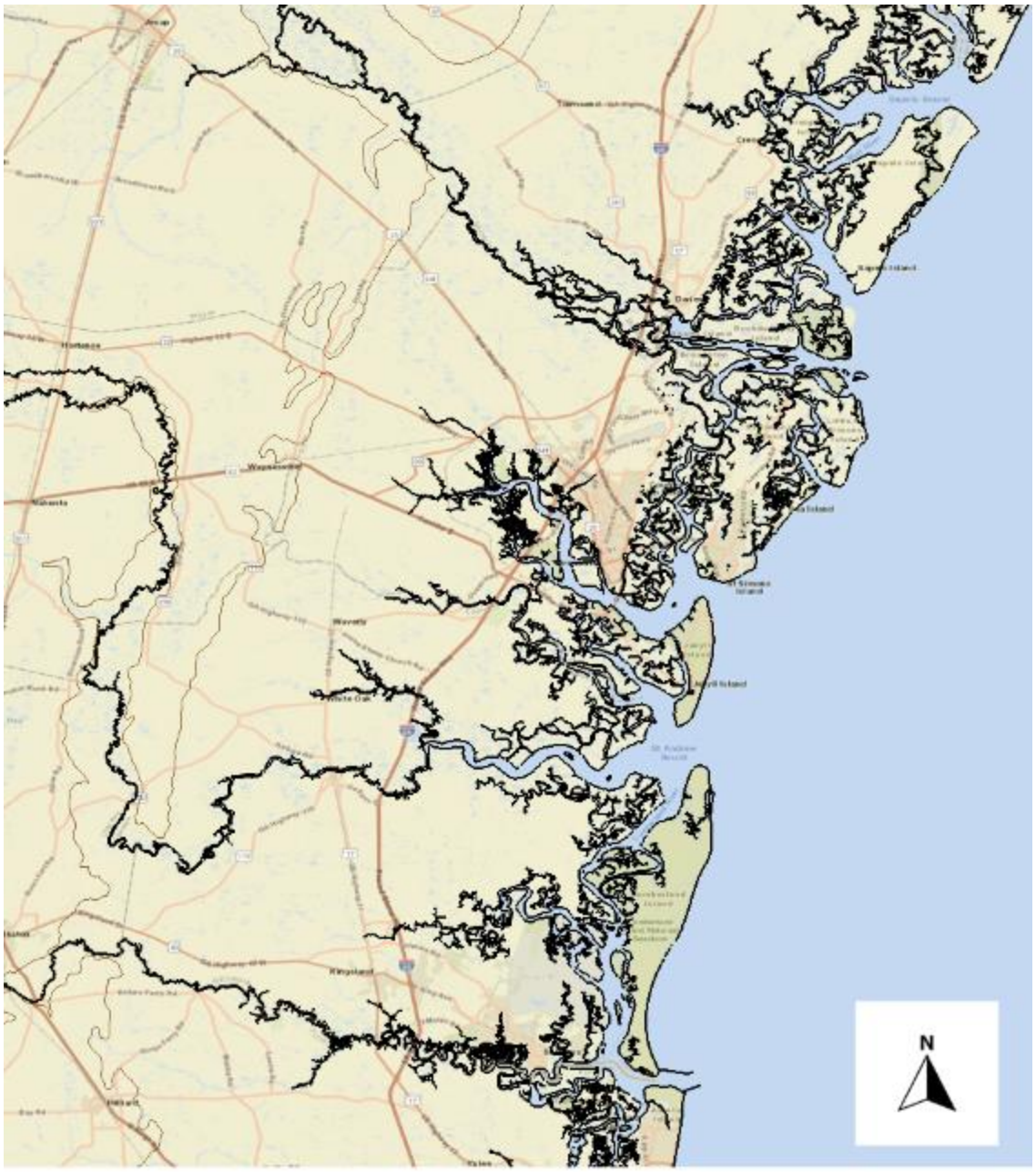

Figure 4.27 Southern coastal Georgia without mapped floodwaters

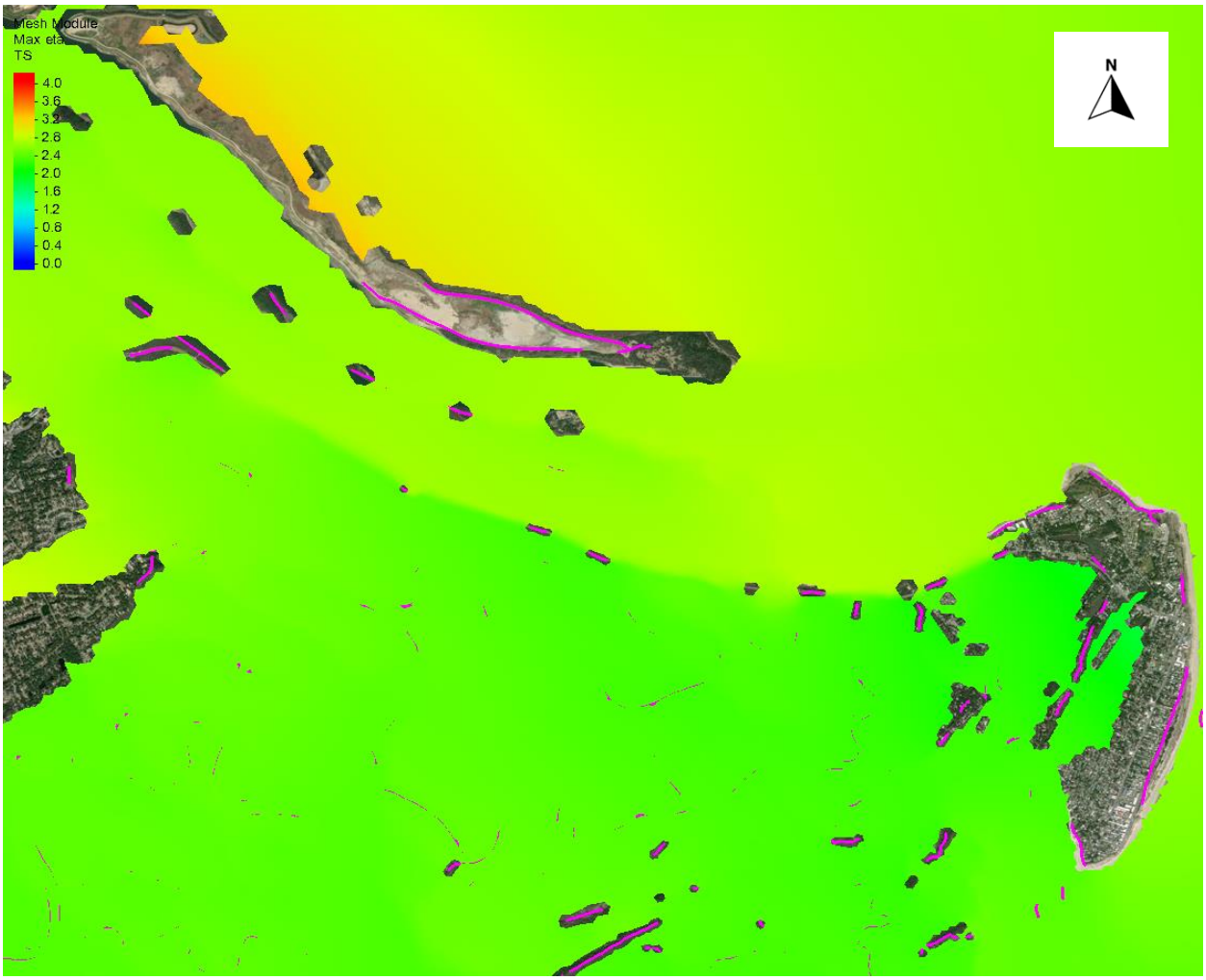

Figure 4.28 Coastal inundation of Outer Savannah, GA and Tybee Island, GA during Hurricane Matthew (2016) simulated by ADCIRC, with VFs outlined in pink

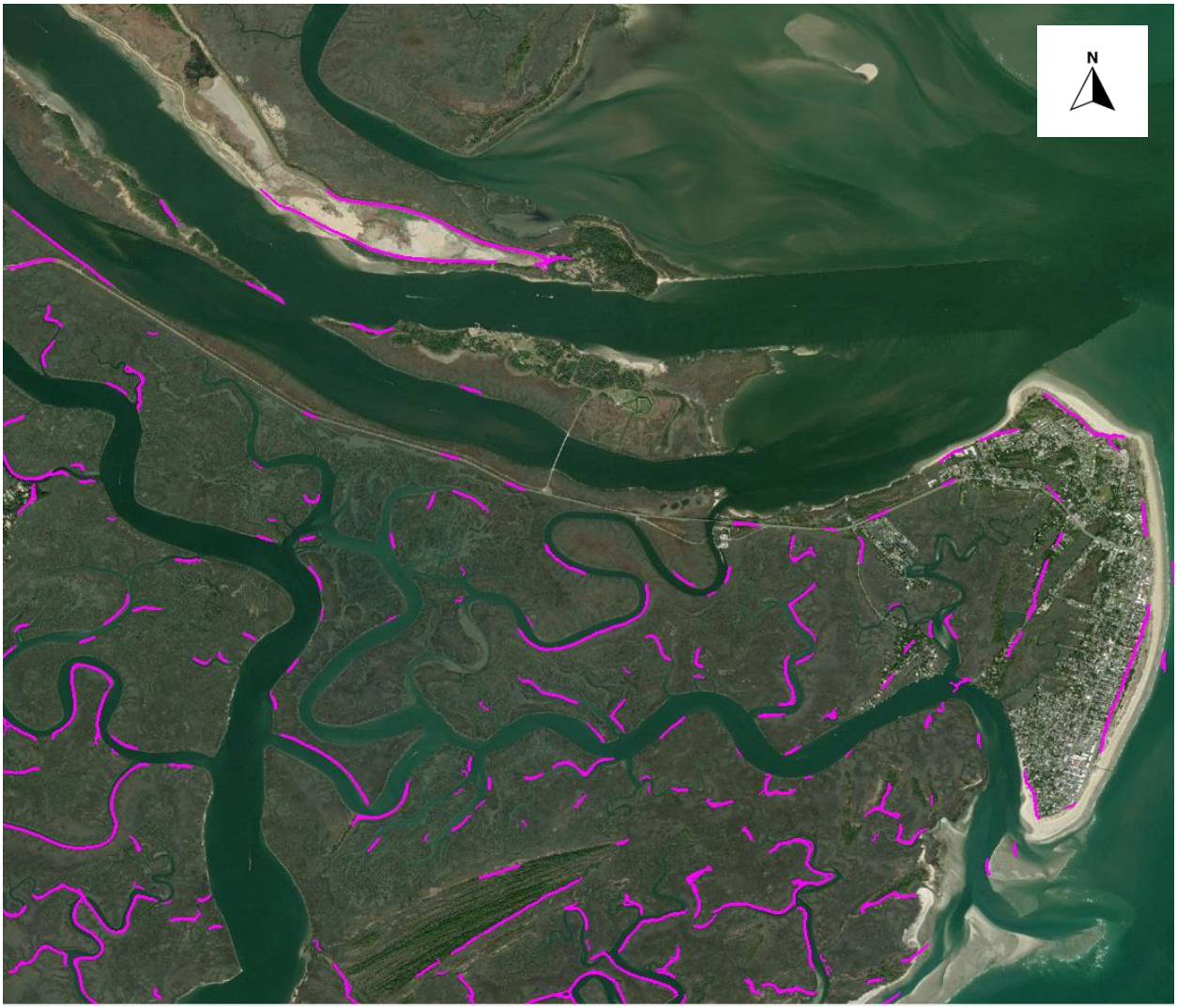

Figure 4.29 Outer Savannah, GA and Tybee Island, GA without mapped floodwaters

5.0 | DISCUSSION

5.1 | Research Significance

Real-time storm surge prediction as well as synthetic storm surge research occurs using a variety of different hydrodynamic models, of which ADCIRC is one of the most prominent (Dietrich et al., 2012; Turan et al., 2018). ADCIRC uses an unstructured mesh as the spatial discretization. There are numerous large domain meshes developed for storm surge modeling, including the SACS mesh developed by the U.S. Army Corps of Engineers (Woodruff et al., 2023). The SACS mesh was generated using two different mesh generation technologies: one for the overland floodplain and another for the wet region. For comparison, the mesh developed for this thesis used only one meshing technology: OM2D.

OM2D was developed with both floodplain and oceanic meshing in mind, and through using an array of different functions, a seamless floodplain-oceanic mesh was able to be developed on a large scale (Roberts et al., 2019). The inclusion of a large scale 1-meter resolution DEM in developing a high-resolution, large domain mesh additionally is significant in developing an effective mesh. The DEMs used within the mesh both in guiding the meshing process as well as the topographic and bathymetric interpolation were developed within 4 years of this study, allowing for an updated coastal morphology profile.

The interpolation function used, PyDEM2GRD, developed by Bilskie, has been used on both large and small scale meshes. However, the smoothing functions integrated into PyDEM2GRD allows a meshes elevation profile to avoid any instabilities (M. V. Bilskie & Hagen, 2013). These smoothing functions used as a part of PyDEM2GRD are more robust than those built into OM2D or other elevation interpolation functions, and thus provided the finalized mesh a more operational mesh (M. V. Bilskie & Hagen, 2013; Roberts et al., 2019).

The SACS mesh as well as other research grade large domain meshes do not have VFs integrated into the mesh on as large of a scale as the finalized Georgia mesh developed as a part of this thesis (*South Atlantic Coastal Study (SACS)*, 2021). The extraction of VFs utilizing PyVF and subsequent appendage to node points in the mesh has only been performed on small scales prior to this research (M. V. Bilskie et al., 2015; Gao, 2021). The Georgia mesh was the first time a mesh generated included automatically extracted VFs were appended as node points on a state-wide scale using automated mesh generation technology.

5.2 | Future Work

One of the areas of future work is that of the VF delineation. When delineating the polylines from the DEM, the user is allotted the option to choose a value known as *dh*. This value represents the relative elevation of a geographical element compared to its surrounding terrain. In this study, a *dh* of 1.5 meters was chosen, meaning that all extruded features below 1.5 meters in height are disregarded, and read into the mesh as *null*. The reason that *dh* was set at 1.5 meters was to reduce the amount of computer processing time required to develop the VFs into a usable polyline. For example, a *dh* value of .25 meters resulted in over 270,000 polylines that needed to be processed, compared to around 17,000 for a *dh* of 2 meters.

Within an ADCIRC simulation and its respective mesh file, elevation values are known only for node points, and then linearly interpolated between those points. Therefore, if an extruded VF is not resolved with a node, ADCIRC will linearly interpolate that region based on the elevation of the surrounding areas. It is recommended that in future work within coastal inundation studies over Georgia that a lower *dh* value is used, which will result in more VFs being resolved into the mesh. How the VFs are resolved into node points additionally depends on element size of the

mesh. With smaller element sizes in the mesh, the curvature and geometry of VFs can be resolved more effectively, and thus ADCIRC will be able to better understand how inundation will propagate inland.

When running ADCIRC, waves were not calculated and thus SWAN was not utilized. In future studies, integrating SWAN and ADCIRC could potentially provide an improved storm surge simulation. Additionally, future work should simulate more historic hurricanes, such as Hurricane Irma (2017) and Hurricane Ian (2022), both of which also had significant storm surge impacts on the state of Georgia.

Future work also must include updated geographic data overtime as the coastal morphology changes. A future mesh would include regions beyond Georgia as well, including the technology used in this project across the vulnerable U.S. coastline and beyond. Additionally, changes in technology in LiDAR would allow for a more accurate coastal elevation profile of the VFs and thalwegs. Future work also could involve the generation of an overall higher resolution mesh, where both more thalwegs and more VFs are integrated into the mesh. Improved computational abilities would allow for increased mesh resolution, allowing for improved ADCIRC runtimes, making a higher resolution mesh more optimal.

6.0 | CONCLUSION

The increased risk of coastal regions has increased the need for accurate storm surge simulation technology (Intergovernmental Panel on Climate Change (IPCC), 2022). The state of Georgia lays along the SAB, and features diverse geographies and coastal morphology. An unstructured, finite element mesh was generated for Georgia and the surrounding SAB for large-domain storm surge modeling in the hydrodynamic model, ADCIRC.

The mesh was generated using mesh generation software OM2D. Both oceanic and overland floodplain regions were included within the meshing domain, expanding the spatial discretization for the ADCIRC simulation to include potentially inundated regions. The mesh generation process triangulated both the overland and oceanic regions simultaneously and completed the mesh in under an hour.

The mesh additionally featured integrated geographic features such as VFs and thalwegs. The inclusion of these geographic elements allowed for the mesh to include higher resolution around significant geographic areas, while reducing mesh resolution in unimportant areas, improving overall computational cost (M. V. Bilskie et al., 2020). The integrated vertical features were appended to the mesh as node points, in order to resolve significantly high regions that could interfere with coastal inundation. Vertical features were extracted from a LiDAR DEM using PyVF for the mesh's node point generation (Gao, 2021). The resulting mesh then was interpolated using PyDEM2GRD in order to avoid instabilities within the mesh's elevation profile (M. V. Bilskie & Hagen, 2013).

Subsequently, the unstructured, finite element mesh generated as a result was employed in ADCIRC to conduct simulations for both the storm surge induced by Hurricane Matthew (2016) and a regular tidal scenario. Simulated results were the best along locations within the Georgia

mesh, where resolution was the highest and VFs were both extracted and subsequently appended to nodes. The model assumed scenarios with no wind waves, and only simulated water levels.

Future contributions to the finalized Georgia mesh will improve the capabilities of the mesh to simulate storm surge and tides in other regions beyond Georgia if geographic elements are expanded beyond Georgia. The finalized Georgia mesh will be implemented for real-time storm surge predictions during future tropical events that affect Georgia and the SAB.

REFERENCES

AQUAVEO. (n.d.). *Surface-water Modeling System (SMS)* [Computer software]. Retrieved June 14, 2023, from https://www.aquaveo.com/software/sms-surface-water-modeling-system-introduction

Bates, P. D., Marks, K. J., & Horritt, M. S. (2003). Optimal use of high-resolution topographic data in flood inundation models. *Hydrological Processes*, *17*(3), 537–557. https://doi.org/10.1002/hyp.1113

Bathi, J. R., & Das, H. S. (2016). Vulnerability of Coastal Communities from Storm Surge and Flood Disasters. *International Journal of Environmental Research and Public Health*, *13*(2), Article 2. https://doi.org/10.3390/ijerph13020239

Bilskie, M. (2012). *Influence of Topographic Elevation Error on Modeled Storm Surge*.

Bilskie, M. V., Akhavian, R., & Hagen, S. (2012). *Bare Earth LiDAR to Gridded Topography for the Pascagoula River, MS: An Accuracy Assessment*. 295–314. https://doi.org/10.1061/9780784412411.00018

Bilskie, M. V., Asher, T. G., Miller, P. W., Fleming, J. G., Hagen, S. C., & Jr, R. A. L. (2022). Real-Time Simulated Storm Surge Predictions during Hurricane Michael (2018). *Weather and Forecasting*, *37*(7), 1085–1102. https://doi.org/10.1175/WAF-D-21-0132.1

Bilskie, M. V., Bacopoulos, P., & Hagen, S. C. (2019). Astronomic tides and nonlinear tidal dispersion for a tropical coastal estuary with engineered features (causeways): Indian River lagoon system. *Estuarine, Coastal and Shelf Science*, *216*, 54–70. https://doi.org/10.1016/j.ecss.2017.11.009

Bilskie, M. V., Coggin, D., Hagen, S. C., & Medeiros, S. C. (2015). Terrain-driven unstructured mesh development through semi-automatic vertical feature extraction. *Advances in Water Resources*, *86*, 102–118. https://doi.org/10.1016/j.advwatres.2015.09.020

Bilskie, M. V., & Hagen, S. C. (2013). Topographic accuracy assessment of bare earth lidar-derived unstructured meshes. *Advances in Water Resources*, *52*, 165–177. https://doi.org/10.1016/j.advwatres.2012.09.003

Bilskie, M. V., Hagen, S. C., & Medeiros, S. C. (2020). Unstructured finite element mesh decimation for real-time Hurricane storm surge forecasting. *Coastal Engineering*, *156*, 103622. https://doi.org/10.1016/j.coastaleng.2019.103622

Bilskie, M. V., Hagen, S. C., Salisbury, M. B., & Coggin, D. (2012). *Low-Versus High-Resolution Finite Element Modeling of Storm Surge in the Yellow River, Florida*. 65–76. https://doi.org/10.1061/41185(417)7

Blain, C. A., Westerink, J. J., & Luettich Jr., R. A. (1994). The influence of domain size on the response characteristics of a hurricane storm surge model. *Journal of Geophysical Research: Oceans*, *99*(C9), 18467–18479. https://doi.org/10.1029/94JC01348

Blanton, B., & Luettich, J., Richard. (2023). *North Carolina Coastal Flood Analysis System Model Grid Generation*.

Bode, L., & Hardy, T. A. (1997). Progress and Recent Developments in Storm Surge Modeling. *Journal of Hydraulic Engineering*, *123*(4), 315–331. https://doi.org/10.1061/(ASCE)0733-9429(1997)123:4(315)

Boender, E. (1994). Reliable Delaunay-based mesh generation and mesh improvement. *Communications in Numerical Methods in Engineering*, *10*(10), 773–783. https://doi.org/10.1002/cnm.1640101003

Booij, N., Holthuijsen, L. H., & Ris, R. C. (2015). *The "Swan" Wave Model for Shallow Water*. 668–676. https://doi.org/10.1061/9780784402429.053

Bunya. (2010). *A High-Resolution Coupled Riverine Flow, Tide, Wind, Wind Wave, and Storm Surge Model for Southern Louisiana and Mississippi. Part II: Synoptic Description and Analysis of Hurricanes Katrina and Rita in: Monthly Weather Review Volume 138 Issue 2 (2010)*. https://journals.ametsoc.org/view/journals/mwre/138/2/2009mwr2907.1.xml

Bunya, S., Dietrich, J. C., Westerink, J. J., Ebersole, B. A., Smith, J. M., Atkinson, J. H., Jensen, R., Resio, D. T., Luettich, R. A., Dawson, C., Cardone, V. J., Cox, A. T., Powell, M. D., Westerink, H. J., & Roberts, H. J. (2010). A High-Resolution Coupled Riverine Flow, Tide, Wind, Wind Wave, and Storm Surge Model for Southern Louisiana and Mississippi. Part I: Model Development and Validation. *Monthly Weather Review*, *138*(2), 345–377. https://doi.org/10.1175/2009MWR2906.1

Cangialosi, J. P., & Landsea, C. W. (2016). An Examination of Model and Official National Hurricane Center Tropical Cyclone Size Forecasts. *Weather and Forecasting*, *31*(4), 1293–1300. https://doi.org/10.1175/WAF-D-15-0158.1

C-CAP Regional Land Cover and Change. (n.d.). Retrieved June 8, 2023, from https://coast.noaa.gov/digitalcoast/data/ccapregional.html

Coastal Model Applications and Field Measurements- Tools and Standards for Ocean Modeling | U.S. Geological Survey. (n.d.). Retrieved March 23, 2023, from https://www.usgs.gov/centers/whcmsc/science/coastal-model-applications-and-field-measurements-tools-and-standards-ocean

Coastal National Elevation Database (CoNED) Applications Project | U.S. Geological Survey. (n.d.). Retrieved June 1, 2023, from https://www.usgs.gov/special-topics/coastal-national-elevation-database-applications-project

Coggin, D. (2008). Lidar In Coastal Storm Surge Modeling: Modeling Linear Raised Features. *Electronic Theses and Dissertations*. https://stars.library.ucf.edu/etd/3478

Continuously Updated Digital Elevation Model (CUDEM)—1/3 Arc-Second Resolution Bathymetric-Topographic Tiles. (n.d.). [dataset]. NOAA National Centers for Environmental Information (Point of Contact). Retrieved June 7, 2023, from https://catalog.data.gov/dataset/continuously-updated-digital-elevation-model-cudem-1-3-arc-second-resolution-bathymetric-topogr

Dietrich, J. C., Tanaka, S., Westerink, J. J., Dawson, C. N., Luettich, R. A., Zijlema, M., Holthuijsen, L. H., Smith, J. M., Westerink, L. G., & Westerink, H. J. (2012). Performance of the Unstructured-Mesh, SWAN+ADCIRC Model in Computing Hurricane Waves and Surge. *Journal of Scientific Computing*, *52*(2), 468–497. https://doi.org/10.1007/s10915-011-9555-6

Dietrich, J. C., Westerink, J. J., Kennedy, A. B., Smith, J. M., Jensen, R. E., Zijlema, M., Holthuijsen, L. H., Dawson, C., Luettich, R. A., Powell, M. D., Cardone, V. J., Cox, A. T., Stone, G. W., Pourtaheri, H., Hope, M. E., Tanaka, S., Westerink, L. G., Westerink, H. J., & Cobell, Z. (2011). Hurricane Gustav (2008) Waves and Storm Surge: Hindcast, Synoptic Analysis, and Validation in Southern Louisiana. *Monthly Weather Review*, *139*(8), 2488–2522. https://doi.org/10.1175/2011MWR3611.1

Dietrich, J. C., Zijlema, M., Westerink, J. J., Holthuijsen, L. H., Dawson, C., Luettich, R. A., Jensen, R. E., Smith, J. M., Stelling, G. S., & Stone, G. W. (2011). Modeling hurricane

waves and storm surge using integrally-coupled, scalable computations. *Coastal Engineering*, *58*(1), 45–65. https://doi.org/10.1016/j.coastaleng.2010.08.001

Exploring digital elevation models—ArcMap | Documentation. (n.d.). Retrieved April 5, 2023, from https://desktop.arcgis.com/en/arcmap/latest/tools/spatial-analyst-toolbox/exploring-digital-elevation-models.htm

Feng, X., Yin, B., & Yang, D. (2012). Effect of hurricane paths on storm surge response at Tianjin, China. *Estuarine, Coastal and Shelf Science*, *106*, 58–68. https://doi.org/10.1016/j.ecss.2012.04.032

Florinsky, I. V. (1998). Combined analysis of digital terrain models and remotely sensed data in landscape investigations. *Progress in Physical Geography: Earth and Environment*, *22*(1), 33–60. https://doi.org/10.1177/030913339802200102

Frey, P., & George, P. (2008). Mesh Generation: Application to Finite Elements: Second Edition. *Mesh Generation: Application to Finite Elements: Second Edition*. https://doi.org/10.1002/9780470611166

Frey, P. J., Borouchaki, H., & George, P.-L. (1998). 3D Delaunay mesh generation coupled with an advancing-front approach. *Computer Methods in Applied Mechanics and Engineering*, *157*(1), 115–131. https://doi.org/10.1016/S0045-7825(97)00222-3

Gallien, T. W., Sanders, B. F., & Flick, R. E. (2014). Urban coastal flood prediction: Integrating wave overtopping, flood defenses and drainage. *Coastal Engineering*, *91*, 18–28. https://doi.org/10.1016/j.coastaleng.2014.04.007

Gao, S. (2021). Vertical Feature Delineation for Flood Hazard Assessments at the Coastal Land Margin. *LSU Doctoral Dissertations*. https://doi.org/10.31390/gradschool_dissertations.5598

Georgas, N., Orton, P., Blumberg, A., Cohen, L., Zarrilli, D., & Yin, L. (2014). The Impact of Tidal Phase on Hurricane Sandy's Flooding Around New York City and Long Island Sound. *Journal of Extreme Events*, *01*(01), 1450006. https://doi.org/10.1142/S2345737614500067

Ghorbanzadeh, M., Vijayan, L., Yang, J., Ozguven, E. E., Huang, W., & Ma, M. (2021). Integrating Evacuation and Storm Surge Modeling Considering Potential Hurricane Tracks: The Case of Hurricane Irma in Southeast Florida. *ISPRS International Journal of Geo-Information*, *10*(10), Article 10. https://doi.org/10.3390/ijgi10100661

Greenberg, D., Dupont, F., Lyard, F., Lynch, D., & Werner, F. (2007). Resolution issues in numerical models of oceanic and coastal circulation. *Continental Shelf Research*, *27*, 1317–1343. https://doi.org/10.1016/j.csr.2007.01.023

Groom, J., Bertin, S., & Friedrich, H. (2018). Evaluation of DEM size and grid spacing for fluvial patch-scale roughness parameterisation. *Geomorphology*, *320*, 98–110. https://doi.org/10.1016/j.geomorph.2018.08.017

Hagen, S. C., Horstmann, O., & Bennett, R. J. (2002). An Unstructured Mesh Generation Algorithm for Shallow Water Modeling. *International Journal of Computational Fluid Dynamics*, *16*(2), 83–91. https://doi.org/10.1080/10618560290017176

Hagen, S. C., Zundel, A. K., & Kojima, S. (2006). Automatic, unstructured mesh generation for tidal calculations in a large domain. *International Journal of Computational Fluid Dynamics*, *20*(8), 593–608. https://doi.org/10.1080/10618560601046846

Hebert, P. J. (1980). Atlantic Hurricane Season of 1979. *Monthly Weather Review*, *108*(7), 973–990. https://doi.org/10.1175/1520-0493(1980)108<0973:AHSO>2.0.CO;2

Heinzer, T. J., Williams, M. D., Dogrul, E. C., Kadir, T. N., Brush, C. F., & Chung, F. I. (2012). Implementation of a feature-constraint mesh generation algorithm within a GIS. *Computers & Geosciences*, *49*, 46–52. https://doi.org/10.1016/j.cageo.2012.06.004

Helderop, E., & Grubesic, T. H. (2019). Social, geomorphic, and climatic factors driving U.S. coastal city vulnerability to storm surge flooding. *Ocean & Coastal Management*, *181*, 104902. https://doi.org/10.1016/j.ocecoaman.2019.104902

Hiester, H. R., Piggott, M., Farrell, P. E., & Allison, P. (2014). Assessment of spurious mixing in adaptive mesh simulations of the two-dimensional lock-exchange. *Ocean Modelling*, *73*, 30–44. https://doi.org/10.1016/j.ocemod.2013.10.003

Hinkel, J., Lincke, D., Vafeidis, A. T., Perrette, M., Nicholls, R. J., Tol, R. S. J., Marzeion, B., Fettweis, X., Ionescu, C., & Levermann, A. (2014). Coastal flood damage and adaptation costs under 21st century sea-level rise. *Proceedings of the National Academy of Sciences*, *111*(9), 3292–3297. https://doi.org/10.1073/pnas.1222469111

Historic Storm Surge Records | Coastal Processes, Hazards, and Society. (n.d.). Retrieved June 3, 2023, from https://www.e-education.psu.edu/earth107/node/1046

Hu, K., Meselhe, E., Rhode, R., Snider, N., & Renfro, A. (2022). The Impact of Levee Openings on Storm Surge: A Numerical Analysis in Coastal Louisiana. *Applied Sciences*, *12*(21), Article 21. https://doi.org/10.3390/app122110884

Intergovernmental Panel on Climate Change (IPCC). (2022). *The Ocean and Cryosphere in a Changing Climate: Special Report of the Intergovernmental Panel on Climate Change*. Cambridge University Press. https://doi.org/10.1017/9781009157964

Irish, J. L., Resio, D. T., & Ratcliff, J. J. (2008). The Influence of Storm Size on Hurricane Surge. *Journal of Physical Oceanography*, *38*(9), 2003–2013. https://doi.org/10.1175/2008JPO3727.1

Kohno, N., Dube, S. K., Entel, M., Fakhruddin, S. H. M., Greenslade, D., Leroux, M.-D., Rhome, J., & Thuy, N. B. (2018). Recent Progress in Storm Surge Forecasting. *Tropical Cyclone Research and Review*, *7*(2), 128–139. https://doi.org/10.6057/2018TCRR02.04

Kojima, S. (2005). Optimization Of An Unstructured Finite Element Mesh For Tide And Storm Surge Modeling Applications In The Western North Atlantic Ocean. *Electronic Theses and Dissertations*. https://stars.library.ucf.edu/etd/457

Li, J., & Nie, B. (2017). Storm surge prediction: Present status and future challenges. *Procedia IUTAM*, *25*, 3–9. https://doi.org/10.1016/j.piutam.2017.09.002

Lin, N., Emanuel, K. A., Smith, J. A., & Vanmarcke, E. (2010). Risk assessment of hurricane storm surge for New York City. *Journal of Geophysical Research, 115*(D18), D18121. https://doi.org/10.1029/2009JD013630

Lin, N., Emanuel, K., Oppenheimer, M., & Vanmarcke, E. (2012). Physically based assessment of hurricane surge threat under climate change. *Nature Climate Change*, *2*(6), 462–467. https://doi.org/10.1038/nclimate1389

Liu, X. (2008). Airborne LiDAR for DEM generation: Some critical issues. *Progress in Physical Geography: Earth and Environment*, *32*(1), 31–49. https://doi.org/10.1177/0309133308089496

Löhner, R., & Parikh, P. (1988). Generation of three-dimensional unstructured grids by the advancing-front method. *International Journal for Numerical Methods in Fluids*, *8*(10), 1135–1149. https://doi.org/10.1002/fld.1650081003

Luettich, R. A. (Richard A., Westerink, J. J., & Scheffner, N. W. (1992). ADCIRC: An advanced three-dimensional circulation model for shelves, coasts, and estuaries. Report 1, Theory and methodology of ADCIRC-2DD1 and ADCIRC-3DL. In *This Digital Resource was created from scans of the Print Resource* [Report]. Coastal Engineering Research Center (U.S.). https://erdc-library.erdc.dren.mil/jspui/handle/11681/4618

Macchione, F., Costabile, P., Costanzo, C., & De Santis, R. (2019). Moving to 3-D flood hazard maps for enhancing risk communication. *Environmental Modelling & Software*, *111*, 510–522. https://doi.org/10.1016/j.envsoft.2018.11.005

Maune, D. F. (2007). *Digital elevation model technologies and applications: The DEM users manual*. Asprs Publications.

Mcinnes, K. L., Walsh, K. J. E., Hubbert, G. D., & Beer, T. (2003). Impact of Sea-level Rise and Storm Surges on a Coastal Community. *Natural Hazards*, *30*(2), 187–207. https://doi.org/10.1023/A:1026118417752

Mudd, L., Wang, Y., Letchford, C., & Rosowsky, D. (2014). Assessing Climate Change Impact on the U.S. East Coast Hurricane Hazard: Temperature, Frequency, and Track. *Natural Hazards Review*, *15*(3), 04014001. https://doi.org/10.1061/(ASCE)NH.1527-6996.0000128

Mukherjee, S., Joshi, P. K., Mukherjee, S., Ghosh, A., Garg, R. D., & Mukhopadhyay, A. (2013). Evaluation of vertical accuracy of open source Digital Elevation Model (DEM). *International Journal of Applied Earth Observation and Geoinformation*, *21*, 205–217. https://doi.org/10.1016/j.jag.2012.09.004

Panthi, J., Pradhanang, S. M., Nolte, A., & Boving, T. B. (2022). Saltwater intrusion into coastal aquifers in the contiguous United States—A systematic review of investigation approaches

and monitoring networks. *Science of The Total Environment*, *836*, 155641. https://doi.org/10.1016/j.scitotenv.2022.155641

Park, K., Federico, I., Di Lorenzo, E., Ezer, T., Cobb, K. M., Pinardi, N., & Coppini, G. (2022). The contribution of hurricane remote ocean forcing to storm surge along the Southeastern U.S. coast. *Coastal Engineering*, *173*, 104098. https://doi.org/10.1016/j.coastaleng.2022.104098

Passeri, D., Hagen, S. C., Smar, D., Alimohammadi, N., Risner, A., & White, R. (2012). *Sensitivity of an ADCIRC Tide and Storm Surge Model to Manning's n*. 457–475. https://doi.org/10.1061/9780784412411.00027

Persson, P.-O. (2006). Mesh size functions for implicit geometries and PDE-based gradient limiting. *Engineering with Computers*, *22*(2), 95–109. https://doi.org/10.1007/s00366-006-0014-1

Resio, D. T., & Westerink, J. J. (2008). Modeling the physics of storm surges. *Physics Today*, *61*(9), 33–38. https://doi.org/10.1063/1.2982120

Roberts, K. J., Pringle, W. J., & Westerink, J. J. (2019). OceanMesh2D 1.0: MATLAB-based software for two-dimensional unstructured mesh generation in coastal ocean modeling. *Geoscientific Model Development*, *12*(5), 1847–1868. https://doi.org/10.5194/gmd-12-1847-2019

Sahoo, B., & Bhaskaran, P. K. (2018). A comprehensive data set for tropical cyclone storm surge-induced inundation for the east coast of India. *International Journal of Climatology*, *38*(1), 403–419. https://doi.org/10.1002/joc.5184

Sea, Lake, and Overland Surges from Hurricanes (SLOSH). (n.d.). Retrieved March 23, 2023, from https://www.nhc.noaa.gov/surge/slosh.php

Sebastian, M., Behera, M. R., & Murty, P. L. N. (2019). Storm surge hydrodynamics at a concave coast due to varying approach angles of cyclone. *Ocean Engineering*, *191*, 106437. https://doi.org/10.1016/j.oceaneng.2019.106437

South Atlantic Coastal Study (SACS). (2021). [Computer software]. U.S. Army Corps of Engineers. https://www.sad.usace.army.mil/SACS/

Storm Surge Overview. (n.d.). Retrieved March 23, 2023, from https://www.nhc.noaa.gov/surge/

Sun, X., Xie, L., Shah, S. U., & Shen, X. (2021). A Machine Learning Based Ensemble Forecasting Optimization Algorithm for Preseason Prediction of Atlantic Hurricane Activity. *Atmosphere*, *12*(4), Article 4. https://doi.org/10.3390/atmos12040522

Tarboton, D. (2005). Terrain analysis using digital elevation models (TauDEM). *Utah State University*.

Thomas, A., Dietrich, J., Asher, T., Bell, M., Blanton, B., Copeland, J., Cox, A., Dawson, C., Fleming, J., & Luettich, R. (2019). Influence of storm timing and forward speed on tides and storm surge during Hurricane Matthew. *Ocean Modelling*, *137*, 1–19. https://doi.org/10.1016/j.ocemod.2019.03.004

Thompson, E. F., & Cardone, V. J. (1996). Practical Modeling of Hurricane Surface Wind Fields. *Journal of Waterway, Port, Coastal, and Ocean Engineering*, *122*(4), 195–205. https://doi.org/10.1061/(ASCE)0733-950X(1996)122:4(195)

Tognin, D., D'Alpaos, A., Marani, M., & Carniello, L. (2021). Marsh resilience to sea-level rise reduced by storm-surge barriers in the Venice Lagoon. *Nature Geoscience*, *14*(12), Article 12. https://doi.org/10.1038/s41561-021-00853-7

Turan, C. K., Kinfu, Y. P., Samad, M. A., Farhadzadeh, A., & Ng, K. (2018). *Comparison of ADCIRC and SLOSH Model Simulations for Hurricanes Andrew and Irma near Miami, Florida*. 176–187. https://doi.org/10.1061/9780784481424.019

Velasquez-Montoya, L., Wargula, A., Tomiczek, T., Sciaudone, E. J., & Smyre, E. (2023). Modeling the hydrodynamics of a tidal inlet during bay-side storms. *Estuarine, Coastal and Shelf Science, 280*, 108145. https://doi.org/10.1016/j.ecss.2022.108145

Villarini, G., Vecchi, G. A., & Smith, J. A. (2012). U.S. Landfalling and North Atlantic Hurricanes: Statistical Modeling of Their Frequencies and Ratios. *Monthly Weather Review*, *140*(1), 44–65. https://doi.org/10.1175/MWR-D-11-00063.1

Weatherill, N. P., & Hassan, O. (1994). Efficient three-dimensional Delaunay triangulation with automatic point creation and imposed boundary constraints. *International Journal for Numerical Methods in Engineering*, *37*(12), 2005–2039. https://doi.org/10.1002/nme.1620371203

Westerink, J. J., Luettich, R. A., Feyen, J. C., Atkinson, J. H., Dawson, C., Roberts, H. J., Powell, M. D., Dunion, J. P., Kubatko, E. J., & Pourtaheri, H. (2008). A Basin- to Channel-Scale Unstructured Grid Hurricane Storm Surge Model Applied to Southern Louisiana. *Monthly Weather Review*, *136*(3), 833–864. https://doi.org/10.1175/2007MWR1946.1

Wolock, D. M., & Price, C. V. (1994). Effects of digital elevation model map scale and data resolution on a topography-based watershed model. *Water Resources Research*, *30*(11), 3041–3052. https://doi.org/10.1029/94WR01971

Woodruff, J., Dietrich, J. C., Wirasaet, D., Kennedy, A. B., & Bolster, D. (2023). Storm surge predictions from ocean to subgrid scales. *Natural Hazards*, *117*(3), 2989–3019. https://doi.org/10.1007/s11069-023-05975-2

Yasuda, T., Nakajo, S., Kim, S., Mase, H., Mori, N., & Horsburgh, K. (2014). Evaluation of future storm surge risk in East Asia based on state-of-the-art climate change projection. *Coastal Engineering*, *83*, 65–71. https://doi.org/10.1016/j.coastaleng.2013.10.003

Zhang, K., Douglas, B. C., & Leatherman, S. P. (2000). Twentieth-Century Storm Activity along the U.S. East Coast. *Journal of Climate*, *13*(10), 1748–1761. https://doi.org/10.1175/1520-0442(2000)013<1748:TCSAAT>2.0.CO;2

Zijlema, M. (2010). Computation of wind-wave spectra in coastal waters with SWAN on unstructured grids. *Coastal Engineering*, *57*(3), 267–277. https://doi.org/10.1016/j.coastaleng.2009.10.011